NONLINEAR LIFTING LINE THEORY FOR PREDICTING STALLING INSTABILITIES ON WINGS OF MODERATE ASPECT RATIO

GENERAL DYNAMICS/CONVAIR

PREPARED FOR
NAVAL AIR AND DEVELOPMENT CENTER

15 JUNE 1976

Unclassified

SECURITY CLASSIFICATION OF THIS PAGE (When Data Entered)

REPORT DOCUMENTATION PAGE		READ INSTRUCTIONS BEFORE COMPLETING FORM
1. REPORT NUMBER CASD-NSC-76-001	2. GOVT ACCESSION NO.	3. RECIPIENT'S CATALOG NUMBER
4. TITLE (and Subtitle) Nonlinear Lifting Line Theory for Predicting Stalling Instabilities on Wings of Moderate Aspect Ratio		5. TYPE OF REPORT & PERIOD COVERED Final Technology Report 6/30/75 - 6/15/76 6. PERFORMING ORG. REPORT NUMBER
7. AUTHOR(s) S. T. Piszkin E. S. Levinsky		8. CONTRACT OR GRANT NUMBER(s) N62269-75-C-0356
9. PERFORMING ORGANIZATION NAME AND ADDRESS General Dynamics Convair Division 5001 Kearny Villa Road, San Diego, Calif. 92138		10. PROGRAM ELEMENT, PROJECT, TASK AREA & WORK UNIT NUMBERS A-3200000/001B/6F41421212
11. CONTROLLING OFFICE NAME AND ADDRESS Naval Air And Development Center, Code 3015 Warminster, PA 18974		12. REPORT DATE June 15, 1976 13. NUMBER OF PAGES 97
14 MONITORING AGENCY NAME & ADDRESS(if different from Controlling Office)		15. SECURITY CLASS (of this report) Unclassified 15a. DECLASSIFICATION/DOWNGRADING SCHEDULE

16. DISTRIBUTION STATEMENT (of this Report)

Approved for Public Release; Distribution Unlimited

17. DISTRIBUTION STATEMENT (of the abstract entered in Block 20, if different from Report)

18 SUPPLEMENTARY NOTES

19. KEY WORDS (Continue on reverse side if necessary and identify by block number)

Departure	Spin Entry
Hysteresis	Stall
Lifting Line Theory	Unsteady Aerodynamics
Nonlinear Aerodynamics	Zero Beta Moments

20. ABSTRACT (Continue on reverse side if necessary and identify by block number)

A computational procedure has been developed for predicting the time dependent longitudinal and lateral aerodynamic characteristics of wing-body configurations at angles of attack up to and beyond stall. The purpose of the procedure is to provide the aircraft designer with a tool for simulating and alleviating such adverse wing stalling characteristics as wing rock, wing drop, loss of roll control or roll control reversal, etc. and thereby lead to the design of aircraft with improved stall,

DD FORM 1 JAN 73 1473 EDITION OF 1 NOV 65 IS OBSOLETE

Unclassified

SECURITY CLASSIFICATION OF THIS PAGE (When Data Entered)

departure and spin resistance characteristics.

The procedure is based on nonlinear lifting line theory which has been modified to include unsteady wake effects. A discrete vortex lattice representation is used for the time dependent wake, whereas a finite element representation is used to describe the time dependent wing load distribution, which is assumed concentrated along a single line at the 25% chord position. In accordance with lifting line theory, each chordwise section is assumed to behave like a two-dimensional airfoil at an effective angle of attack defined by geometry and induced flow angularity. The usual assumptions of lifting line theory apply to the method, viz. moderate to high wing aspect ratio, moderate sweep angle and incompressible flow. Additional assumptions are also implicit regarding effects of the unsteady flow on section chordwise load distributions and stall.

Arbitrary nonlinear section lift curves may be introduced, and time histories of the overall wing longitudinal and lateral aerodynamic characteristics and spanwise load distribution may be examined as the wing is pitched (up or down) through the stall range. Lateral asymmetries (e.g. aileron deflection) may also be introduced and removed during the pitching motion to simulate effects of control actuation.

Calculations are presented which compare the method with existing theory and test data and which show effects of various planform modifications and airfoil section variations on wing stalling characteristics. For airfoils which have a negative lift curve slope (subsequent to stall), the solutions sometimes exhibit abrupt losses in lift, lift hysteresis, and asymmetric stall (even with zero lateral asymmetry). These results are due to the existence of multiple solutions to the lifting line equations, which have been known to occur with negative section lift curves (e.g. References 1 - 3). The transient flow nature of the present formulation may provide a means of choosing between the various possible loadings at a given angle of attack.

The theory predicts that lift hysteresis during stall is strongly influenced by wing planform shape and by the steepness of the negative lift curve slope beyond stall. Increasing aspect ratio and decreasing the section negative lift curve slope tend to reduce stall hysteresis. Laterally asymmetrical span load distributions are produced, even at zero yaw, by introducing and then removing an aileron deflection. This gives rise to a "zero beta" rolling and yawing moment not unlike those observed in tests at post stall angles of attack. The zero beta asymmetries are shown to be alleviated by the same factors which reduced stall hysteresis. Definitive wind tunnel tests involving dynamic measurements of aerodynamic force and moment coefficients and of span load distribution are required to evaluate the accuracy of the method.

FOREWORD AND DEDICATION

This research was undertaken by the Convair Division of General Dynamics Corporation, San Diego, California, under Naval Air and Development Center Contract N62269-75-C-0356. The NADC Scientific Officer was Mr. A. Piranian, Code 3015A. The program was administered by Professor L. Schmidt, U.S. Navy Postgraduate School, who was acting as Navy Technology Administrator for Aerodynamics, Code 320D.

The Principal Investigator was Mr. Stanley T. Piszkin, who passed away suddenly and without warning shortly after completing the formulation and computer check-out phases of the contract. Mr. Piszkin also performed the majority of the computer calculations and was able to demonstrate the occurance of zero beta rolling and yawing moments. The second author was priviledged to have worked closely with Mr. Piszkin during the formulative stages of the program, and hopes that he has been able to convey the ideas and results of Mr. Piszkin in a clear and precise manner.

Mr. Piszkin, as an aerodynamicist and as a private pilot with experience in aerobatics, not only dealt with the theory of stalling instabilities from a theoretical standpoint, but also from a very practical flight safety point of view. It was his hope that these efforts would someday lead to a better understanding of the nature and cause of the adverse departure and spin entry characteristics of high performance aircraft and thereby result in improved flight safety. It is to this goal and to Mr. Piszkin's memory that the present report has been dedicated.

The authors wish to thank Mr. Herbert Sinnen for his efficient programming of the computational procedure, and for his cooperation in acquainting the second author with its use when the need arose.

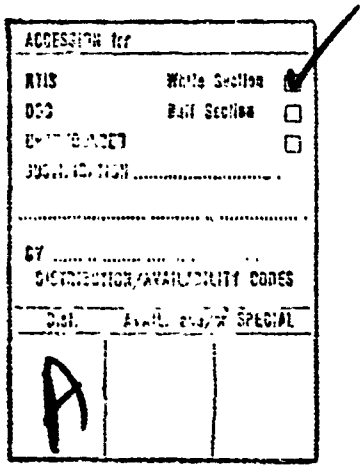

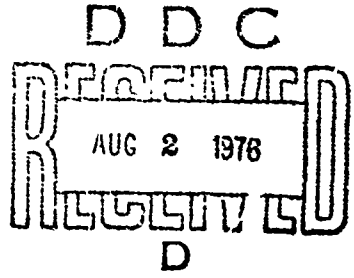

ABSTRACT

A computational procedure has been developed for predicting the time dependent longitudinal and lateral aerodynamic characteristics of wing-body configurations at angles of attack up to and beyond stall. The purpose of the procedure is to provide the aircraft designer with a tool for simulating and alleviating such adverse wing stalling characteristics as wing rock, wing drop, loss of roll control or roll control reversal, etc., and thereby should lead to the design of aircraft with improved stall, departure and spin resistance characteristics.

The procedure is based on nonlinear lifting line theory which has been modified to include unsteady wake effects. A discrete vortex lattice representation is used for the time dependent wake, whereas a finite element representation is used to describe the time dependent wing load distribution, which is assumed concentrated along a single line at the 25% chord position. In accordance with lifting line theory, each chordwise section is assumed to behave like a two-dimensional airfoil at an effective angle of attack defined by geometry and induced flow angularity. The usual assumptions of lifting line theory apply to the method, viz. moderate to high wing aspect ratio , moderate sweep angle and incompressible flow. Additional assumptions are also implicit regarding effects of the unsteady flow on section chordwise load distributions and stall.

Arbitrary nonlinear section lift curves may be introduced. and time histories of the overall wing longitudinal and lateral aerodynamic characteristics and spanwise load distribution may be examined as the wing is pitched (up or down) through the stall range. Lateral asymmetries (e.g. aileron deflection) may also be introduced and removed during the pitching motion to simulate effects of control actuation.

Calculations are presented which compare the method with existing theory and test data and which show effects of various planform modifications and airfoil section variations on wing stalling characteristics. For airfoils which have a negative lift curve slope (subsequent to stall), the solutions sometimes exhibit abrupt losses in lift, lift hysteresis , and asymmetric stall (even with zero lateral asymmetry). These results are due to the existence of multiple solutions to the lifting line equations, which have been known to occur with negative section lift curves (e.g. References 1-3). The transient flow nature of the present formulation may provide a means of choosing between the various possible loadings at a given angle of attack.

The theory predicts that lift hysteresis during stall is strongly influenced by wing planform shape and by the steepness of the negative lift curve slope beyond stall. Increasing aspect ratio and decreasing the section negative lift curve slope tend to reduce stall hysteresis. Laterally asymmetrical span load distributions are produced,

even at zero yaw, by introducing and then removing an aileron deflection. This gives rise to a "zero beta" rolling and yawing moment not unlike those observed in tests at post stall angles of attack. The zero beta asymmetries are shown to be alleviated by the same factors which reduced stall hysteresis. Definitive wind tunnel tests involving dynamic measurements of aerodynamic force and moment coefficients and of span load distribution are required to evaluate the accuracy of the method.

TABLE OF CONTENT

LIST OF FIGURES

LIST OF FIGURES (CONT'D)

LIST OF FIGURES (CONT'D)

SYMBOLS

a	section lift curve slope
AR	aspect ratio
b	absolute value of maximum negative lift curve slope, also wing span
C	weighting factor in iteration procedure
c	local wing chord
C_D	drag coefficient
C_{D_P}	profile drag coefficient
C_L	lift coefficient
C_ℓ	rolling moment coefficient
C_{L_o}	value of C_L at α 0
C_M	pitching moment coefficient
C_N	yawing moment coefficient
C_Y	side force coefficient
h	width of vortex elements in y direction
i_W	incidence angle of wing root with respect to fuselage centerline
L	lift
M	maximum number of spanwise rows of vortex elements (see Figure 3)
N	number of vortex element across exposed span of wing
n	number of chord lengths traveled by wake vortex elements per time step
R_B	fuselage radius
R_I	radial distance of image vortex from center of fuselage in y-z plane
R_P	radial distance of wing trailing vortex element from fuselage centerline in y-z plane
S	wing reference area
t	time
V_∞	freestream velocity
W	downwash matrix

w	downwash velocity (positive in negative z direction)
x, y, z	body axis coordinate system with x and y axes in chordwise and spanwise directions, respectively, (see Figure 2)
x_{cp}	distance of control point from leading edge
α_D	downwash angle, Equation (6)
α_{EFF}	effective section angle of attack
α_p	geometric angle of attack at wing root
α_T	wing twist angle with respect to wing root
α_1	maximum angle of attack for linear region of tri-linear section lift curve
α_2	minimum angle of attack for fully stalled region of tri-linear section lift curve.
α_{2D}	downwash angle due to two-dimensional bound vortex element, Equation (9)
α_{3D}	downwash angle due to three-dimensional bound vortex element, Equation (7)
β	side slip angle
Γ	circulation of vortex element
γ	wing dihedral angle
γ_{ij}	downwash influence coefficient used with tri-linear lift curve slope
Δ	incremental
δ	angle defined by Equation (11) and shown in Figure 4, also Kronecker Delta symbol with subscripts ij
$\Delta\alpha_R$	differential lateral control deflection
ϵ	distance of first shed vortex behind wing trailing edge
Λ	local quarter chord sweep angle
ρ	density
λ	taper ratio

Subscripts

A	aft shed vortex element
B	bound or shed vortex element, also body upwash angle
F	forward bound or shed vortex element
I	image vortex element

i	index of spanwise control station
j,k	indicies locating vortex elements along the span (j) and in the wake (k)
L	left trailing vortex
R	right trailing vortex, also roll asymmetry angle
T	trailing vortex element, also twist angle

Superscripts

-	mean value
( )	iteration number
^	normalized circulation, $\hat{\Gamma} = 2\,\Gamma/V_\infty\,c$

INTRODUCTION

As is well known, there are a large number of aerodynamic effects which may limit the maneuverability of a fighter, especially as thrust to weight ratios, structural placards and physiological limits on the pilot are raised. These include such phenomena as shock induced buffet, wing rock and wing drop (probably due to asymmetrical separation with a subsequent rolling-yawing motion), nose slicing (possibly due to the establishment of asymmetrical flow and yawing moments in the nose region), pitch-up (loss of longitudinal stability due to flow separation at the tips), loss of lateral stability at high angles of attack, loss of roll control and roll control reversal at high angles of attack, and large drag increases (which lower the maximum sustained load factor). It is generally believed that some type of flow separation is responsible for each of these phenomena. The present report deals with the development of a simplified aerodynamic tool for estimating the aerodynamic characteristics of wings and wing-body configurations of moderate to high aspect ratio undergoing transient pitching motion with flow separation. Hence, the method developed in this study should prove useful for the prediction, simulation and possible inhibition of those adverse stalling phenomena included within the framework of the theory.

As noted above, the present formulation is for wings of moderate to high aspect ratio to which lifting line theory may be applied. In this regard there has appeared some interesting analytical work (1-3), based on Prandtl lifting line theory, which indicates that multiple solutions of the lifting line equations are possible under certain conditions. The multiple solutions are predicted only if the two-dimensional lift curves have either discontinuities or regions of high negative slope, beyond stall, as illustrated in Figure 1. One interesting feature of the multiple solutions is that they can yield span load distributions which are either symmetrical or asymmetrical about the wing centerline even at zero sidelsip angle. According to Sears [1], the asymmetrical solutions suggested to von Karman that large rolling moments could be produced near the stall without postulating any initial rolling velocity (or other asymmetries such as slight sideslip or wing panel misalignment). Sears states that the usual "textbook" explanation for the large rolling moments near stall, which is based on an initial rolling velocity which stalls one panel and destalls the other, fails to account for the violence of the rolling moments experienced in a wind tunnel with a model held fixed to the sting. The establishment of any one particular load distribution (either symmetrical or asymmetrical) probably depends on the relative stability of the corresponding circulation distribution to small disturbances.

The present report attempts to apply nonlinear lifting line theory to the modeling and prediction of aerodynamic effects during stall penetration at high angles of attack. Previous discussions of stall aerodynamics have noted the occurrence of asymmetrical flow separation at zero yaw angle as a possible forcing mechanism for wing rock and

and other types of pre and post-stall motions (e.g. References 4-7). It is postuated herein that the time dependent zero beta yawing and rolling moments predicted by the nonlinear lifting line theory are contributory to the limit cycle type of motions apt to occur during stall. This, of course, will require careful experimental verification.

The lifting line formulation utilized herein is a finite element, unsteady wake, incompressible flow theory and is somewhat more general than the General Dynamics/Convair nonlinear lifting line procedure reported in References 8 - 10. Besides excluding time dependent wake effects, the later procedure was limited to laterally symmetric load distributions at zero yaw angle, did not include effects of yaw, and could not handle body interference effects. Nevertheless, the procedure was found to correlate reasonably well with wind tunnel data through the stall (Ref. 9).

The procedure as formulated herein may be applied at either zero or non zero yaw angle (yaw is handled by skewing the wing panels). Both symmetrical and asymmetrical load distributions may be obtained, even at zero yaw angle. Three dimensional unsteady aerodynamic effects are included by allowing shed vortices in the wake to vary in strength with distance and time. The strengths of the shed vortices are related to those of the corresponding bound elements at an earlier time, based on the convective time delay at free stream velocity between the bound vortex and the particular wake station. Although the theory is unsteady from the point of view of wake induced effects, it is assumed that the two-dimensional airfoil chordwise loadings and sectional characteristics in stall are steady state. Thus, the assumption is implicit that such two dimensional phenomena as associated with the dynamic stall of helicopter blades are of a shorter time scale than the unsteady wake effects (see also Section 2.2).

The present approach makes use of the key assumption in lifting line theory, viz. that each chordwise section acts like a two-dimensional airfoil at an effective angle of attack equal to the local geometric angle of attack less the induced angle of attack. In order for this assumption to remain valid, (i.e. for the chordwise load distribution to remain two-dimensional) the aspect ratio must be sufficiently large to limit spanwise flow effects , and vortex effects associated with high leading edge sweep angles must not be dominant in the stall. Besides the assumptions noted above the method requires the selection of (or switching between) the various multiple span load solutions which may exist at a given angle of attack. Some of these solutions may be indicative of unstalled load distributions, some of partly stalled distributions and some of nearly fully stalled distributions. The criterion used for selecting among the various matematically possible solutions is empirical, and it is recognized that this aspect of the formulation requires further analysis. Because of this empiricism, and as a result of the assumptions noted previously, the need for wind tunnel tests involving dynamic measurements of aerodynamic forces, moments and span load distribution can not be over-emphasized.

The mathematical basis for the present theory is formulated in Section II. Results of some simplified analyses and properties of the solutions are also presented in Section II.

The method of solution and a dicussion of the stability and convergence of the iteration procedure are presented in Section III. More extensive numerical results involving comparison with existing test data and linear theory, are found in Section IV. Also presented in Section IV are parametric studies showing effects of planform shape and of two-dimensional lift curve characteristics on stalling properties. Mathematical details of the formulation and a listing of the computer program, along with detailed instructions for its use, may be found in Reference 12.

---

* The reader is also referred to Reference 25, which came to the attention of the author just prior to completion of the present report, and which also applies nonlinear lifting line theory to the design of wings which minimize aircraft departure and spin entry tendencies.

THEORY AND ASSUMPTIONS

The present section presents the mathematical basis and assumptions for the nonlinear lifting line theory with a time dependent wake as utilized herein. The theory may be used to obtain the time dependent span load distribution and corresponding time dependent wing force and moment coefficients for wings and wing-bodies of arbitrary planform experiencing a predetermined schedule of pitching motion and/or of lateral control deflections.

The present lifting line theory is similar to that used by Weissinger in his L-method [11], but has been modified to include nonlinear section aerodynamics, body interference effects and time dependent wake effects. Effects of sideslip, or yaw, are represented as differential right and left sweep angles (like a skewed wing). No fuselage cross flow terms are included in this sideslip representation. The theory as presented below allows for the arbitrary chordwise positioning of the wing control points, although the bound vortex location is always retained at the 25% chord location.

2.1 VORTEX SYSTEM

The vortex system used in the analysis is pictured in Figures 2 and 3, and is assumed planar except for the vertical displacement of the image vortices in the fuselage. The exposed wing, as shown in Figure 2, is segmented into N equal-span elements (up to 20) of width h in the spanwise y direction. Each element is a parallelogram in shape and consists of a bound vortex segment along the 1/4 chord line (which may be swept), two streamwise trailing segments and a closing shed vortex element at a downstream distance $\Delta x = V_\infty \Delta t$, where V_∞ is the free stream velocity and Δt is the time step. In the time dependent solution the strength $\Gamma_{j,1}(t)$ of this vortex element represents the circulation carried by the wing at the j 'th spanwise element (j = 1, 2 ... N) at the current time t. The downstream trailing vortex elements are of identical shape, but are of varying strength as

$$\Gamma_{j,k}(t) = \Gamma_{j,k-1}(t - \Delta t) \tag{1}$$

where k is an index describing the vortex element number in the wake (see Figure 3). If the maximum number of downstream parallelogram elements to be included is M-1, then

$$1 \leq k \leq M$$

where k = 1 corresponds to the wing element at the current time t, and k = M refers

to the final wake element, which is assumed unclosed. If M = 1, the solution reduces to that for a steady state wake.

Representation of the fuselage (assumed an infinite circular cylinder) by image vortex elements, as depicted in Figures 3 and 4, has found extensive use in the literature, e.g. References 13-16. The body images are located at identical axial positions as the primary (wing and wake) vortices. Since only the trailing vortex segments are properly imaged (cancellation of primary vortex induced velocities normal to the fuselage) the lateral and vertical locations of the image vortices is based on location of the primary trailing vortices. As shown in Figure 4, the images are located along a straight line in the y-z plane between the primary trailing vortex and the fuselage center at a radial distance R_I from the centerline

$$R_I = R_B^2/R_P \tag{2}$$

where R_B is the body radius and R_P is the radius to the primary vortex.

The velocities induced by the connecting bound elements between the image vortices are also included, based on Ref. 13, even though the bound image vortices do not satisfy the no flow condition through the fuselage. However, these velocities were not further augmented by the factor suggested in Reference 14, since it was believed that the justification for this correction was insufficient. The bound image vortices were included in the evaluation of the overall force on the wing-body combination, in accordance with the Trefftz-plane relationships given in Reference 16.

2.2 LIFTING LINE EQUATIONS

The lifting line assumption states that each spanwise station i of a wing acts like a two-dimensional airfoil at an effective angle of attack α_{EFF_i} equal to the local geometric pitch angle of attack α_{p_i} (includes effects of wing incidence, twist, control deflection, and body cross flow) less the downwash angle of attack α_{D_i} induced by the trailing vortex systems, viz.

$$\alpha_{EFF_i} = \alpha_{P_i} - \alpha_{D_i} \tag{3}$$

Thus, for an airfoil with lift, pitching moment, and profile drag curves of functional form

$$C_L = C_L(\alpha_p),\ C_M = C_M(\alpha_p),\ \text{and}\ C_{D_P} = C_{D_P}(\alpha_p), \tag{4}$$

lifting line theory assumes that

$$C_{L_i}(t) = C_{L_i}\left[\alpha_{EFF_i}(t)\right]$$

$$C_{M_i}(t) = C_{M_i}\left[\alpha_{EFF_i}(t)\right] \qquad (5)$$

$$C_{D_{P_i}}(t) = C_{D_{P_i}}\left[\alpha_{EFF_i}(t)\right]$$

Equations (5) indicate also that the unsteady effects to be included in the theory enter only through the time dependence of α_{EFF_i}, viz. through changes with time in α_{p_i} and/or α_{D_i}. As noted in the Introduction, the basic section characteristics as defined functionally by Equations (4) are assumed independent of time. This requires that various linear and nonlinear two-dimensional unsteady flow effects, such as dynamic stall (e.g. Reference 17), be of an appreciably shorter time scale than the wake and geometric effects included herein. This assumption is equivalent to assuming that the chordwise pressure distribution, which affects the nature of flow separation on the airfoil, rapidly approach the steady state distribution for the current angle of attack. Combining unsteady two-dimensional effects with the nonlinear lifting line theory was assumed beyond the scope of the present effort.

The control point for evaluating α_{EFF_i} is taken at an axial distance x_{cp_i} from the leading edge. In the usual Prandtl lifting line formulation $x_{cp_i} = c_i/4$. Hence, there would be no induced velocity contribution from the wing bound vortex segments. In order to generalize the formulation for arbitrary x_{cp_i}, the downwash angle α_{D_i} has been defined as the difference between the total three-dimensional downwash angle α_{3D_i} at the control point and an equivalent two-dimensional downwash angle α_{2D_i} from an infinite span bound vortex along the c/4 line and equal in strength to $\Gamma_{i,1}(t)$. Thus

$$\alpha_{D_i} = \alpha_{3D_i} - \alpha_{2D_i} \qquad (6)$$

In terms of downwash velocity components Δw induced by the parallelogram lattice elements of unit circulation strength

$$\alpha_{3D_i} = \frac{w_i}{V_\infty} = \frac{1}{V_\infty} \sum_{j=1,k=1}^{j=N,k=M} \Delta w_{i_{j,k}} \cdot \Gamma_{j,k}(t) \qquad (7)$$

where for each j,k lattice element and at each control point i

$$\Delta w = \Delta w_{T_L} + \Delta w_{T_R} + \Delta w_{B_F} + \Delta w_{B_A} + \Delta w_{I_{T_L}} + \Delta w_{I_{T_R}} + \Delta w_{I_{B_F}} + \Delta w_{I_{B_A}} \qquad (8)$$

The subscripts in Equation (8) are T trailing element, B bound or shed element, I image, L left, R right, F forward and A aft. Mathematical expressions for each of the elements in Equation (8), based on the law of Biot and Savart, are given in Reference 12.

The equivalent two-dimensional downwash angle is

$$\alpha_{2D_i} = \left(\frac{1}{V_\infty}\right) \Delta w_{2D_i} \Gamma_{i,1}(t) = \frac{1}{V_\infty} \quad \frac{\Gamma_{i,1}(t)}{2\pi (x_{cp} - x_{c/4})_i \cos(\Lambda_i - \beta)} \tag{9}$$

where Λ_i is the quarter chord sweep angle (assumed negative for the left wing panel, $1 \le i \le N/2$, and positive for the right wing panel, $N/2 + 1 \le i \le N$), and β is the side slip angle. The usual sign convention taking the downwash as positive has been employed in the above expressions.

The pitch angle of attack is composed of the elements

$$\alpha_{P_i}(t) = \alpha(t) + \alpha_{T_i} + \Delta\alpha_{R_i}(t) + \Delta\alpha_{B_i}(t) \tag{10}$$

where $\alpha(t)$ is the angle of attack of the root section, α_{T_i} is the built in geometric twist, $\Delta\alpha_{R_i}(t)$ is the effective roll asymmetry angle of attack due to deflection of ailerons, and $\Delta\alpha_{B_i}(t)$ is the additional angle of attack due to the body upwash.

$$\Delta\alpha_{B_i}(t) = [\alpha(t) - i_w] \frac{R_B^2}{y_i^2} \cos 2\delta_i \cos \delta_i \tag{11}$$

where

$$\cos \delta_i = \frac{|y_i|}{\{[z_B - (|y_i| - y_B)\tan\gamma]^2 + y_i^2\}^{1/2}}$$

Here i_w is the wing root incidence angle, and the remaining quantities are defined in Figure 4.

The unknowns are the current time values of the circulation on the wing $\Gamma_{i,1}(t)$, and may be found by solving Equation (3) and the first of Equations (5). Thus, inserting Equations (6), (7), (9) and (10) into Equation (3) gives

$$\alpha_{EFF_i}(t) = \alpha_{P_i}(t) - \alpha_{3D_i}(t) + \alpha_{2D_i}(t)$$

$$= \alpha(t) + \alpha_{T_i} + \Delta\alpha_{R_i}(t) + \Delta\alpha_{B_i}(t)$$

$$- \frac{1}{V_\infty} \sum_{j=1, k=1}^{j=N, k=M} \Delta w_{i_{j,k}} \Gamma_{j,k}(t)$$

$$+ \frac{1}{V_\infty} \Delta w_{2D_i} \Gamma_{i,1}(t) \qquad (12)$$

Expressing $C_{L_i}(t)$ in Equation (5) in terms of the bound circulation gives

$$\frac{2\Gamma_{i,1}(t)}{V_\infty c_i} = C_{L_i}[\alpha_{EFF_i}(t)] \qquad (13)$$

Equation (13) implies that the Kutta- Joukowski law $L_i(t) = \rho V_\infty \Gamma_i(t)$ holds in the unsteady as well as in the steady state case. This assumption is discussed further in Section 2.5.

Equations (12) and (13) constitute the set of lifting line equations to be solved for $\alpha_{EFF_i}(t)$ and $\Gamma_{i,1}(t)$. The $\Gamma_{j,k}(t)$, $k > 1$, are known from solutions at previous times through Equation (1). Before describing the general method of solution several simplified solutions of these equations, which do not require any computer calculations, are discussed below.

2.3 SIMPLIFICATIONS FOR A LINEAR LIFT CURVE

In general, Equations (12) and (13) must be solved by an iterative method, because of the nonlinear nature of the lift curve as expressed in Equation (13). It is precisely these nonlinearities which lead to the occurance of multiple span loadings, lift hysteresis, and zero beta rolling and yawing moments. However, it is beneficial to examine several simplifications which occur when the lift curve is linear, in order to compare the theory with existing methods and to better understand the nature of the complications due to the nonlinear effects.

2.3.1 LINEAR LIFT CURVE - In the case of a linear lift curve Equation (13) becomes

$$\frac{2\Gamma_{i,1}(t)}{V_\infty c_i} = a_i \alpha_{EFF_i}(t) \tag{14}$$

where a_i is the section lift curve slope. Combining Equation (14) with Equation (13) then gives a single set of linear equations which may be solved directly for $\Gamma_{i,1}(t)$.

The result is

$$\left[\frac{\Delta w_{i,j,1}}{V_\infty} + \delta_{ij}\left(\frac{2}{V_\infty a_i c_i} - \frac{\Delta w_{2D_i}}{V_\infty}\right)\right]\Gamma_{j,1}(t) = \alpha_{p_i}(t) - \frac{\Delta w_{i,j,k}}{V_\infty}\Gamma_{j,k}(t) \qquad 2 \le k \le M \tag{15}$$

where the repeated indices indicate a summation, and δ_{ij} is the Kronecker delta symbol.

Equation (15) represents a linear set of algebraic equations which may be solved directly for each step in time. If the problem is initiated from a steady state condition, then M = 1 for t = 0 and the double summation term vanishes. In matrix notation Equation (15) now becomes

$$[\Delta W]\{\Gamma_1(0)\} = \{\alpha_p(0)\} \tag{16}$$

where elements of the $[\Delta W]$ square matrix are given by the term in square brackets in Equation (15), whereas $\{\Gamma_1(0)\}$ and $\{\alpha_{p_i}(0)\}$ are column matrices made up of the elements $\Gamma_{j,1}(0)$ and $\alpha_{p_i}(0)$ respectively. Inverting Equation (16) gives

$$\{\Gamma_1(0)\} = [\Delta W]^{-1}\{\alpha_p(0)\} \tag{17}$$

At subsequent time steps terms in the double summation plays a role in the solution. Thus, according to Equation (1), with $t = \Delta t$, $k = 2$ now corresponds to the solution $\Gamma_{j,1}(0)$. Hence, we require $M \ge 2$ in order to account for unsteady wake effects.

2.3.2 EQUIVALENCE WITH WEISSINGER THEORY

2.3.2.1 Steady State - The present lifting line formulation becomes identical to the Weissinger L-method[11] for a linear lift curve in the steady state case provided the control point x_{cp} is placed at distance equal to 50% of chord from the lifting line

(75% chord for zero sweep angle). This may be shown by considering a single horseshoe vortex element (k = 1 only), with a bound segment and two trailing segments. By Equation (6)

$$\alpha_{D_i} = \alpha_{3D_i} - \alpha_{2D_i}$$

and from Equation (9) with $(x_{cp} - x_{c/4})_i \cos(\Lambda_i - \beta) = (1/2)\, c_i$

$$\alpha_{2D_i} = \frac{\Gamma_{i,1}}{\pi V_\infty c_i}$$

According to Equation (3)

$$\alpha_{EFF_i} = \alpha_{p_i} - \alpha_{3D_i} + \frac{\Gamma_{i,1}}{\pi V_\infty c_i} \tag{18}$$

For thin airfoil aerodynamics, $a_i = 2\pi$; therefore by the steady state form of Equation (14)

$$\frac{\Gamma_{i,1}}{\pi V_\infty c_i} = \alpha_{EFF_i}$$

and substitution in Equation (18) yields

$$\alpha_{3D_i} = \alpha_{p_i} \tag{19}$$

which is the flow tangency boundary condition at the 75% chord control point used in the Weissinger approach. The nonlinear lifting line formulation, with the control point location such that

$$(x_{cp} - x_{c/4}) \cos(\Lambda - \beta) = c/2 \tag{20}$$

may therefore be taken equivalent to a nonlinear Weissinger formulation.

2.3.2.2 Unsteady Theory (Two-Dimensional). It should be noted that the theory also reduces to an unsteady form of the Weissinger theory, both for two-dimensional and three-dimensional flows. Thus, for a two-dimensional unsteady flow Equations (6) and (7) become

$$\alpha_{EFF}(t) = \frac{1}{V_\infty} \Delta w_k \Gamma_k(t) - \frac{\Gamma_1(t)}{2\pi V_\infty (x_{cp} - x_{c/4})}$$

where Δw_k is the downwash at x_{cp} due only to forward and aft spanwise segments of the k'th element. Thus, from Equation (8)

$$\Delta w_k = \Delta w_{B_{F_k}} + \Delta w_{B_{A_k}} \tag{21}$$

$$\alpha_{EFF}(t) = \alpha_p(t) - \frac{1}{V_\infty} \Delta w_k \Gamma_k(t) + \frac{\Gamma_j(t)}{2\pi V_\infty (x_{cp} - x_{c/4})}$$

Using the linearized form of the unsteady Kutta-Joukowski law, Equation (14), assuming the lift curve slope $a = 2\pi$, and taking $x_{cp} - x_{c/4} = c/2$ then gives

$$\frac{1}{V_\infty} \Delta w_k \Gamma_k(t) = \alpha_p(t) \qquad k = 1, 2, \ldots \tag{22}$$

Equation 22 states that the instantaneous downwash angle at the 75% chord position from all bound and shed spanwise vortex segments is equal to the instantaneous angle of attack.

Equation (22) may be expressed in terms of the differential vortex strengths. Referring to Figure 5

$$\Delta\Gamma_k(t) = \Gamma_k(t) - \Gamma_{k-1}(t)$$

Thus, from Equation (21)

$$\Delta w_k \Gamma_k(t) = (\Delta w_{B_{F_k}} + \Delta w_{B_{A_k}}) \Gamma_k(t)$$

and since $\Delta w_{B_{A_k}} = -\Delta w_{B_{F_{k+1}}}$

substitution in Equation (22) yields

$$\frac{1}{V_\infty} \Delta w_{B_{F_k}} \Delta\Gamma_k(t) = \alpha_p(t) \tag{23}$$

where as seen from Figure 5,

$$\Delta\Gamma_1(t) = \Gamma_1(t) - \Gamma_0(t) = \Gamma_1(t)$$

is the instantaneous bound vortex strength on the airfoil at the 25% chord position. As also noted in Figure 5, the force free convection of the wake requires

$$\Delta\Gamma_k(t + \Delta t) = \Delta\Gamma_{k-1}(t) \tag{24}$$

whereas the condition that the total vorticity (bound and shed) remain zero for all time requires

$$\Delta\Gamma_2(t + \Delta t) = -[\Gamma_1(t + \Delta t) - \Gamma_1(t)] \tag{25}$$

Equation (25) requires that the first time step be taken with k = 2, for which the first shed vortex is at a distance $\epsilon = (n - 3/4)\,c$ from the trailing edge, as shown in Figure 5. Here n is the number of chord lengths per time step.

Equations (22) and (23) both show that the unsteady theory reduces to satisfying a flow tangency condition in the two-dimensional case when the control station is taken at the 75% chord position.

The equivalence of the present unsteady wake lifting line formulation with the classical solution of Wagner (Reference 18) for a two dimension airfoil in unsteady flow is readily shown through use of Equations (23) - (25). Thus, Figure 6 compares the calculated value of the change in lift coefficient $\Delta C_L(t)$ due to a step change in angle of attack $\Delta\alpha_p$, as calculated from Equation (23) - (25), with the Wagner function. Lift coefficient was calculated from the bound circulation strength $\Gamma_1(t)$ through the unsteady Kutta-Joukowski law, Equation (13).

The step size used in the compution for the shedding of discrete vortices was one chord length. The close correspondence between the discrete vortex formulation and the continuous vortex sheet theory of Wagner shows that very little accuracy is lost in the discrete vortex model. It is also clear that unsteady wake effects, due to the variation of shed as well as of trailing vorticity are accounted for in the formulation. Effects of wake vorticity on chordwise load distribution are not included as was mentioned previously. Incorporation of these effects would require addition bound vortex elements and control point locations on the wing.

2.3.2.3 Unsteady Theory (Three-Dimensional)

The unsteady finite element representation may also be readily shown to lead to a flow tangency condition at the 75% chord position in the three dimensional case. The

The demonstration is similar to that in Section 2.3.2.1 for the steady state case, except that the unsteady form of the Kutta-Joukowski law is used as given by Equation (13) and the summation is carried out over k = 1, 2, ... M rows of vortex elements in the wake. The result is,

$$\alpha_{3D_i}(t) = \frac{1}{V_\infty} \Delta w_{i_{j,k}} \Gamma_{j,k}(t) = \alpha_{p_i}(t) \qquad (26)$$

provided the control point is located according to Equation (20) and provided the steady state thin airfoil theory lift curve slope value is used.

2.4 SIMPLIFIED SOLUTIONS FOR A NONLINEAR LIFT CURVE

Several calculations have been performed with N = 2 (one vortex per wing panel) and a tri-linear 2D lift curve. The two-vortex representation is the simplest possible model for obtaining asymmetrical load distributions at zero yaw angle and should be illustrative of the type of results obtainable with a larger number of horseshoe vortex elements. Only simplified steady state solutions are discussed below, since the corresponding simplified unsteady solutions did not include effects of the shed vortex segments. Unsteady nonlinear solutions will be presented in connection with the iterative procedure described for solving Equations (12) and (13) in Section 3.

As illustrated geometrically in Figure 7, several different steady state load distributions, both symmetrical and asymmetrical, may be possible for a wing with a tri-linear lift curve at geometric angle of attack α_p when $\alpha_p > \alpha_2 > \alpha_1$. Thus, solutions 1 through 6 represent the following loadings (see also Figure 1b):

1. Symmetrical, both panels unstalled with positive lift curve slope a.

2. Symmetrical, both panels stalled with negative lift curve slope - b.

3. Symmetrical, both panels stalled with zero lift curve slope

4. Asymmetrical, one panel unstalled and other panel stalled with lift curve slope -b.

5. Asymmetrical, one panel unstalled and other panel stalled with lift curve slope 0.

6. Asymmetrical, both panels stalled, one with lift curve slope -b and the other with lift curve slope 0.

The determination or which load distribution will occur depends on the airfoil 2-D lift characteristics (b/a, α_1 and α_2), on the geometric angle of attack, and on wing aspect ratio.

Symmetrical (unstalled with lift curve slope a)

For loading 1, the lifting line equations, [Equations (12) and (13)], simplify, respectively, to

$$C_{L_1} = a(\alpha_p - \gamma_{11} C_{L_1} - \gamma_{12} C_{L_2}) \tag{27}$$

provided the effective angle of attack α_{EFF}, which is

$$\alpha_{EFF} = \alpha_p - \gamma_{11} C_{L_1} - \gamma_{12} C_{L_2} \tag{28}$$

is less than α_1. Here γ_{11} is the downwash angle induced at control point 1 (assumed at the center of bound element 1) due to horseshoe vortex 1 of strength such that $C_{L_1} = 1$. Similarly, γ_{12} is the downwash angle induced at control point 1 due to horseshoe vortex 2 of strength such that $C_{L_2} = 1$. The influence coefficients γ_{ij} are related to the downwash terms $\Delta w_{ij}/V_\infty$ used in previous sections through the expression $\gamma_{ij} = (V_\infty c_i/2)\, \Delta w_{ij}/V_\infty$. Here also, the control point position has been taken on the bound vortex, so that Δw_{2D} in Equation (12) cancels the contribution from the bound vortex.

For symmetrical loadings, $C_{L_1} = C_{L_2}$. From the Biot-Savart law the coefficients γ_{11} and γ_{12} are readily shown to be

$$\gamma_{11} = \frac{c_1/\bar{c}}{\pi AR}$$

$$\gamma_{12} = \frac{-c_2/\bar{c}}{3\pi AR}$$

where c_1 and c_2 are the respective chords and $\bar{c}$ is the average chord. For a wing of symmetrical planform with only two horseshoe vortices $c_1/\bar{c} = c_2/\bar{c} = 1$. Solving Equation (27) for $C_{L_1}/a\alpha_1$ gives

$$\frac{C_{L_1}}{a\alpha_1} = \frac{\alpha_p/\alpha_1}{1 + a\gamma_{11}(1 + \gamma_{12}/\gamma_{11})} \tag{29}$$

for the unstalled 3-D lift curve. Equation (29) may be compared with the analogous lifting line result with a constant downwash angle for $a = 2\pi$. The latter is

$$C_L/2\pi = \frac{\alpha_p}{1 + 2/AR}, \text{ whereas Equation (29) gives}$$

$$C_L/2\pi = \frac{\alpha_p}{1 + \frac{4}{3\,AR}}$$

Symmetrical (stalled with lift curve slope -b)

For loading 2, the effective angle of attack defined by Equation (28) must lie between α_1 and α_2. The lifting line equation is now

$$C_{L_1} = a\alpha_1 - b\,(\alpha_p - \gamma_{11}\,C_{L_1} - \gamma_{12}\,C_{L_2} - \alpha_1)$$

Solving for $C_{L_1}/a\,\alpha_1$ gives, assuming symmetry,

$$\frac{C_{L_1}}{a\alpha_i} = \frac{1 + \frac{b}{a}\,(1 - \alpha_p/\alpha_1)}{1 - (b/a)\,a\gamma_{11}\,(1 + \gamma_{12}/\gamma_{11})} \tag{30}$$

Symmetrical (stalled with lift curve slope 0)

For loading 3, the three dimensional lift coefficient is simply given by

$$C_L/a\alpha_1 = 1 - \Delta C_L/a\alpha_1 \tag{31}$$

where ΔC_L is the drop in lift coefficient between α_1 and α_2. For loading 3 we require that α_{EFF} as given by Equation (28) exceed α_2.

Asymmetrical (panel #1 unstalled, panel #2 stalled with $dC_L/d\alpha = -b$)

For loading 4, the lifting line equations give

$$C_{L_1} = a\,(\alpha_p - \gamma_{11}\,C_{L_1} - \gamma_{12}\,C_{L_2}) \tag{32}$$

$$C_{L_2} = a\alpha_1 - b\,(\alpha_p - \gamma_{21}\,C_{L_1} - \gamma_{22}\,C_{L_2} - \alpha_1) \tag{32}$$

where

$$\alpha_{EFF_1} = \alpha_p - \gamma_{11} C_{L_1} - \gamma_{12} C_{L_2} \tag{33}$$

$$\alpha_{EFF_2} = \alpha_p - \gamma_{21} C_{L_1} - \gamma_{22} C_{L_2}$$

We require that α_{EFF_1} be less than α_1 and that α_{EFF_2} lie between α_1 and α_2. Solving Equations (32) and (33) with

$\gamma_{12} = \gamma_{21}$ and $\gamma_{11} = \gamma_{22}$ due to the symmetrical wing planform yields

$$C_{L_1}/a\alpha_1 = N_1/D, \tag{34}$$

$$C_{L_2}/a\alpha_1 = N_2/D \tag{35}$$

and $$C_{L_2}/C_{L_1} = N_2/N_1 \tag{36}$$

where

$$N_1 = \left(\frac{\alpha_p}{\alpha_1}\right)\left[1 - \frac{b}{a}\,(a\gamma_{11} - a\gamma_{12})\right] - (1 + \frac{b}{a})\, a\gamma_{12}$$

$$N_2 = \left(\frac{\alpha_p}{\alpha_1}\right)\left[1 - \frac{b}{a}\,(a\gamma_{11} - a\gamma_{12}) - (1 + \frac{b}{a})\right] + (1 + \frac{b}{a})\,(1 + a\gamma_{11})$$

and $$D = (1 + a\gamma_{11})\,(1 - \frac{b}{a}\, a\gamma_{11}) + \frac{b}{a}\,(a\gamma_{12})^2$$

Equation (36) has been plotted in Figure 8 for AR = 4. Also indicated in Figure 8 is the maximum angle of attack limit above which α_{EFF_1} exceeds α_1. As seen from Figure 8, Equation (36) predicts an asymmetrical rolling moment at angles of attack below that for 3-D $C_{L_{max}}$ when $b/a \geq 1.5$. Hence, some deterioration in aircraft departure characteristics might be expected under these conditions.

Asymmetrical (panel #1 unstalled, panel #2 stalled with $dC_L/d\alpha_p = 0$)

For loading #5, the lifting line equations reduce to

$$C_{L_1} = a\,(\alpha_p - \gamma_{11}\,C_{L_1} - \gamma_{12}\,C_{L_2})$$

$$C_{L_2} = a\alpha_1 - \Delta C_L. \tag{37}$$

We also require that α_{EFF_1} be less than α_1 and that α_{EFF_2} be greater than α_2, where α_{EFF_1} and α_{EFF_2} are defined according to Equations (33). Solving Equations (37) gives

$$\frac{C_{L_1}}{a\alpha_1} = \frac{(\alpha_p/\alpha_1) - (\gamma_{12}/\gamma_{11})\,a\,\gamma_{11}\,(1 - \frac{\Delta C_L}{a\alpha_1})}{1 + a\,\gamma_{11}} \tag{38}$$

$$\frac{C_{L_2}}{a\alpha_1} = 1 - \frac{\Delta C_L}{a\alpha_1} \tag{39}$$

$$C_{L_2}/C_{L_1} = \left[\frac{(\alpha_p/\alpha_1)\,(1 - \frac{\Delta C_L}{a\alpha_1})^{-1} - (\gamma_{12}/\gamma_{11})\,a\,\gamma_{11}}{1 + a\,\gamma_{11}}\right]^{-1} \tag{40}$$

Equation (40) has been plotted in Figure 9 for values of $\Delta C_L/a\alpha_1$ between 0 and 1 and AR = 4. Also shown in Figure 9 is the maximum angle of attack at which $\alpha_{EFF_1} \leq \alpha_1$ (unstalled panel limit) and the minimum angle of attack at which $\alpha_{EFF_2} \geq \alpha_2$ (stalled panel limit). The latter limit is dependent upon b/a. Figure 9 shows that with $b/a \geq 1.5$, asymmetric loadings of type 5 may exist over an α_p zone which increases in width with increasing b/a and $\Delta C_L/a\alpha_1$.

Asymmetrical (panel #1 stalled with $dC_L/d\alpha = -b$, panel #2 stalled with $dC_L/d\alpha = 0$)

In this case the lifting line equations give

$$C_{L_1} = a\alpha_1 - b\,(\alpha_p - \gamma_{12}\,C_{L_2} - \gamma_{11}\,C_{L_1} - \alpha_1) \tag{41}$$

$$C_{L_2} = a\alpha_1 - \Delta C_L$$

with the requirement that α_{EFF_1} lie between α_1 and α_2, and that α_{EFF_2} be greater than α_2. Equations (41) were solved for C_{L_2}/C_{L_1} giving

$$\frac{C_{L_2}}{C_{L_1}} = \left\{ \frac{1 + \frac{b}{a}\left[1 - \frac{\alpha_p}{\alpha_1} + \left(\frac{\gamma_{12}}{\gamma_{11}}\right) a\gamma_{11}\left(1 - \frac{\Delta C_L}{a\alpha_1}\right)\right]}{\left(1 - \frac{\Delta C_L}{a\alpha_1}\right)\left[1 - \left(\frac{b}{a}\right) a\gamma_{11}\right]} \right\}^{-1} \tag{42}$$

In summary, we have demonstrated the possibility of six different steady state loadings near stall for wings with a tri-linear section lift curve. Taking a wing with $AR = 4$, $b/a = 4$ and $\Delta C_L/a\alpha_1 = 0.6$, it is readily shown that all six loadings will satisfy the lifting line equations at an angle of attack $\alpha_p = 1.3\,\alpha_1$, which is just below the value $\alpha_p = 4/3\,\alpha_1$ for the maximum 3-D lift coefficient. The values of C_{L_1} and C_{L_2} for these six loadings are listed in the table on Figure 10. The corresponding values of α_{EFF_1} and α_{EFF_2} are shown in the plot.

The question naturally arises; which of the six possible loadings will occur physically? This question was posed by Sears[1] who stated "The choice between the various solutions must involve the question of the relative stabilities of the flows." The question will be readdressed in connection with the iterative method of solving the time dependent nonlinear lifting line equations.

2.5 GENERALIZED FORM OF THE KUTTA-JOUKOWSKI LAW FOR UNSTEADY FLOW

A generalized form of the two-dimensional Kutta-Joukowski law, viz.

$$L(t)_i = \rho V_\infty \Gamma_1(t)_i \tag{43}$$

has been used throughout the formulation in Sections 2.2 and 2.3 and is the basis for Equation (13). In the present section we derive Equation (43) from the condition that the negative rate of change of total momentum associated with the spanwise vortex segments gives the magnitude of the lift. The total momentum perpendicular to x for a two-dimensional vortex system composed of discrete elements $\Delta\Gamma_k(t)$ spaced along the x axis at distances x_k from the leading edge, as shown in Figure 5b, is

$$\rho\Delta\Gamma_k(t)\, x_k$$

where the double index implies a summation. Hence, the unsteady two-dimensional lift becomes

$$L(t) = -\rho \frac{d}{dt} [\Delta\Gamma_k(t)\, x_k] \tag{44}$$

where the subscript i has been dropped for simplicity of notation [see also Eq. (1) of Reference (1)].

The conditions that the shed vortex elements, $k \geq 2$, are convected downstream at velocity V_∞, and that the total vorticity $\sum_{k=1}^{M-1} \Delta\Gamma_k(t)$ remain zero for all time are given by Equations (24) and (25), respectively. The instantaneous bound vortex strength is $\Delta\Gamma_1(t) = \Gamma_1(t)$.

Referring to Figure 5b, taking time steps with n = 1 (one chord length between elements), placing the bound vortex at the 25% chord position, the momentum at time $t = c/V_\infty$ is

$$\rho\, \Delta\Gamma_k(c/V_\infty)\, x_k = \Delta\Gamma_1(c/V_\infty)\, c/4 + \Delta\Gamma_2(c/4)\, 5c/4$$

$$= -\Gamma_1(c/V_\infty)\, c$$

where we have made use of Equation (25).

Similarly, for $t = 2c/V_\infty$

$$\rho\, \Delta\Gamma_k(2c/V_\infty)\, x_k = \Delta\Gamma_1(2c/V_\infty)c/4 + \Delta\Gamma_2(2c/V_\infty)\, 5c/4 + \Delta\Gamma_3(2c/V_\infty)\, 9c/4$$

$$= -\Gamma_1(2c/V_\infty)\, c - \Gamma_1(c/V_\infty)\, c$$

where we have made use of Equations (24) and (25).

For $t = (M-1)\, c/V_\infty$, the result generalizes to

$$\rho\, \Delta\Gamma_k[(M-1)\, c/V_\infty]\, x_k = -c \sum_{k=1}^{M-1} \Gamma_1(kc/V_\infty) \tag{45}$$

Taking $t = (M-2)c/V_\infty$ and subtracting the result from Equation (45) gives

$$\rho \left\{ \Delta\Gamma_k[M-1)c/V_\infty]\, x_k - \Delta\Gamma_k[(M-2)c/V_\infty]\, x_k \right\} = -c\Gamma_1[(M-1)c/V_\infty]$$

Dividing by $\Delta t = c/V_\infty$, we obtain

$$\frac{\rho \Delta \left\{ \Delta \Gamma_k \left[(M-1)\, c/V_\infty \right] x_k \right\}}{\Delta t} = -V_\infty \Gamma_1 \left[(M-1) c/V_\infty \right]$$

and Equation (44) in difference form becomes

$$L \left[(M-1) c/V_\infty \right] = \rho V_\infty \Gamma_1 \left[(M-1) c/V_\infty \right] \tag{46}$$

which is identical to Equation (43). The same result may be obtained for arbitrary step sizes n, and in the limit $n \to 0$ the generalized Kutta-Joukowski law is found.

METHOD OF SOLUTION AND ITERATION PROCEDURE

The set of nonlinear lifting line expressions as given by Equations (12) and (13) constitute a system of 2N algebraic equations in the 2N unknowns $\Gamma_i(t)$ and $\alpha_{EFF_i}(t)$, $i = 1, 2, \ldots, N$, which must be solved for each step in time. The equations are nonlinear; because the functional relation between $\Gamma_i(t)$ and $\alpha_{EFF_i}(t)$, expressing the two-dimensional lift curve at station i, is generally nonlinear in the stall region and beyond. Hence an iteration procedure is required for their solution.

The nonlinear lifting line equations and corresponding wing and fuselage geometric relations were programmed for solution on the CDC Cyber 70 computer. Details of the computer program and of the method of solution have been presented in Reference 12, as was noted previously. However, the method of solution will also be reviewed below, because of the limited distribution of Reference 12 and because several of the assumptions in the iteration procedure may require further discussion.

3.1 ITERATION PROCEDURE

The iteration procedure assumes the aircraft wing and fuselage geometry, sideslip angle, etc., are given, and that the schedule of pitch angle $\alpha_p(t)$ and lateral control deflection $\Delta\alpha_R(t)$ have been specified. Two iteration loops will be described, one for $t = 0$ and the second for $t > 0$.

3.1.1 INITIAL SOLUTION. The method is started by determining the steady state solution for $t = 0$. The root solving procedure consists of a simple iteration loop on the induced angle of attack $\alpha_{D_i}(0)$. A guess is first made for the spanwise variation of induced angle of attack $\alpha_{D_i}^{(1)}(0)$. This, together with the known $\alpha_{p_i}(0)$, establishes $\alpha_{EFF_i}^{(1)}(0)$ through Equation (3). The wing bound vortex strengths $\Gamma_{i,1}^{(1)}(0)$ are then found by table look-up from the input aerodynamic lift curves expressed by Equation (13). For $t = 0$ we may take $M = 1$, or equivalently take $\Gamma_{i,k}(0) = \Gamma_{i,1}(0)$, hence no wake vortices need be considered. The induced angles are then recalculated, based on the downwash velocity components $\Delta w_{i,k}$ and Δw_{2D_i}, and on the initial iterate for the vortex strengths $\Gamma_{i,1}^{(1)}(0)$, and compared with the assumed values of $\alpha_{D_i}^{(1)}(0)$. The differences may be designated $\Delta\alpha_{D_i}^{(1)}(0)$. The values to be used in the next iteration are

$$\alpha_{D_i}^{(2)}(0) = \alpha_{D_i}^{(1)}(0) + C\,\Delta\alpha_{D_i}^{(1)}(0) \tag{47}$$

where C is a weighting factor. The value of C affects the stability and convergence of the iteration procedure. Increasing C speeds up convergence (reduces the number

of required iterations), but may destablize the iteration procedure. In general, the maximum value for C depends on wing aspect ratio, the number N of spanwise elements, and on lift curve slope. Some further discussion of effects of C on stability are contained in Section 3.1.3.

With $\alpha_{D_i}^{(2)}(0)$ given by Equation (47) the procedure is repeated, viz.

$$\alpha_{D_i}^{(2)}(0) \rightarrow \alpha_{EFF_i}^{(2)}(0) \rightarrow \Gamma_{i,1}^{(2)}(0) \rightarrow \Delta\alpha_{D_i}^{(2)}(0), \text{ etc.}$$

until either convergence is obtained, or until a maximum number of iterations has occurred. Convergence is assumed when $\Delta\alpha_D^{(m)}(0) \leq 0.1$ degree for all i.

3.1.2 SOLUTION AT SUBSEQUENT TIME STEPS - The iteration procedure at succeeding time steps $t > 0$ is similar to that at $t = 0$ with the following exceptions:

(i) The vortex strengths $\Gamma_{i,k}(t)$ in the wake are no longer identical to those on the wing ($k = 1$), but are found by indexing from the previous time step according to Equation (1).

(ii) A special logic is used to specify the initial guess $\alpha_{D_i}^{(1)}(t)$.

The later requirement was found necessary, especially near stall, because of the possibility of multiple solutions, and because the iteration procedure apparently tends to disallow roots on the steep negative slope regions of the section lift curves. Therefore, the wing elements appear in the solutions as either unstalled or fully stalled (region where the post stall lift curve is near zero). A dominant form for the solution in the stall region appears to be a spanwise alternating pattern of unstalled and fully stalled elements. The significance of this saw-tooth type of solution was not entirely clear. For example, if a very large number of spanwise elements were modeled, then such a pattern over a given spanwise portion of the wing may well correctly represent partial stall or heavy buffeting in that region. However, since the present computer program is limited to 10 elements per wing panel ($N_{max} = 20$), this type of saw-tooth stall pattern does not appear to be physically realistic. It was found that the saw-tooth stall pattern could be avoided in most cases by choosing the initial guess for $\alpha_{D_i}(t)$ according to the following special logic.

a) When no wing sections are stalled at the prior time step (i.e. all converged values of $\alpha_{EFF_i}(t - \Delta t)$ are less than α_{max_i}, corresponding to the section angle of attack for maximum C_l), then the $\alpha_{D_i}^{(1)}(t)$ are taken equal to the converged values from the previous time step $\alpha_{D_i}(t - \Delta t)$. This will produce solutions with all spanwise elements unstalled, if such solutions exist.

b) When the iteration procedure at the end of the previous time step, or during the current iteration, gives a solution with one or more stalled sections on a wing panel (e.g. $\alpha_{EFF_i}(t - \Delta t)$ exceeds α_{max}), then the iteration procedure is started (or restarted) with the assumption that the induced angles are zero on that particular wing panel. This procedure tends to force solutions with as many stalled elements on that panel as the lifting line equations will allow.

The special logic represented by a) forces the spanwise wing elements to remain unstalled until such time that one or more elements must be stalled to satisfy the governing equations. Partially stalled solutions with either saw-tooth stall patterns or uniform stall patterns, are avoided during this time, even though they satisfy the lifting line equations. The special logic given by b) assumes that once any spanwise element has stalled, it tends to induce all adjacent elements of the same panel to stall within the limits of the lifting line equations. Shielding of stall progression from one side of the airplane to the other is assumed provided by the presence of the fuselage (at least for low and mid-wing configurations). Unstalled solutions, or solutions with saw-tooth stall patterns, are avoided during this time even though they are mathematically acceptable.

It should be noted that the above logic will tend to maximize the extent of any stall hysteresis loop which occurs for a wing undergoing a pitching motion through the stall. Thus, stall will be delayed to the maximum possible angle of attack while $\alpha_p(t)$ is increasing, and destall will be delayed to the minimum possible angle of attack while $\alpha_p(t)$ is decreasing.

Thus the sample computations presented in Section 4 may well tend to exaggerate the stall hysteresis loops (and the angle of attack range for the occurrance of zero beta rolling and yawing moments). The user is cautioned that the physical validity of these assumptions has yet to be established, since there are at present insufficient wind tunnel test data with dynamic type measurements. An alternative type of mathematical formulation, wherein the selection between the various multiple solutions is based on their physical stability, rather than on a special logic for the initial iterate, is clearly desirable.

3.1.3 STABILITY OF ITERATION PROCEDURE

The stability of the iteration procedure may be readily shown to be dependent upon the spanwise extent of the wing vortex elements, upon lift curve slope a and upon the weighting factor C. We consider for example the highly idealized case of a wing with a single vortex element and no unsteady wake effects (M = N = 1). Neglecting the subscripts i, j, k the first iterate at time t is

$$\alpha_D^{(1)}(t) = \frac{\Delta w}{V_\infty} \hat{\Gamma}(t - \Delta t)$$

where

$$\frac{\Delta w}{V_\infty} = \frac{V_\infty c}{2}\left[\frac{\Delta w_{3D}}{V_\infty} - \frac{\Delta w_{2D}}{V_\infty}\right], \text{ and } \hat{\Gamma}(t-\Delta t) = \frac{2\Gamma(t-\Delta t)}{V_\infty c}$$

is the normalized circulation (lift coefficient) from the previous time step. According to Sections 3.1.1 and 3.1.2, with the section unstalled, the initial iterate for $\hat{\Gamma}^{(1)}(t)$ is

$$\hat{\Gamma}^{(1)}(t) = a\left[\alpha_p(t) - \left(\frac{\Delta w}{V_\infty}\right)\hat{\Gamma}(t-\Delta t)\right] + C_{L_o} \tag{48}$$

where a is the unstalled lift curve slope, and C_{L_o} is the section lift coefficient at $\alpha = 0$. The value for $\Delta\alpha_D^{(1)}(t)$ which appears in Equation (47) is simply

$$\Delta\alpha_D^{(1)}(t) = \left(\frac{\Delta w}{V_\infty}\right)\hat{\Gamma}^{(1)}(t)$$

Introducing the weighing factor C into Equation (47) gives for the second iteration in downwash angle

$$\alpha_D^{(2)}(t) = (1-C)\,\hat{\Gamma}(t-\Delta t) + C\left(\frac{\Delta w}{V_\infty}\right)\hat{\Gamma}^{(1)}(t)$$

The second iteration for $\hat{\Gamma}^{(2)}(t)$ follows as

$$\hat{\Gamma}^{(2)}(t) = a\left[\alpha_p(t) - (1-C)\hat{\Gamma}(t-\Delta t) - C\left(\frac{\Delta w}{V_\infty}\right)\hat{\Gamma}^{(1)}(t)\right] + C_{L_o}$$

which may be written, upon making use of Equation (48), as

$$\hat{\Gamma}^{(2)}(t) = (1-C)\hat{\Gamma}^{(1)}(t) + C\left\{a\left[\alpha_p(t) - \left(\frac{\Delta w}{V_\infty}\right)\hat{\Gamma}^{(1)}(t)\right] + C_{L_o}\right\} \tag{49}$$

Similarly, for the third iteration

$$\hat{\Gamma}^{(3)}(t) = (1-C)\,\hat{\Gamma}^{(2)}(t) + C\left\{a\left[\alpha_p(t) - \left(\frac{\Delta w}{V_\infty}\right)\hat{\Gamma}^{(2)}(t)\right] + C_{L_o}\right\} \tag{50}$$

Subtracting Equations (49) and (50) gives

$$\frac{\hat{\Gamma}^{(3)}(t) - \hat{\Gamma}^{(2)}(t)}{\hat{\Gamma}^{(2)}(t) - \hat{\Gamma}^{(1)}(t)} = 1 - C - a\,C\left(\frac{\Delta w}{V_\infty}\right) \tag{51}$$

The iteration procedure should be stable when the absolute value of this ratio is below one, but convergence becomes very slow as the ratio approaches zero. Since $a > 0$, the ratio is generally negative, and convergence and stability require

$$0 < \underbrace{\frac{1}{1 + \left(\frac{a}{2\pi}\right) 2\pi \left(\frac{\Delta w}{V_\infty}\right)}}_{\text{Convergence Limit}} < C < \underbrace{\frac{2}{1 + \left(\frac{a}{2\pi}\right) 2\pi \left(\frac{\Delta w}{V_\infty}\right)}}_{\text{Stability Limit}} \leq 1 \tag{52}$$

The product of h/c and $2\pi\,(\Delta w/V_\infty)$ has been plotted in Figure 11 versus h/c for a horseshoe vortex of span h and with control point locations at either c/4 or 3 c/4. Examination of Figure 11 shows that the allowable value of C must increase as the number of spanwise elements N decreases, or as aspect ratio increases. The value of C should also increase with decreasing positive lift curve slope a, and C should be taken somewhat smaller when the control point is at 3c/4 instead of at c/4.

Equation (51) was derived in order to illustrate the functional dependence of C on paneling geometry and on lift curve slope, and is quantitatively correct only for the highly simplified formulation M = N = 1. Several trial values for C may be required in order to find the value which gives the best convergence properties for a particular nonlinear calculation. According to Reference 12, C should range from about 0.1 for values of $AR \simeq 5$ up to $C \simeq 0.3$ for $AR \simeq 12$. These values were based on $N \simeq 15$. A default value C = 0.1 is used in the computer program.

3.2 COMPUTATION OF FORCE AND MOMENT COEFFICIENTS

Once the converged vortex strength distribution has been determined at a particular time step, total force and moment coefficients for the wing body combination may be found by integrating the section force and moment coefficients over the N wing elements. The integration includes contributions from the bound image elements in the fuselage in order to account for fuselage lift, as noted previously. These fuselage terms are, however, omitted from the computation of drag, side force, and rolling moment coefficient, since the fuselage is believed to make only a negligibly small contribution to these coefficients.

The overall coefficients of lift C_L, drag C_D, side force Cy, pitching moment C_M, rolling moment C_ℓ, and yawing moment C_N are, in terms of the section coefficients (subscript i),

$$C_L = \sum_{i=1}^{N} \left(\frac{hc_i}{S}\right) C_{L_i} \cos \alpha_{D_i} \left[1 + \left(y_{I_{L_i}} - y_{I_{R_i}}\right) / h \right] \tag{53}$$

$$C_D = \sum_{i=1}^{N} \left(\frac{hc_i}{S}\right) \left(C_{D_i} \cos \alpha_{D_i} + C_{L_i} \sin \alpha_{D_i}\right) \tag{54}$$

$$C_y = -(\tan \gamma) \sum_{i=1}^{N} \left(\frac{hc_i}{S}\right) \left(\frac{y_i}{|y_i|}\right) \left[C_{L_i} \cos\left(\alpha_p - \alpha_{D_i}\right) + C_{D_i} \sin\left(\alpha_p - \alpha_{D_i}\right) \right] \tag{55}$$

$$C_M = \sum_{i=1}^{N} \frac{hc_i^2}{S\bar{c}} \left\{ C_{M_i} - \left[C_{L_i} \left(1 + \frac{y_{I_{L_i}} - y_{I_{R_i}}}{h}\right) \cos\left(\alpha_p - \alpha_{D_i}\right) + C_{D_i} \sin\left(\alpha_p - \alpha_{D_i}\right) \right] \left[\frac{x_{c/4_i} - \bar{x}_c}{c_i} \right] \right\} \tag{56}$$

$$C_\ell = -\sum_{i=1}^{N} \left(\frac{hc_i\, y_i}{Sb}\right) C_{L_i} \cos \alpha_{D_i} \tag{57}$$

$$C_N = \sum_{i=1}^{N} \left(\frac{hc_i\, y_i}{Sb}\right) \left(C_{D_i} \cos \alpha_{D_i} + C_{L_i} \sin \alpha_{D_i}\right) \tag{58}$$

The coefficient are referenced to wing area S, mean aerodynamic chord $\bar{c}$ and wing span b. The angle γ refers to wing dihedral. The effective downwash angle α_{D_i} is taken positive in the downward direction, and therefore is of opposite sense to the angle $\Delta\alpha_i$ in Reference 12. Several higher ordered terms, such as $C_{D_i} \sin \alpha_{D_i}$ have been neglected in the lift and rolling moment expressions. Furthermore, there is no geometric contribution of dihedral angle nor of sweep angle to effective angle of attack. Such effects are important at high angles of attack and sideslip, and corrections may be required to correlate with test data, especially with sideslip.

4

SAMPLE CALCULATIONS

An extensive series of computations were made with the nonlinear lifting line computer program described in Sections 2 and 3. The computations were made to compare with test data, with previous theories and to assess effects of wing planform geometry and section lift curve shape on stalling characteristics.

4.1 COMPARISON WITH AVAILABLE THEORY

Several computations were made in order to compare the current method with existing theories in order to evaluate the accuracy and generality of the procedure. A comparison of the accuracy of the finite element representation with the essentially exact potential theory results of Wagner (Reference 18) has been given previously in Figure 6 for the case of a two-dimensional airfoil with a linear lift curve subject to a step change in angle of attack. Because of the simplifications introduced by two-dimensional flow, results by the present method in Figure 6 were hand computed instead of being run on the digital computer. The similarity of the present finite element method with the exact results is apparent in Figure 6. Both methods give an initial lift increment equal to 1/2 of the steady state value.

The present method is compared with calculations by W. P. Jones (Reference 19) and Djojodihardjo and Widnall (Reference 20) in Figure 12, for the response to a step change in angle of attack for a rectangular wing of aspect ratio 6. The lift curve was again linear, and as can be seen from the figure good correlation with the more exact theories was found. Both the present and more exact methods show that the initial lift increment is greater than 1/2 of the steady state value when the aspect ratio is finite. The computations in Figure 12 were carried out on the digital computer with values M = 20 and N = 14.

Figure 13 depicts the variation in span load distribution with time from the current method for the same sample computation. Also shown in Figure 13 are the section lift coefficients at the 12 1/2% and 87 1/2 % semi span stations as obtained by the method of Reference 20. Once again, good correlation is shown with the more exact computations.

The present method was also used to determine the development of lift following a step change in angle of attack for rectangular wings of various aspect ratios, again with linear lift curves. The results are plotted in Figure 14 and compare well with similar variations obtained by Jones (Ref. 19) for wings of elliptic planform. Once again we note that the starting circulatory lift increment exceeds one-half the

steady state value for the finite aspect ratio cases, with the excess increasing for the lower aspect ratios. The computations in Figure 14 are with M = 20 and N = 14.

Normalized steady state lift increments are plotted versus aspect ratio in Figure 15, to examine the aspect ratio range over which the current formulation may be expected to hold. The current method appears to provide an accurate representation for lift down to aspect ratios below 2, for an unswept wing of rectangular planform, when compared with References 21 and 22 and with slender body theory. However, agreement to such low aspect ratios is much less likely for planforms of moderate to high sweep angle and for more sensitive coefficients such as induced drag, section C_L, etc..

4.2 COMPARISON WITH TEST DATA

The wing planform of the T-2C Navy trainer aircraft served as the basic geometry for the remaining computations (with various modifications and adjustments). Lift and rolling moment data from Reference 23 will be compared with the T-2C computations using a steady state wake (M=1), since the testing was done with the model held fixed at a given angle of attack (pitch and pause).

The basic T-2C configuration has a wing of aspect ratio AR = 5.07, taper ratio τ = 0.495, a quarter chord sweep angle Λ = 2.27 degrees, a wing root incidence angle i = 1.7 degrees with 2.5 degrees of washout at the tips, and a dihedral angle γ = 3°. The airfoil is a NACA 64_1A212 section with an a = 0.8 (mod) camber line (flaps and ailerons rigged 3 degrees up), and is constant across the span. The wing was mounted at mid-height to a fuselage whose shape was approximated in the computations by a circular cylinder of radius R_B=0.119 (b/2). The wing paneling used for the computations is shown in Figure 16 in the case of N = 14. The number of spanwise elements was varied for different computations. Nonlinear aerodynamic section data used for the T-2C computations (and for the parametric computations) are plotted in Figures 17 and 18, respectively. Curves labeled #1, #2 and #3 in Figure 17 are for a NACA 64_1A212 section at Reynolds number 3×10^6, 6×10^6 and $> 6 \times 10^6$. Curves labeled #11, #12 and #13 in Figure 17 were adjusted for the -3° trailing edge rigging of the T-2C model, and are to be used in comparing with the wind tunnel data. Curves labeled #4 and #5 in Figure 18 are for a NACA 64-209 section at Reynolds numbers 3×10^6 and 6×10^6, respectively, and were used in the parametric calculations together with curves #6-#8 to examine effects of the steepness of the negative lift curve slope -b in the post stall region. The airfoil section characteristics in Figures 17 and 18 were extrapolated from published NACA data (e.g. Reference 24).

A comparison between the calculated and measured lift values for the T-2C at zero and ten degrees yaw angle is shown in Figure 19. The tests were conducted tail on, and corrections were made for the estimated tail lift contribution as shown in Figure 19b. The test data are static measurements and average out any fluctuating values of C_L. The model was not pitched in a manner to produce lift hysteresis (by taking

transient measurements with α_p increasing and then decreasing with time), whereas the calculations were made with a pitch rate of 8 degrees/second (first increasing and then decreasing). Even though it is difficult to evaluate the accuracy of the unsteady method on the basis of the comparison with the static test data, the calculations appear to indicate a hysteresis loop which extends over a somewhat broader angle of attack band ($11° \leq \alpha_p \leq 18°$) than might be expected. This would be in accordance with the special computational logic employed in the method, which as discussed in Section 3.1.2 may well tend to lead to the maximum allowable hysteresis.

On the other hand, Reference 23 shows the sudden occurence of a rolling moment at zero yaw angle at angles of attack beyond 12 degrees. This may be taken as an indication of the stall (or partial stall) of one wing panel, and may correspond to the lower limit of any zone of lift hysteresis. The T-2C zero beta rolling moment data has been plotted in Figure 20. Also shown in Figure 20 are computations made with the current method, wherein a roll asymmetry is introduced for a very short period and then removed, in order to perturb the asymmetrical loadings. As seen from Figure 20, the resulting rolling moment coefficients (with the roll asymmetry removed) correlate well with the test data.

The present nonlinear lifting line method predicts the occurance of lift hysteresis and zero beta rolling and yawing moments for a symmetrical model with wing section characteristics similar to the T-2C aircraft. Its proper evaluation requires dynamic wind tunnel testing wherein the model may be pitched (up or down) at a given rate, and for which instantaneous (as well as time averaged) data are recorded. It is recommended that any such test be made with a wing whose two-dimensional section characteristics are known. In addition, a program of this type should include measurements of span load distribution, in order to afford a more explicit evaluation of the theory.

4.3 PARAMETRIC STUDIES

A series of parametric calculations have been made, using the current method, to determine effects of wing planform (aspect ratio, taper ratio, sweep back angle, and twist) and of airfoil section characteristics (steepness of negative lift slope beyond stall) on the occurence of lift hysteresis and zero-beta rolling moment. The purpose of the calculations was to obtain trends and guidelines which might lead to the design of safer aircraft which are less subject to adverse departure and spin entry characteristics during high performance maneuvers.

4.3.1 EFFECT OF NEGATIVE LIFT CURVE SLOPE AND ASPECT RATIO.

Effects of the abruptness of the negative lift curve slope beyond stall and of aspect ratio for zero yaw angle are shown in Figures 21-23. Each plot represents a pitch hysteresis computation through the stall with the angle of attack first increasing and then decreasing at a rate of 8 degrees/second. Points with increasing angle of attack are denoted by circles, whereas triangles are used for points with decreasing angle

of attack. Where no triangles appear, the points are coincident with the increasing α_p points. This notation has been used throughout the present section.

Figure 21 is for $\mathcal{AR}$ = 5.07, and shows that the zone over which lift hysteresis occurs gradually decreases as the steepness of the negative lift curve slope diminishes. The same trend is shown in Figure 22 ($\mathcal{AR}$ = 8) and Figure 23 ($\mathcal{AR}$ = 12). The figures also show that increasing aspect ratio reduces the zone of hysteresis for a given negative lift curve slope.

A similar set of pitch sweeps were made for a yaw angle $\beta = 10°$. Lift hysteresis characteristics similar to those in Figures 21-23 were obtained. The corresponding variations of rolling moment coefficient versus angle of attack have been plotted in Figures 24-26 for $\mathcal{AR}$ = 5.07, 8 and 12, respectively. The figures show a hysteresis loop for rolling moment coefficient, which behaves with respect to lift curve slope and aspect ratio in a manner very similar to lift coefficient.

4.3.2 EFFECTS OF TAPER RATIO, SWEEP ANGLE AND TWIST. Effects of taper ratio, sweepback angle and twist on lift hysteresis were obtained for the $\mathcal{AR}$ = 8 case with section lift curves #4, 6 and 7. Thus figures 27-29 show effects of varying τ from 0.2 to 1.0 on lift hysteresis. The calculations for the intermediate value τ = 0.495 are the same as those presented previously in Figure 22, and exhibit a slightly greater tendency for lift hysteresis for all negative lift curve slopes than do either of the other two τ cases. This may be true, because the τ = 0.495 taper ratio provides a more uniform spanwise distribution of section C_L, and hence causes the initial stall to be delayed to higher values of overall lift coefficient when the pitch rate is positive.

Lift hysteresis curves with a sweepback angle $\Lambda = 20°$ have been plotted in Figure 30 for section lift curves #4, 6 and 7. Figure 30 may be compared with Figure 22 (a-c) to evaluate effects of the increased sweep angle. Although these figures show only a minor sweep effect, it should be noted that the present lifting line approach may well apply only for low sweep angles, because of the assumption in the present analysis that the section stalling characteristics remain two-dimension. The introduction of even a moderate degree of wing sweep is known to modify the chordwise pressure distribution and to promote spanwise velocity components, thereby compromising the assumption of locally two-dimensional stall.

Effects of wing twist angle are shown in Figures 31-33. Each figure is for a different negative lift curve slope and presents results for the cases of -3° linear wash out ($0 \leq \alpha_T \leq -3°$), an untwisted wing (α_T=0), and a wing with positive linear twist ($0 \leq \alpha_T \leq +3°$). The calculations for the untwisted case are the same as presented previously in Figure 22(a-c). As is apparent from Figures 31-33, twist has only a minor influence on the extent of life hysteresis for lift curves #6 and #7. However, for lift curve #4, going from wash out ($\alpha_T = 0 \rightarrow -3°$) to wash in ($\alpha_T = 0 \rightarrow +3°$) is seen

to increase the extent of stall hysteresis. This may be due to the more uniform spanwise distribution of section C_L produced by wash in at the tip, as was the case with the effect of taper ratio.

It is recognized that the effects of twist, taper ratio, aspect ratio, and sweep back on stall hysteresis are interrelated. The particular combination of wing geometric parameters which provides the most uniform spanwise distribution of section C_L should also exhibit a greater degree of stall hysteresis. Because of the correspondance between the occurrence of stall hysteresis and zero beta rolling and yawing moments (see Section 4.3.3), it is expected that similar conclusions may be made with regard to the effects of wing planform parameters on the zero-beta moments.

4.3.3 ZERO BETA ROLLING (AND YAWING) MOMENTS. A set of computations was made to illustrate the occurence of zero-beta rolling and yawing moments during the pitch sequence. This is shown in Figures 34 and 35 for the T-2C planform, ($AR = 5.07$). In this case the pitching motion was initiated at $\alpha_p = 12°$ with the wing symmetrical. The pitching motion was halted at $\alpha_p = 14.4°$ and an asymmetry $\Delta\alpha_R = \pm 1°$ was applied to each wing plane and then subsequently removed, in order to simulate an aileron perturbation. The pitching motion was then resumed, either positive or negative, with the wing again symmetrical. Figure 34 shows the lift variation during this process for various lift curves. The corresponding rolling moment variations are shown in Figure 35. The theory predicts the occurence of zero-beta rolling and yawing moments (not plotted) over nearly the same α_p zone as that for which lift hysteresis occurs. Reducing the abruptness of the stall (steepness of the negative lift curve slope) is seen to ameliorate the effect.

A similar set of computations is shown in Figures 36 and 37 for an $AR = 8$ wing. Here the roll asymmetry was introduced and removed at $\alpha_p = 12.4°$, since the wing was already completely stalled at $\alpha_p = 14.4°$. The results show that increasing aspect ratio from 5.07 to 8.0 considerably reduces the zone of angle of attack over which zero-beta lateral moments occur, especially with the less abrupt section lift characteristics.

4.3.4 EFFECTS OF NUMBER OF ELEMENTS. All of the parametric calculations presented so far were made with 14 vortex elements across the span, in order to conserve computer time. It is recognized that requirements for improved computational accuracy could well dictate the use of an increased number N of spanwise elements (the existing computer program is limited to N = 20). Figure 38 shows the effect of varying N from 10 to 20 on lift hysteresis, for the section characteristics with the most abrupt stall (curve #4) and with the most gradual stall (curve #8). Although changing N appears to effect the instantaneous C_L value somewhat, especially for the case with the most gradual stall, the overall stalling characteristics appear virtually uneffected by N. It is recognized that further studies of the effect of N, covering a wider range well beyond N = 20, and for various values of aspect ratio

and taper ratio, are needed to determine an optimum value for the computations. In lieu of any comprehensive study of this type, the value N=14 used in the majority of the computations appears reasonable.

Most of the parametric computations have been made with only four rows of vortex elements in the wake (M=4), the last row being horseshoe in shape. Calculations were made with values of M as high as 40 (and as low as 1). The value M = 4 was set as a compromise for including the major contribution from the unsteady wake (up to distances of $3\bar{c}$ behind the airfoil), while reducing computer time to a minimum

4.4 HYSTERESIS CORRELATION

An attempt was made to correlate the results of the various computations of lift hysteresis with the abruptness of the wing stall and with planform geometry. One such correlation is shown in Figure 39, wherein the product $\Delta C_{L_H} \cdot \Delta\alpha_H$ has been plotted versus $57.3b/\pi AR$. Here ΔC_{L_H} is the maximum C_L difference in the hysteresis zone, and $\Delta\alpha_H$ is the width of the zone. The product $\Delta C_{L_H} \cdot \Delta\alpha_H$ is a measure of the area of the lift hysteresis loop. The value b is the maximum negative lift curve slope (per degree), and the ratio $57.3\ b/\pi AR$ represents the ratio of this slope to the slope $dC_L/d\alpha_D$ for a wing with constant downwash angle α_D across the span.

It is readily seen from Figure 1 that multiple solutions (symmetric case) will not occur unless $b/(dC_L/d\alpha_D) \geq 1$, corresponding to $57.3\ b/\pi\ AR \geq 1$ in the constant downwash angle case. For a wing with AR = 4 and a trilinear lift curve, as used in the examples of Section 2.4, multiple asymmetric solutions occur when $b/a = (57.3\ b)/(2\pi\ AR/4) \geq 1.5$, (or equivalently $57.3\ b/\pi\ AR \geq 0.75$), as seen from Figures 7-9. Thus, the parameter $57.3\ b/\pi AR$ appears reasonable for predicting the occurence of multiple asymmetric as well as of symmetric solutions.

The correlations in Figure 39 predict the occurrence of lift hysteresis wherever $57.3\ b/\pi AR > 0.18$, although the area of the hysteresis loop is seen to be dependent on other planform characteristics as well, such as sweep back angle, twist and taper ratio. Thus, the method predicts the occurrence of lift hysteresis for wings with negative lift curve slopes only approximately 1/5 as abrupt as thought necessary based on the idealized constant downwash angle criterion. This may be due to the ratio $dC_L/d\alpha_D$ being much less than $\pi AR/57.3$ over local regions of the wing with stalled or partially stalled flow. Additional analysis of the parametric computations and dynamic wind tunnel testing are required to further substantiate the correlation in Figure 39.

5

CONCLUSIONS AND RECOMMENDATIONS

A nonlinear lifting line theory, with an unsteady wake, has been developed and has been applied to the prediction of forces and moments on aircraft undergoing a pitching motion through the stall region. The procedure is an outgrowth of the steady state, nonlinear lifting line approaches in Reference 1-3, which predicted the occurrence of multiple solutions to the lifting line equations under certain conditions. The present theory predicts the occurrence of lift hysteresis and of rolling and yawing moments, even at zero yaw angle, for wings where section characteristics exhibit a negative lift curve slope of sufficient steepness subsequent to stall. It is anticipated that the theory (and parametric computations presented herein) may serve as a guide in predicting the susceptibility of various aircraft designs of moderate to high aspect ratio and low sweep angle to adverse stall and departure characteristics.

5.1 CONCLUSIONS

Conclusions relating to the numerical computations and to the assumptions in the theory are summarized below.

(i) The method has been programmed for solution on the CDC Cyber 70 computer. Computer solutions are simple to execute and reasonably economical, requiring about one-minute of micro-processor time for a complete pitch sweep and hysteresis loop.

(ii) Computations by the present method agree reasonably well with previous more exact, unsteady, linear, two-dimensional and three-dimensional theories down to aspect ratios of 3 and less for wings of zero sweep.

(iii) The present method compares well with steady state T-2C test data (aspect ratio 5.07), both for lift and rolling moment. No lift hysteresis effect appeared in the test data, but both test data and theory showed the occurrence of zero-beta rolling and yawing moments in the stall region.

(iv) The present theory predicts the occurence of lift hysteresis (and of zero beta rolling and yawing moments) when the parameter $57.3b/\pi AR > 0.18$ ($-b$ is the maximum negative lift curve slope of the two-dimensional airfoil sections comprising the wing). The angle of attack range over which these effects occur, and their severity is found to increase with increasing b and with decreasing aspect ratio. Other planform parameters, such as sweep-back angle, twist and taper ratio have also been shown to affect the extent of these adverse stalling characteristics to a lesser degree.

(v) The converged solutions obtained at angles of attack for which multiple roots exist are non unique and depend upon the starting solutions used in the integration procedure.

(vi) The iteration procedure used in the present method employed a special logic, which used either the converged solution from the previous time step as the initial iterate (unstalled) case, or set the initial iterate for downwash angle equal to zero over a wing panel (stalled case). This special logic was somewhat empirical, and led to the elimination of solutions with saw-tooth stalling patterns. However, the special logic delayed stall during pitch-up motions, and postponed destall during pitch-down motions, thereby maximizing the zone over which lift hysteresis (and zero beta rolling and yawing moments) occur.

(vii) The formulation does not include geometric effects of sweep angle and dihedral angle on the effective section angle of attack. These effects should be included to produce satisfactory correlation with test data, particularly for the sideslip case.

5 2 RECOMMENDATIONS

Recommendations for improving the present method, by removing several of the restrictive assumptions noted above, by conducting additional comparisons with test data, and by generalizing the procedure for a wider class of aircraft configurations (e.g. lower aspect ratio fighters) are given below.

(i) A less empirical approach is required for selecting a particular loading when multiple solutions exist. This would lead to an improved prediction of the angle of attack zone over which lift hysteresis and attendant zero-beta lateral moments may exist. One approach may be the introduction of rate dependent equations for the vorticity on the wing. Such a formulation may require chordwise relocation of the control point and/or modification of the time stepping procedure (see also iv below).

(ii) A more definative evaluation of the method should be carried out by conducting wind tunnel tests with a model which may be pitched and yawed continuously while obtaining instantaneous readings of forces and moments. It is recommended that the model consist of a circular fuselage with replaceable straight wings of various aspect ratio and of known two-dimensional section characteristics, in order to determine limits of applicability of the method. Pressure data should be obtained over the wing, so that transient span and chordwise load distributions may be obtained and compared with those predicted by the theory.

(iii) The formulation should be extended to treat yaw and dihedral effects directly, rather than by simulating a yawed wing by a skewed wing. In addition, a capability for time dependent yawing motions should be incorporated into the program in order to provide for coupling the lifting line formulation with the equations of motion for an aircraft.

(iv) In order to extend the method to lower aspect ratio fighter type wings, it is recommended that the lifting line formulation be expanded into an unsteady, nonlinear, lifting surface theory. The new formulation would employ at least two spanwise lifting lines, and control points for satisfying flow tangency would be placed at two or more chordwise positions. The expanded theory would also include unsteady effects on chordwise load distribution, and might provide insight into the mechanism of dynamic stall. The later effects are excluded from the current lifting line formulation, which assumes that chordwise load distributions are always steadystate.

REFERENCES

1. Sears, W.R., "Some Recent Developments in Airfoil Theory," Journ. Aerospace Sciences, Vol. 23, No. 5, May 1956, pp 490-499.

2. Schairer, R.S., "Unsymmetrical Lift Distributions on a Stalled Monoplane Wing," California Institute of Technology, Thesis, 1939.

3. Sears, W.R., "A New Treatment of Lifting Line Theory with Applications to Rigid and Elastic Wings," Quat. Appl. Math., Vol. VI, No. 3, Oct. 1948, pp. 239-255.

4. Cord, T.J., "Hysteresis Induced Wing Rock," Air Force Flight Dynamics Lab. Rept., AFFDL-TM-75-76-FGC, June 1975.

5. Anderson, C.A., "Stall/Post-Stall Characteristics of the F-111 Aircraft," AGARD Proceedings #102, Fluid Dynamics of Aircraft Stalling, 1972, pp. 18-1 to 18-9.

6. Jones, J.G., "The Dynamic Analysis of Buffeting and Related Phenomena," AGARD Proceedings #102, Fluid Dynamics of Aircraft Stalling, 1972, pp. 23-1 to 23-10.

7. Shaw, D.E., "Pre-Stall Behavior of Combat Aircraft," AGARD Lecture Series #74, Aircraft Stalling and Buffeting, 1975, pp. 6-1 to 6-18.

8. Marks, K.E., "Method for Calculating Wing High Lift Characteristics Using Non-Linear Section Data," General Dynamics Convair Report GDC-ERR-1560, December 1970.

9. Levinsky, E.S., and Ramsey, J.C., "Methodology for Estimating STOL Aircraft High Lift Systems Characteristics," AIAA Paper 72-779, August 1972.

10. Herbert, J., Levinsky, E.S., Ramsey, J.C., Laudeman, E.C., Altman, H.G., and Barbee, L.G., "STOL Tactical Aircraft Investigation", Vol. II, Design Compendium, General Dynamics Convair, AFFDL TR73-21, Vol. II, May 1973.

11. J. Weissinger, "The Lift Distribution of Swept-Back Wings," TM 1120 National Advisory Committee for Aeronautics, March 1947.

12. Piszkin, S. T., "Dynamic Nonlinear Span Load Program," General Dynamics/Convair Aerodynamics, TN-75-CRAD-03, Nov. 1975.

13. J. Lennertz, Beitrag Zur theoretischen Behandlung des genenseitigen Einflusses von Tragfläche und Rumpf," Z. f.a.M.M., Bd, August 1927, pp. 249-276.

14. Zlotnick M. and Robinson, S.W., Jr., "A Simplified Mathematical Model for Calculating Aerodynamic Loading and Downwash for Midwing Wing-Fuselage Combinations with Wings of Arbitrary Planform," NACA RM L52J27a, 16 January 1953.

15. Gray, W.L. and Schenk, K.M., "A Method for Calculating the Subsonic Steady-State Loading on an Airplane with a Wing of Arbitrary Plan Form and Stiffness," NACA TN 3030, Boeing Airplane Company, December 1953.

16. Lawrence, H.R. and Flax, A.H., "Wing Body Interference at Subsonic and Supersonic Speeds - Survey and New Developments," Journ. of the Aeronautical Sciences, Vol. 24, No. 5, May, 1954, pp. 289-324.

17. Ham, N.D. and Johnson, W., "On the Mechanism of Dynamic Stall," Journal of the American Helicopter Society, Vol. 17, No. 4, Oct. 1972.

18. Wagner, H., "Dynamischer Auftreib von Tragflügeln," Zeitschrift für Angew. Math. v. Mech., Bd. 5, 1925, 11. 17-35.

19. Jones, W.P., "Aerodynamic Forces on Wings in Non-Uniform Motion," British, A.R.C., R&M 2117, 1945.

20. Djojodihardjo, R.H. and Widnall, S.E., "A Numerical Method for the Calculation of Nonlinear Unsteady Lifting Potential Flow Problems," AIAA Journal, Vol. 7, No. 10, Oct. 1969, pp. 2001-2009.

21. Margason, R.F. and Lamar, L.E., "Vortex Lattice Fortran Program for Estimating Subsonic Aerodynamic Characteristics of Complex Planforms," NASA TN D-6142, Feb., 1971.

22. Glauert, H., The Elements of Aerofoil and Airscrew Theory, University Press, Cambridge, 1947.

23. Schuetz, A.J., and Bailey, D.B., "Low Speed Wind Tunnel Investigation of a 0.09 Scale, Navy Model T-2C Subsonic Jet Trainer Aircraft from -8 to +83 Degrees Angle of Attack," Naval Air Dev. Center Report NADC 73259-30, Dec '73.

24. Abbott, I.H. and Von Doenhoff, A.E., Theory of Wing Sections, Dover Publications, N.Y., N.Y., 1959.

25. Kroeger, R. A., and Feistel, T. W., "Reduction of Stall-Spin Entry Tendencies Through Wing Aerodynamic Design," SAE Paper 760481, April 6-9, 1976.

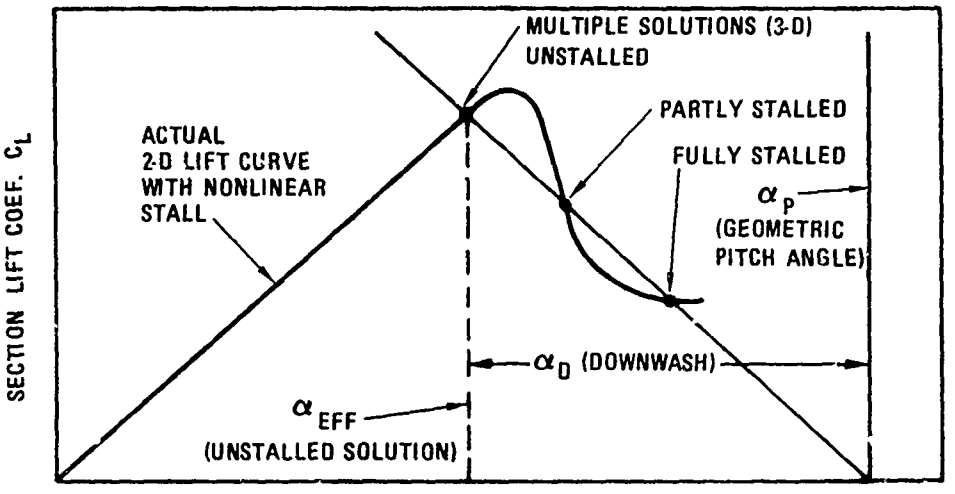

A. TYPICAL SECTION LIFT CURVE

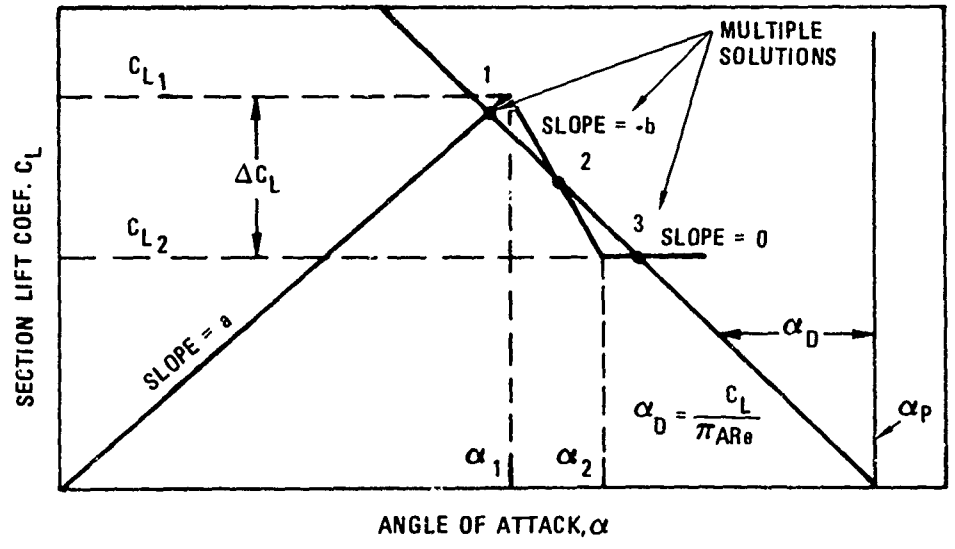

B. TRI-LINEAR SECTION LIFT CURVE
USED FOR SIMPLIFIED CALCULATIONS

Figure 1. Nonlinear Two-Dimensional Section Lift Curves Which Yield Multiple Solutions of the Lifting Line Equations

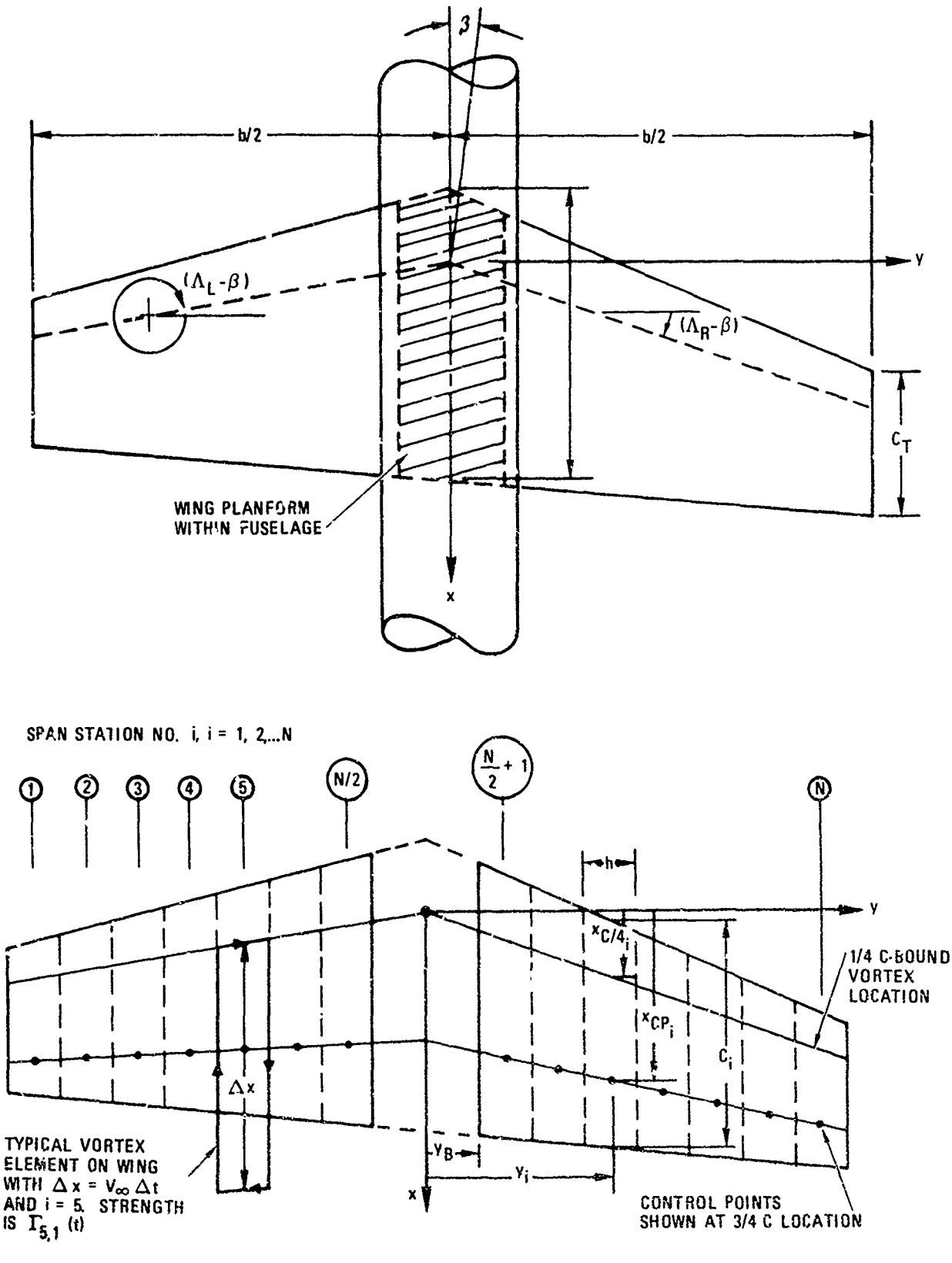

Figure 2. Wing Planform Geometry and Vortex Element Placement

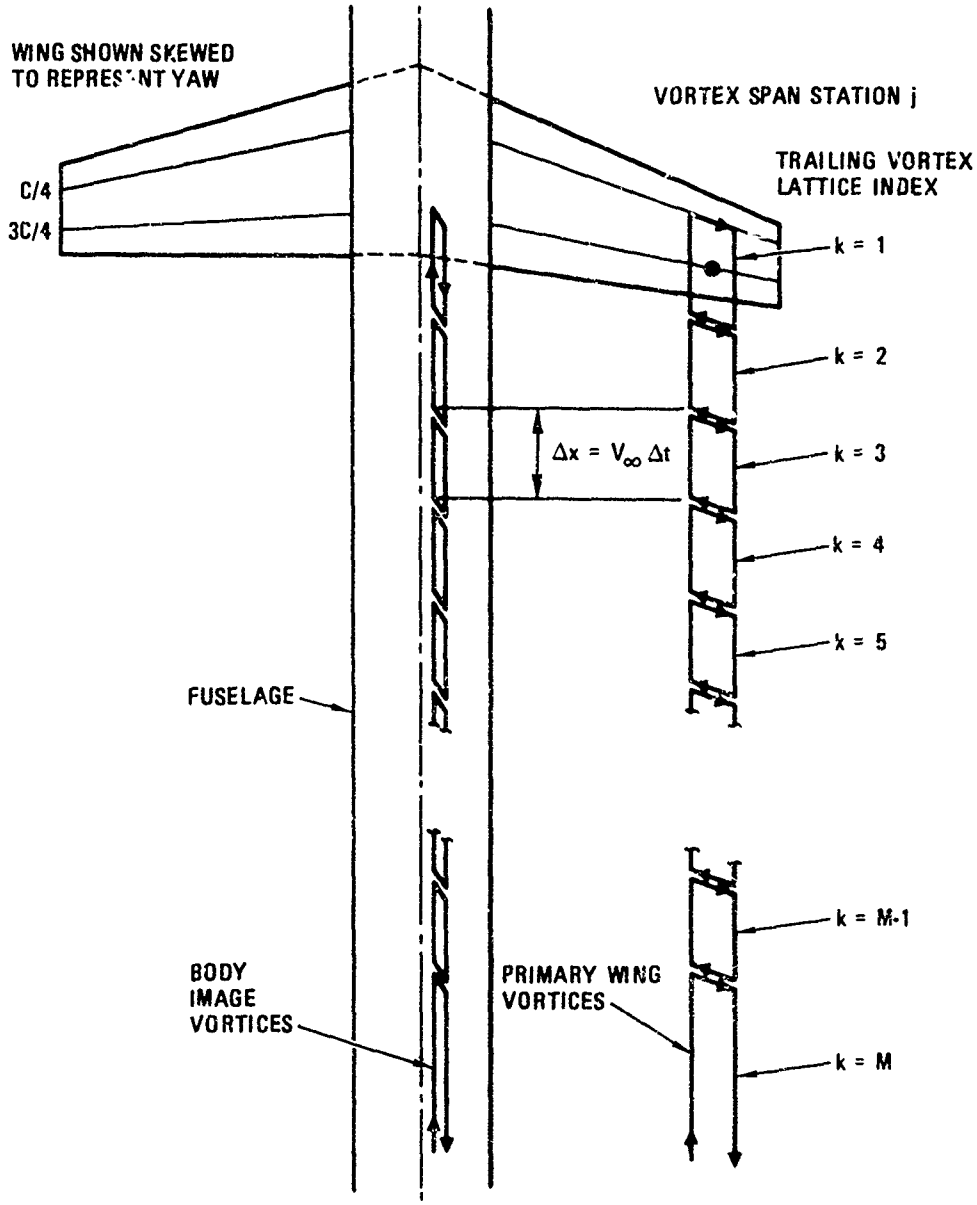

Figure 3. Vortex Elements for Unsteady Wake Formulation

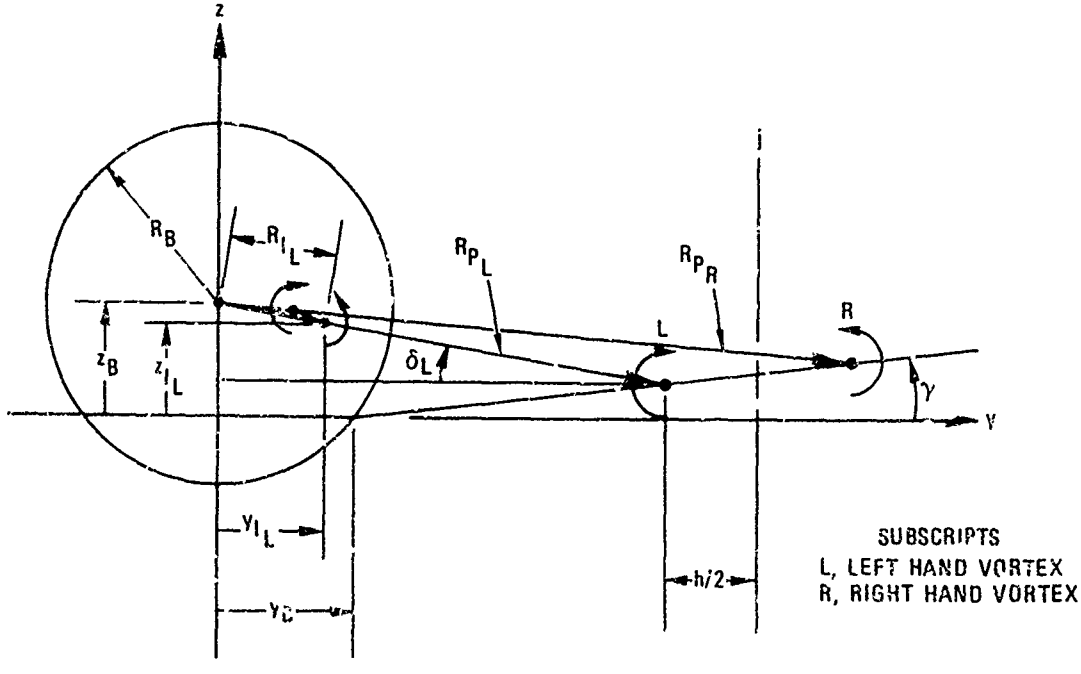

Figure 4. Image System Trailing Element Geometry

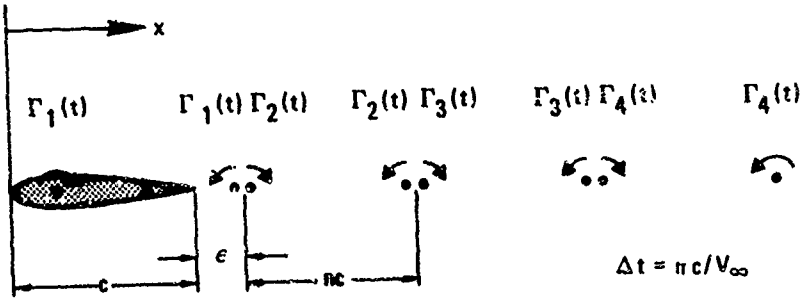

A. FORMULATION IN TERMS OF Γ_k

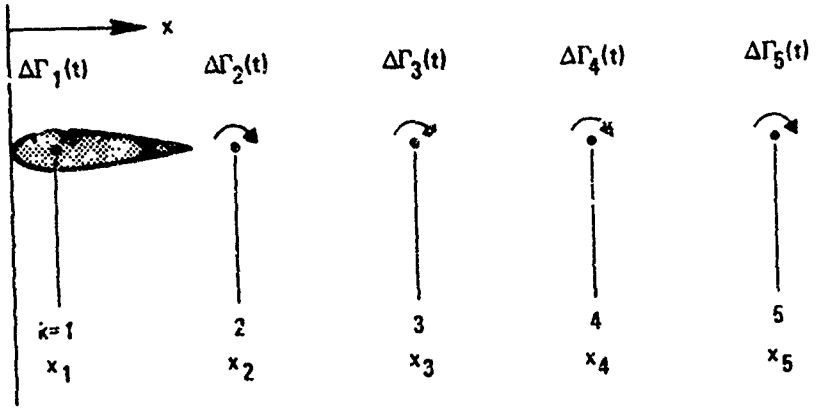

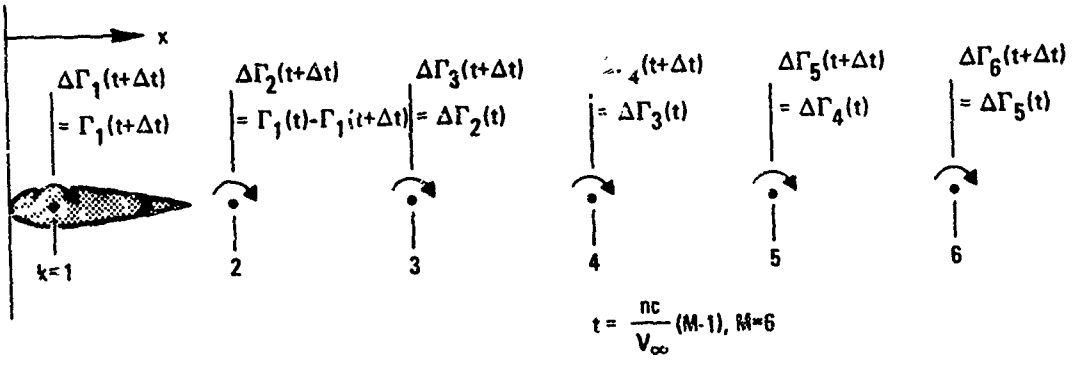

B. FORMULATION IN TERMS OF $\Delta\Gamma_k = \Gamma_k - \Gamma_{k-1}$

Figure 5. Two-Dimensional Representations of Unsteady Wake

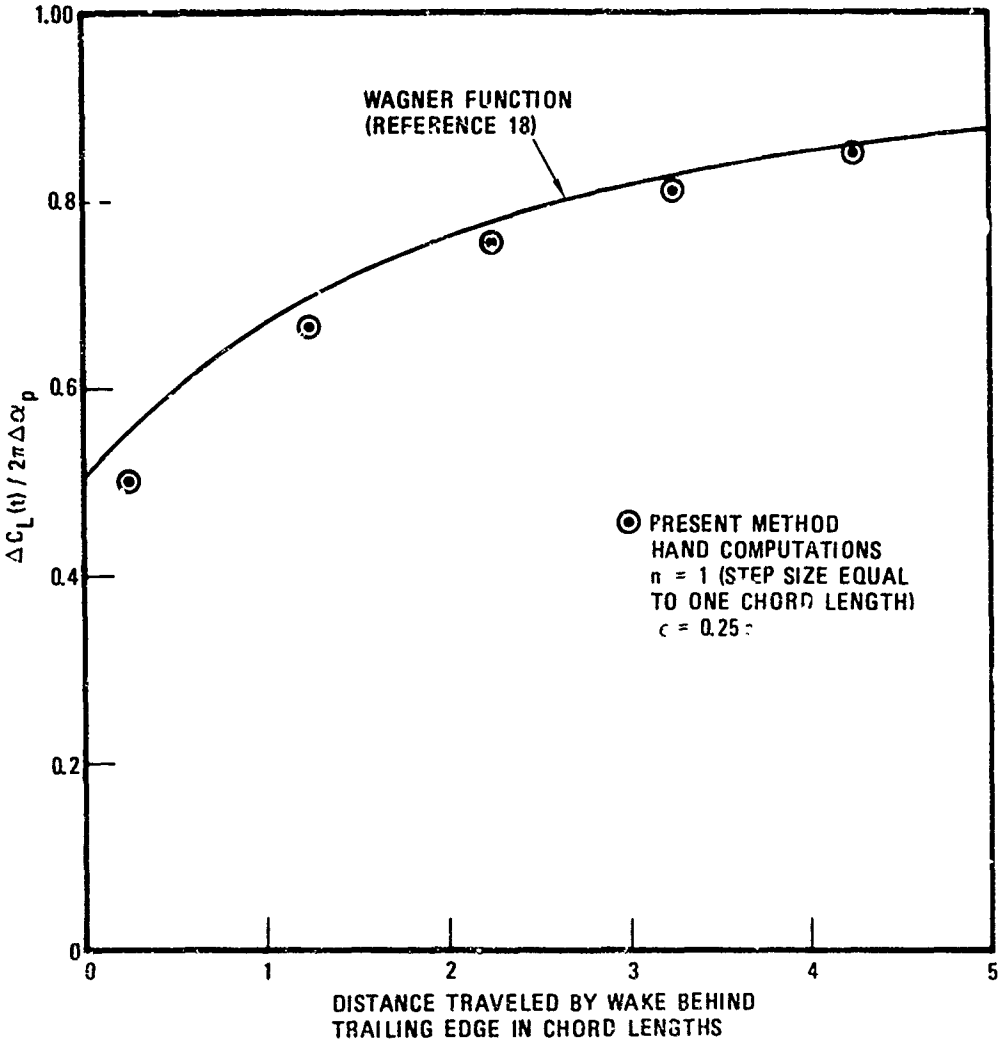

Figure 6. Comparison of Discrete Vortex Wake Model with Wagner Function (Continuous Vortex Wake) for Two-Dimensional Flow

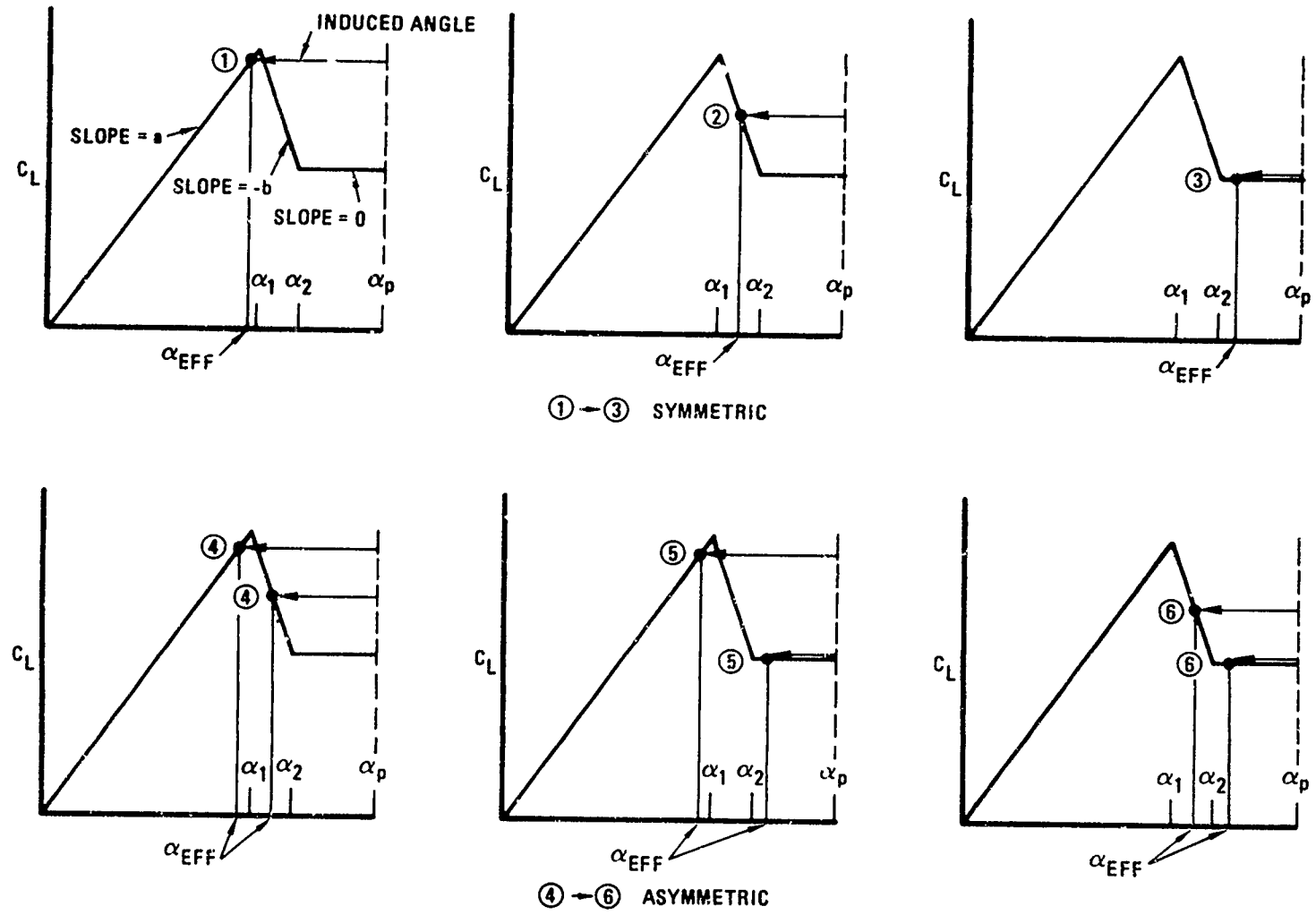

Figure 7. Possible Symmetrical and Asymmetrical Loadings with Tri-Linear Lift Curve when $\alpha_p > \alpha_2$

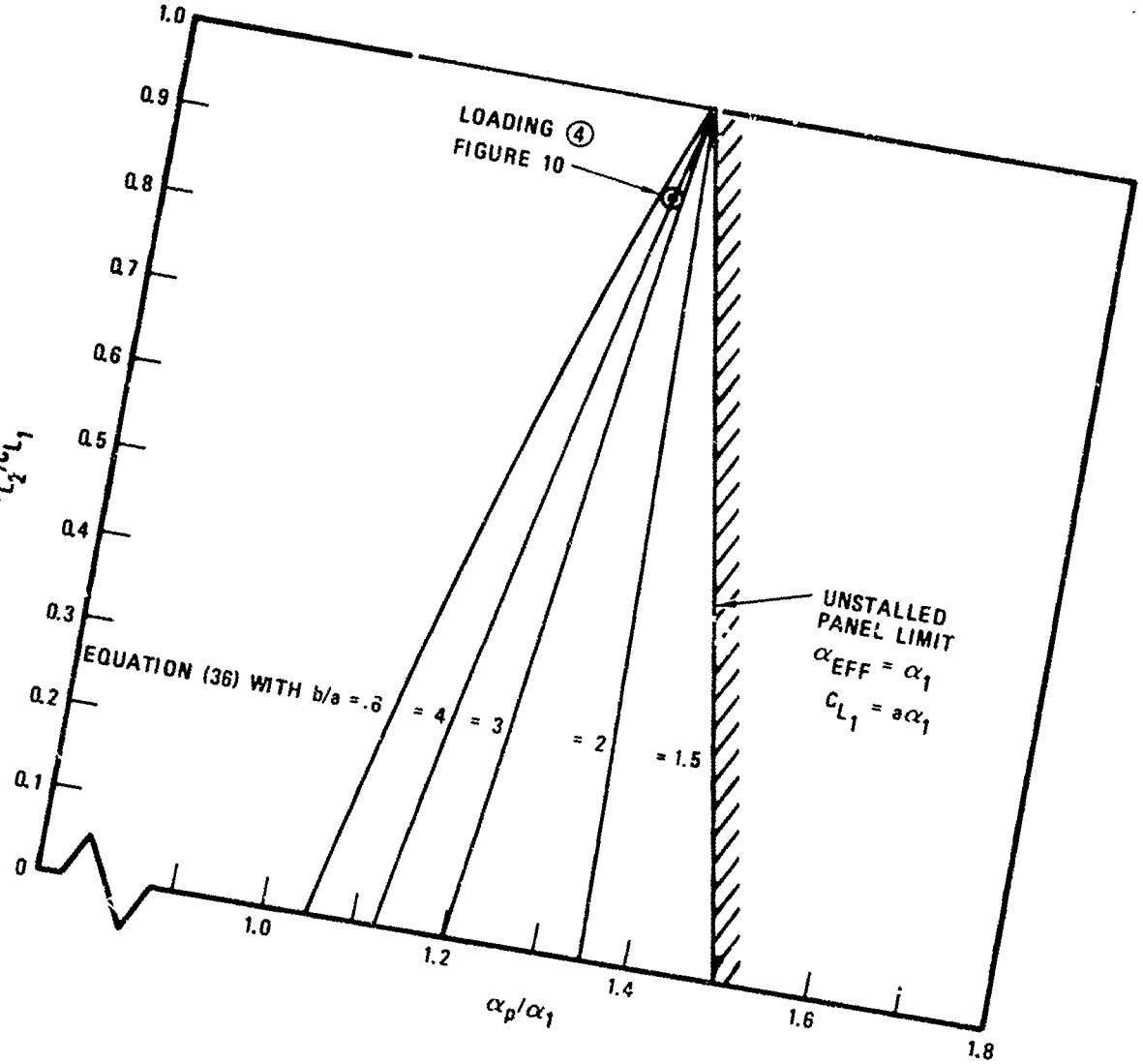

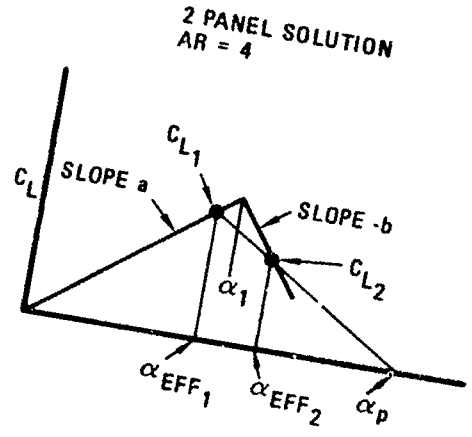

Figure 8. Asymmetric Loadings for Wings with One Panel Unstalled ($dC_L/d\alpha = a$) and the Other Panel Partially Stalled ($dC_L/d\alpha = -b$)

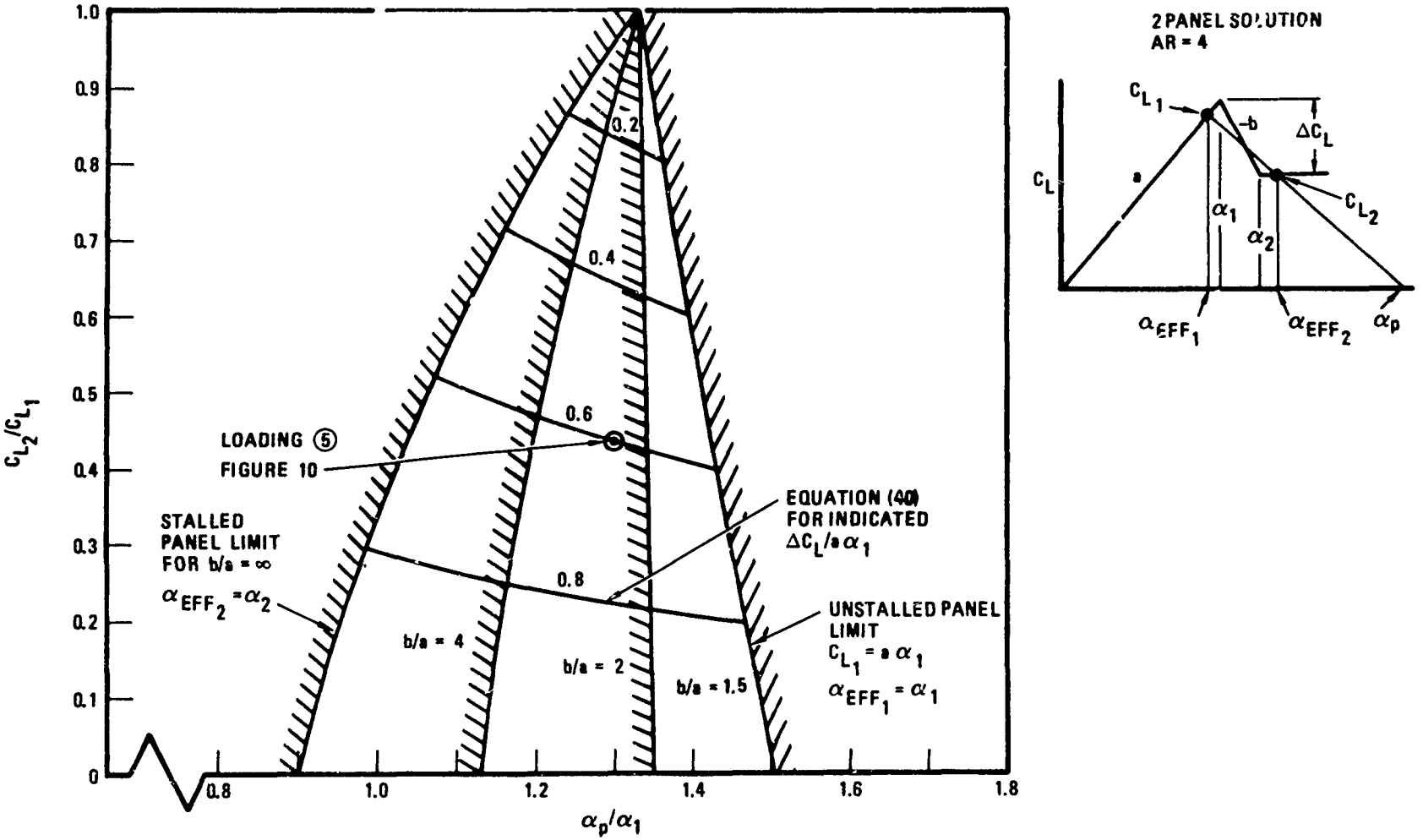

Figure 9. Asymmetric Loadings for Wings with One Panel Unstalled ($dC_L/d\alpha = a$) and the Other Fully Stalled ($dC_L/d\alpha = 0$)

TABULATION OF SYMMETRICAL AND ASYMMETRICAL LOADINGS FOR 2 PANEL SOLUTION, AR=4 WING WITH b/a=4, $\Delta C_L/C_{L_{MAX}}$=0.7, AND α_p/α_1=1.3.

LOADING NO.	SYMBOL	LOADING TYPE	$C_{L_1}/C_{L_{MAX}}$	$C_{L_2}/C_{L_{MAX}}$	C_{L_2}/C_{L_1}
①	●	SYMMETRIC	0.98	0.98	1.00
②	▲	SYMMETRIC	0.65	0.65	1.00
③	■	SYMMETRIC	0.40	0.40	1.00
④	◇	ASYMMETRIC	0.96	0.84	0.87
⑤	◁	ASYMMETRIC	0.91	0.40	0.44
⑥	◇	ASYMMETRIC	0.46	0.40	0.87

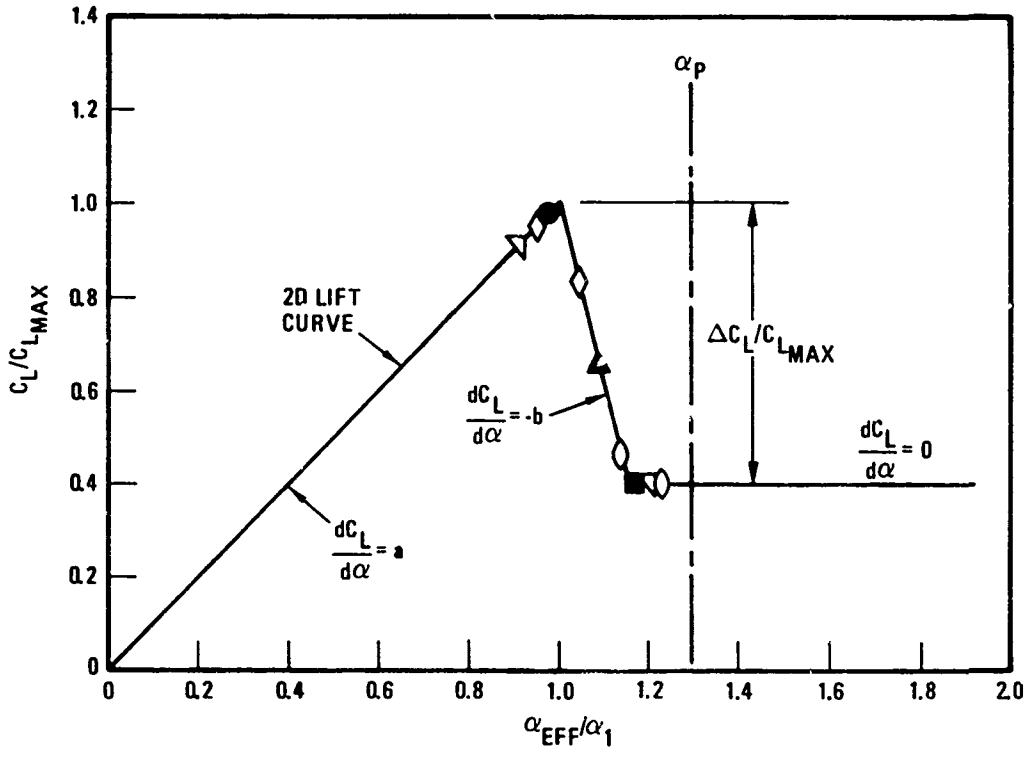

Figure 10. Example of the Occurance of Six Possible Loadings with a Tri-Linear Lift Curve

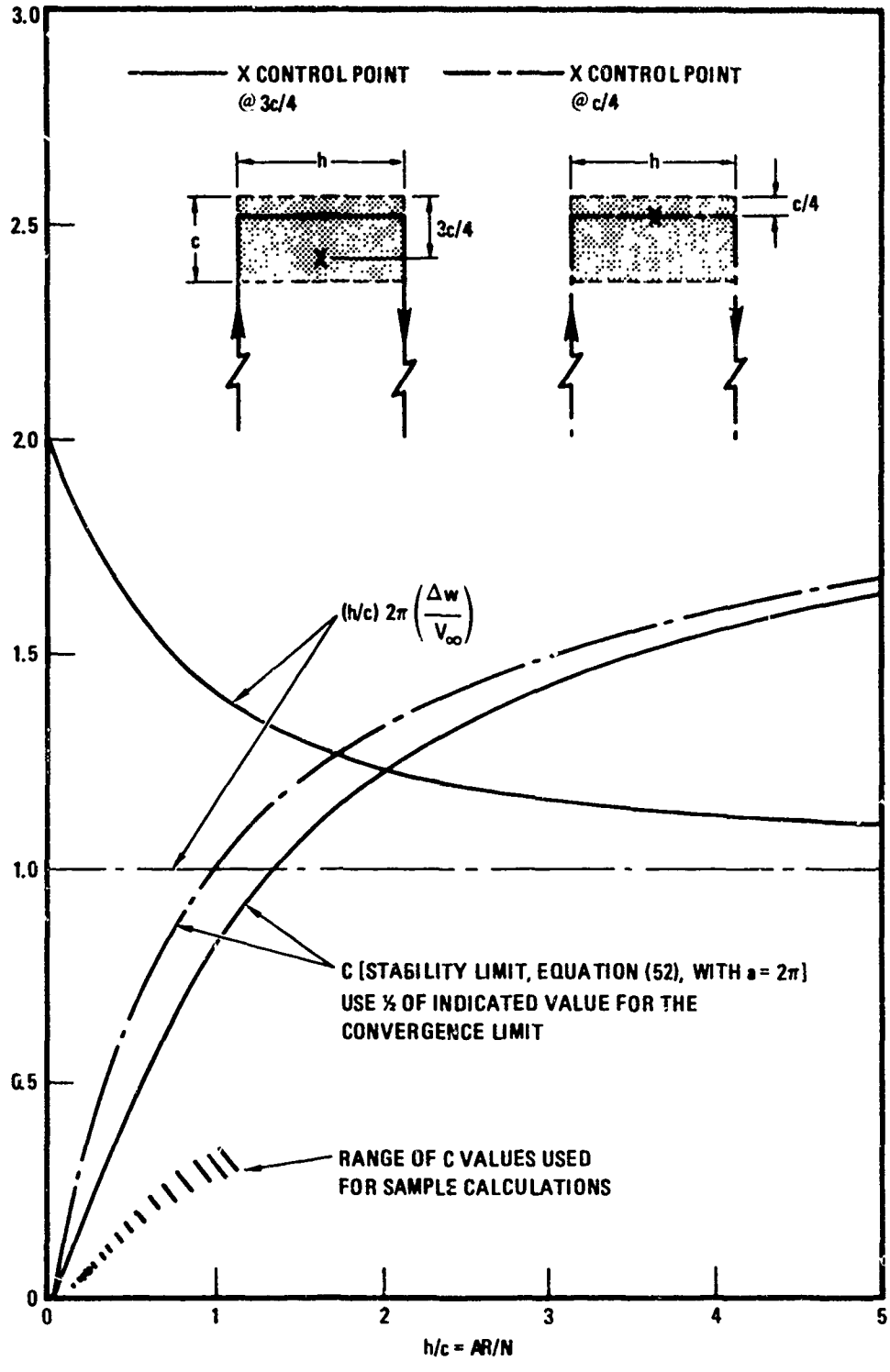

Figure 11. Predicted Stability and Convergence Limits for Iteration Procedure with a Single Vortex Element

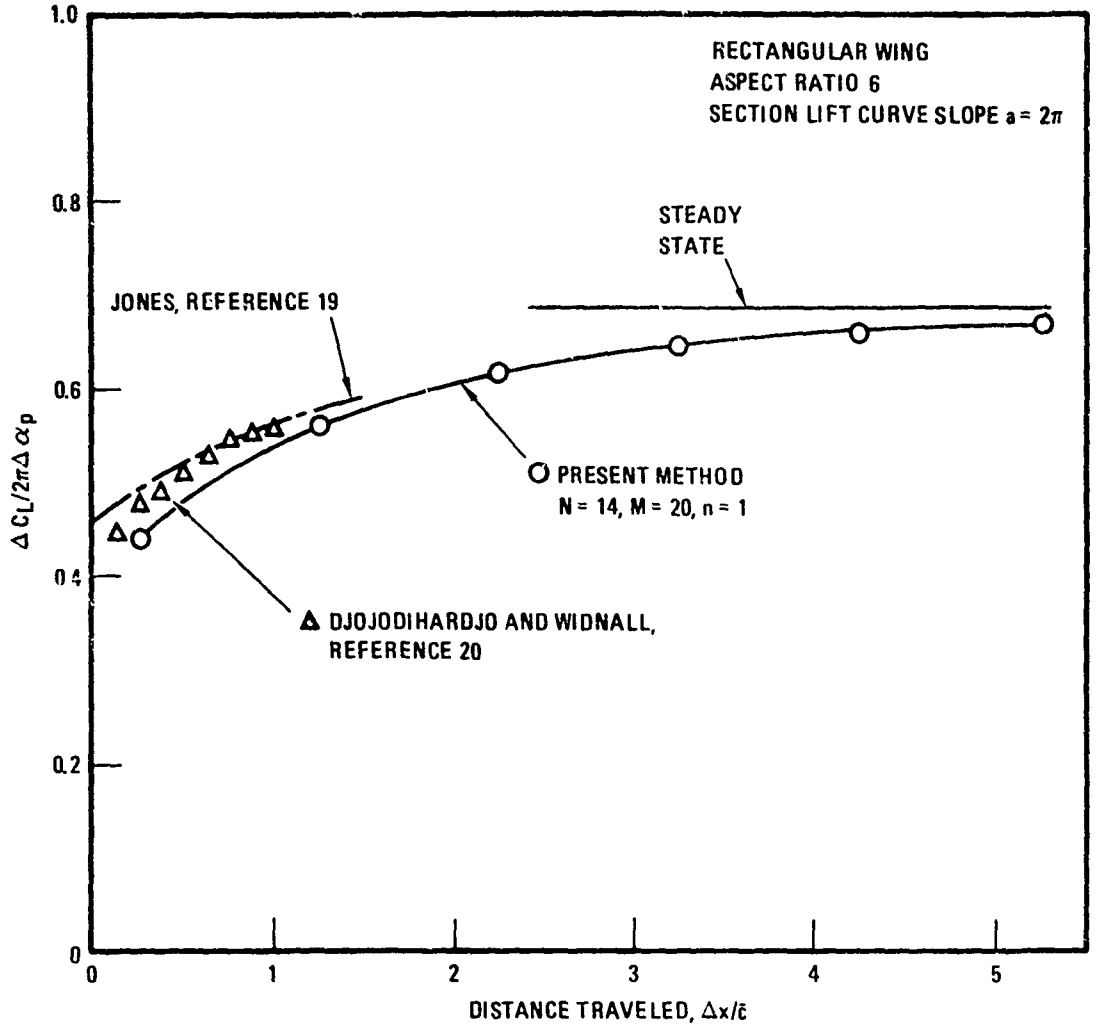

Figure 12. Effect of a Step Change in Angle of Attack on Lift, AR - 6.

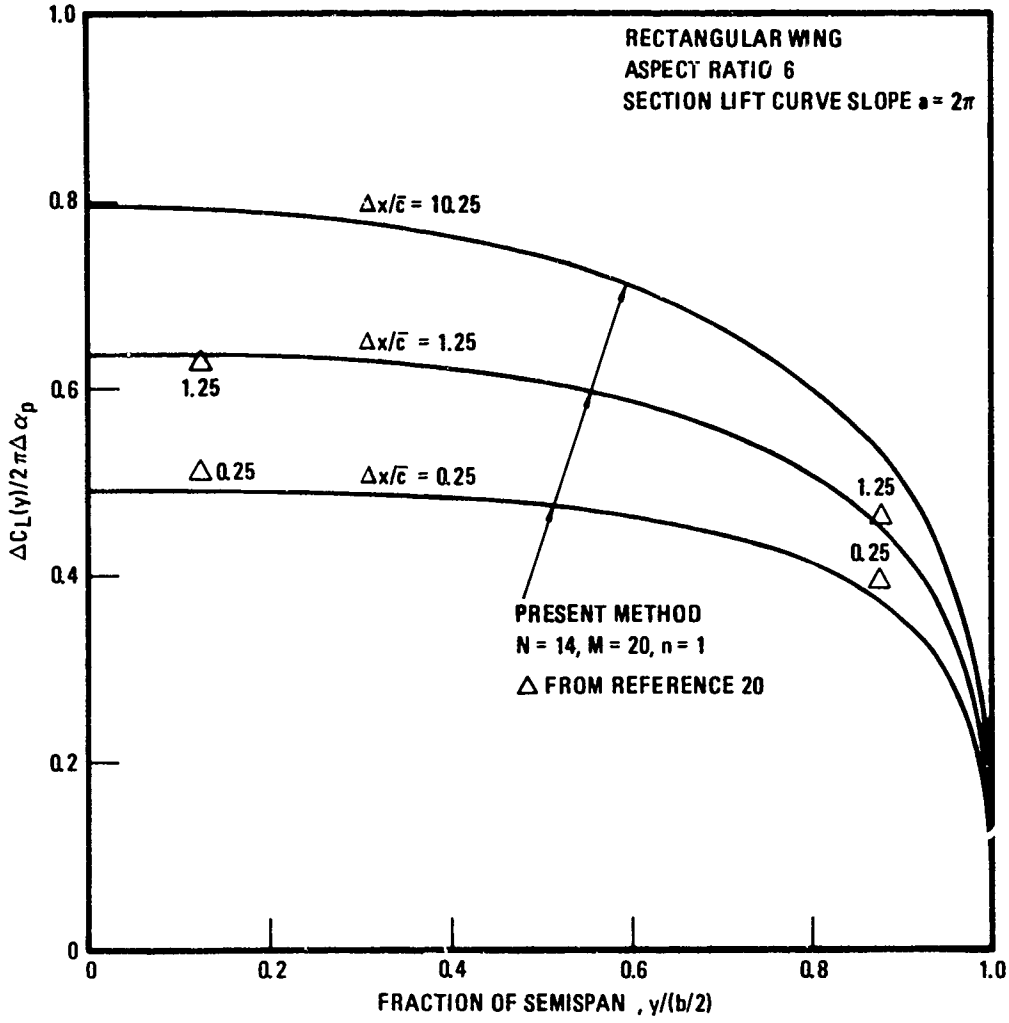

Figure 13. Effect of a Step Change in Angle of Attack on Span Load Distribution AR = 6

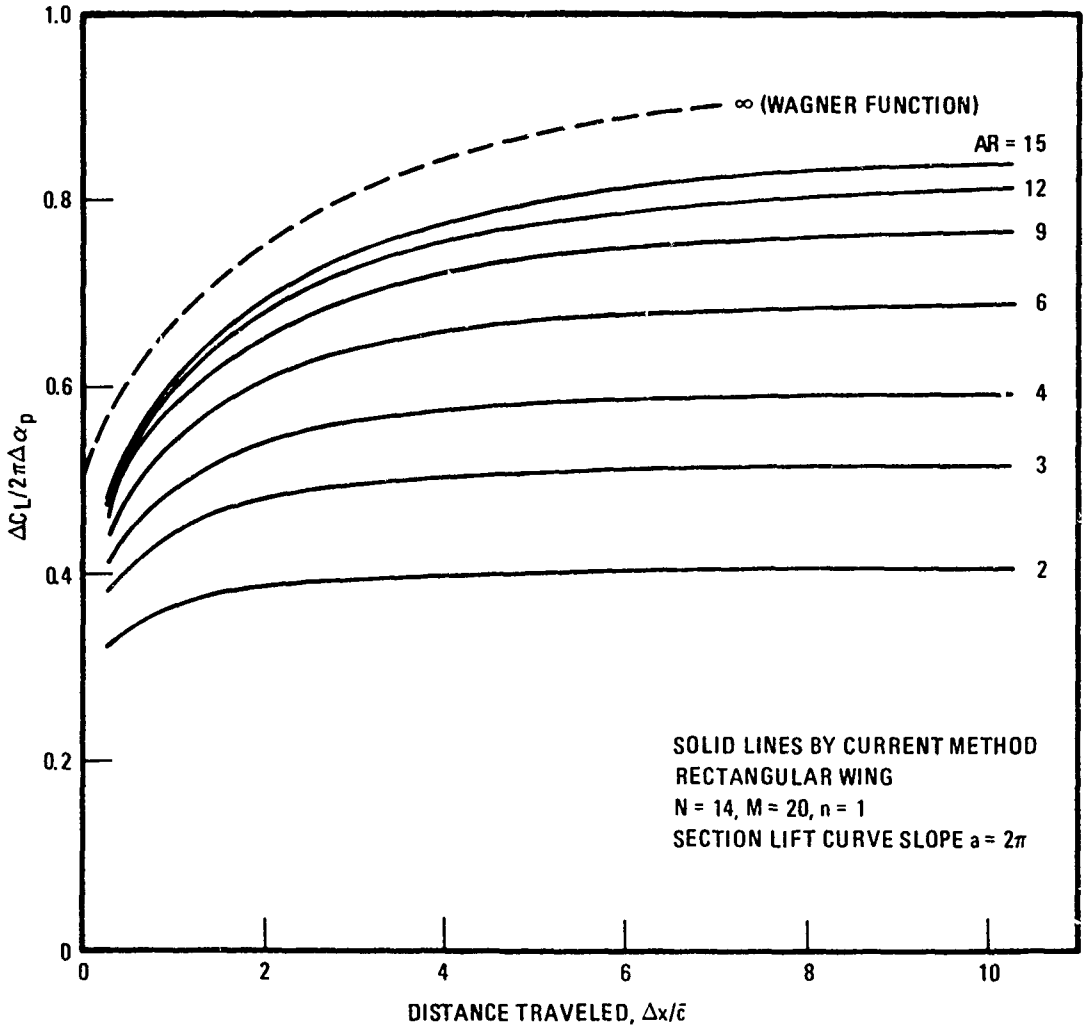

Figure 14. Effect of Aspect Ratio on Lift Following a Step Change in Angle of Attack

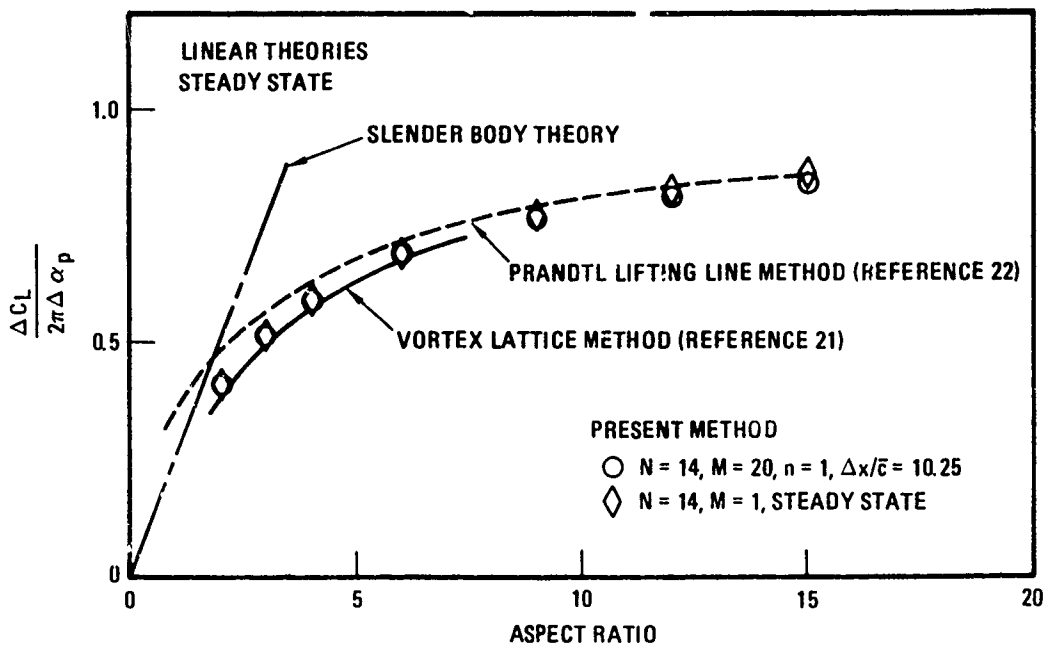

Figure 15. Comparison of Present Method with Steady State Theories for Rectangular Wing

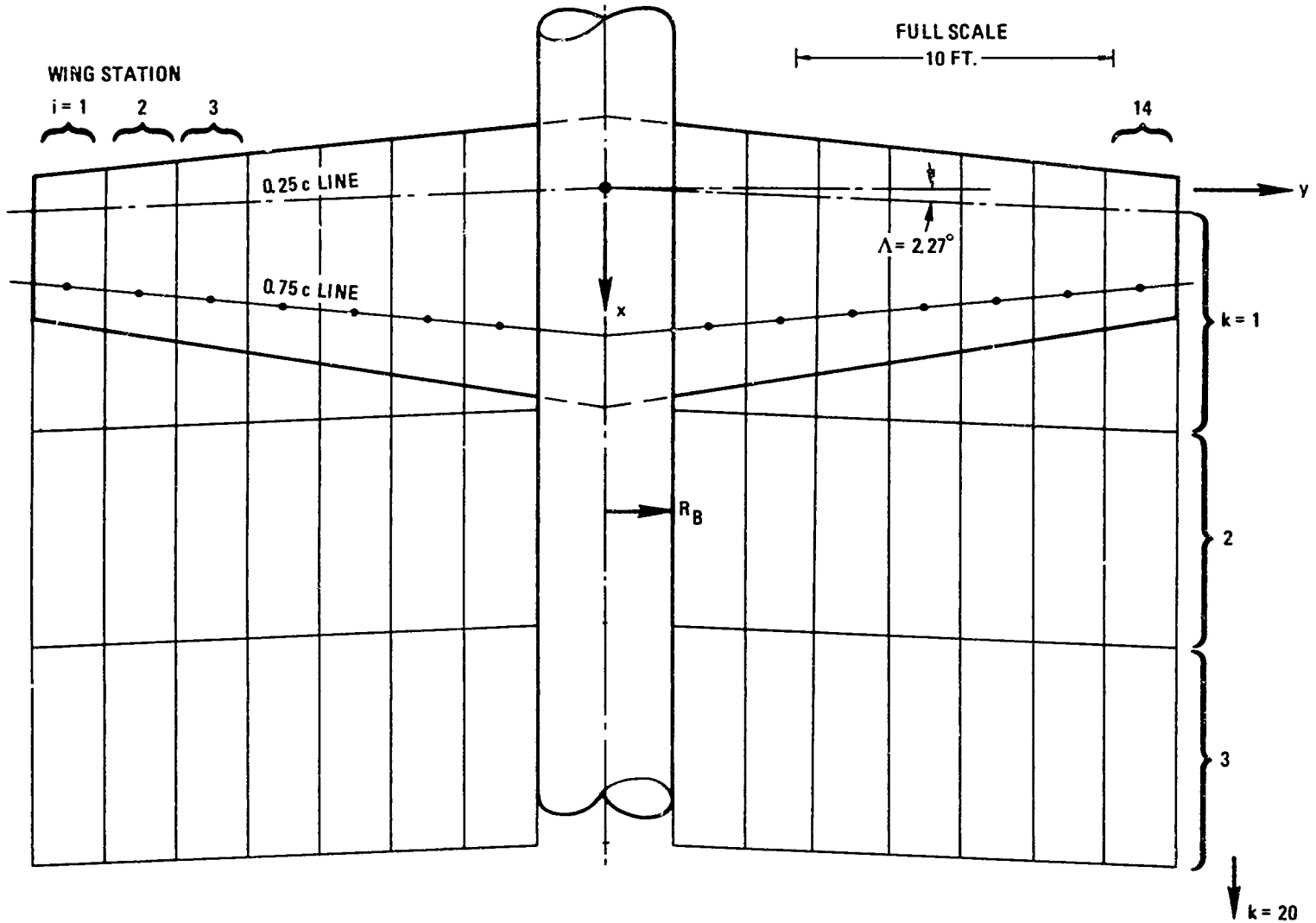

Figure 16. Planform Geometry and Paneling Used for T-2C Computations (N = 14)

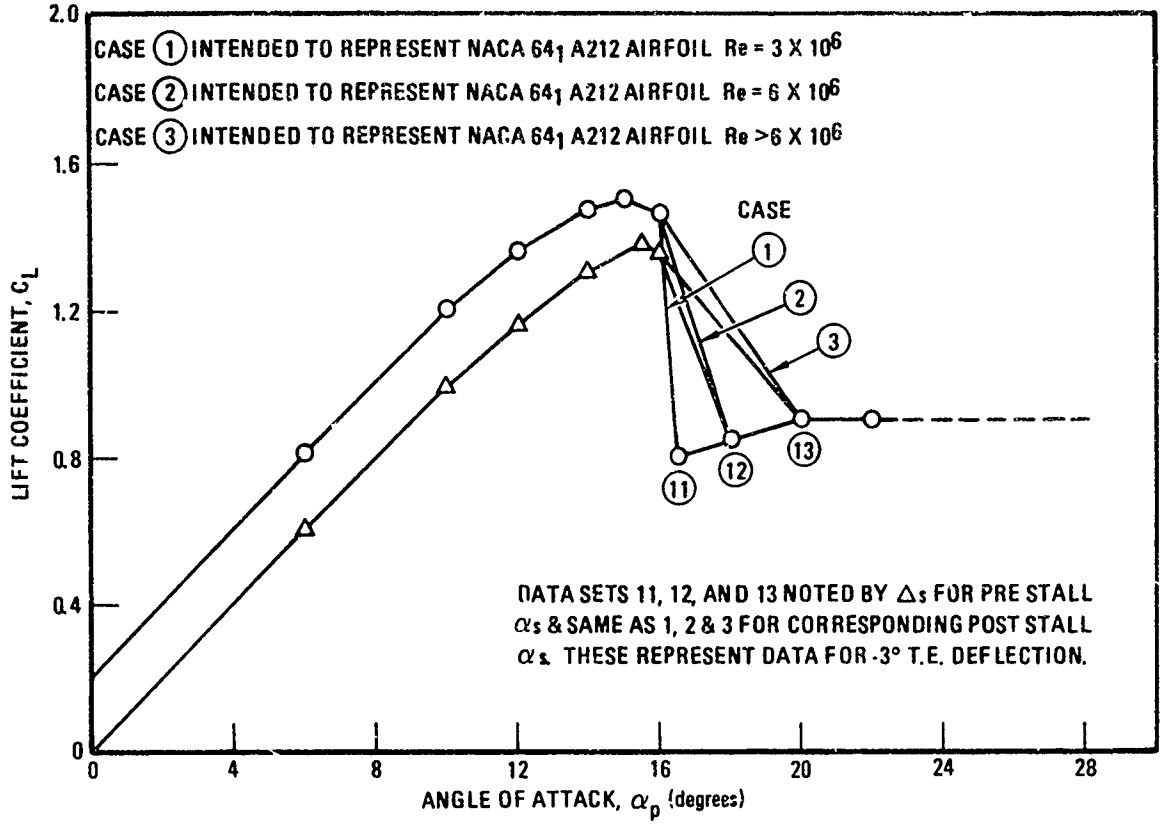

A. LIFT COEFFICIENT

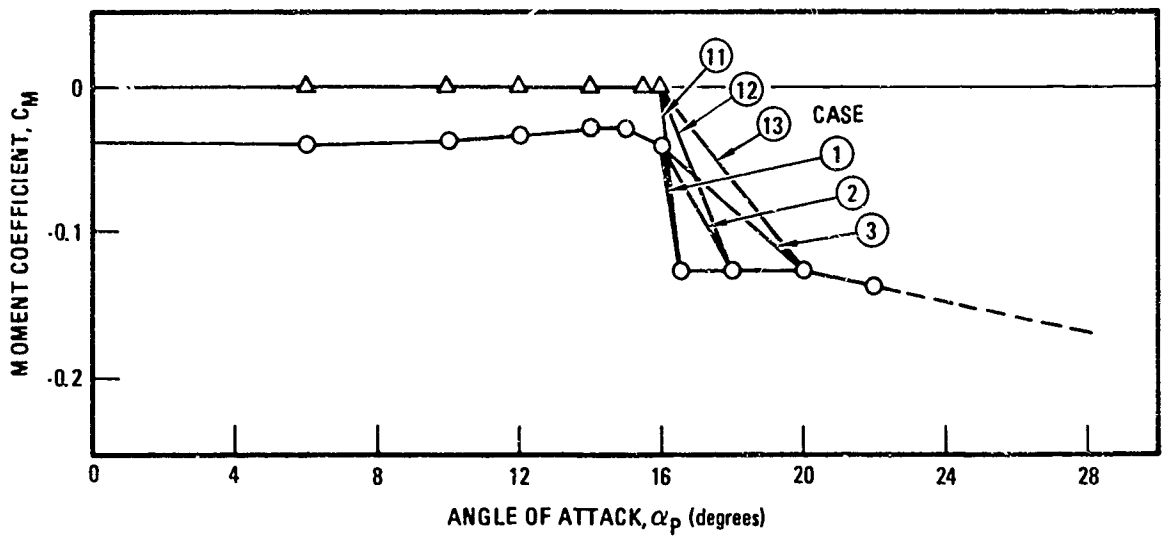

B. PITCHING MOMENT COEFFICIENT ABOUT 25% CHORD POINT

Figure 17. Section Characteristics of NACA 64$_1$ A212 and T-2C Airfoils

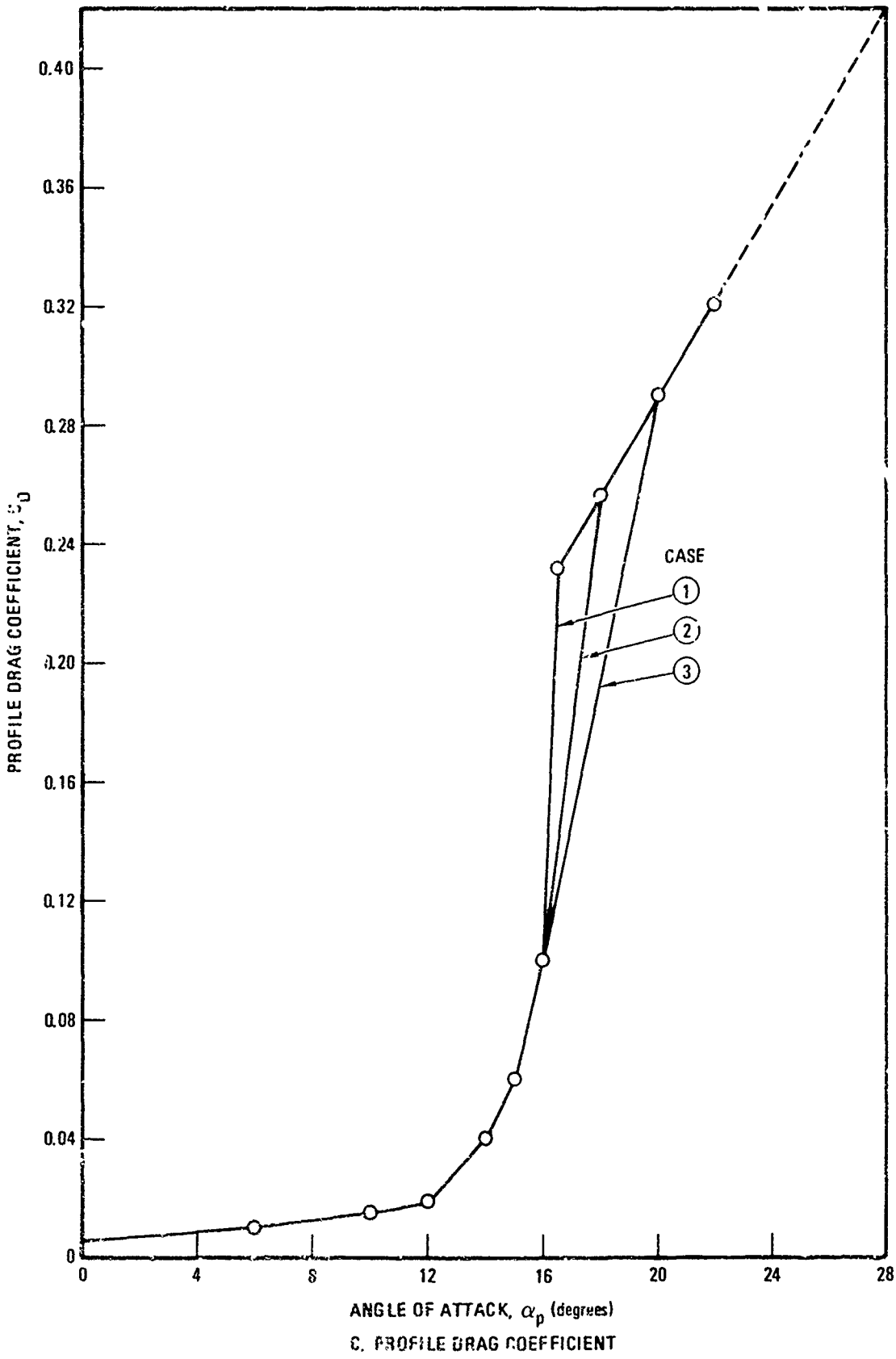

Figure 17. Section Characteristics of NACA 64_1 A212 and T-2C Airfoils (Concluded)

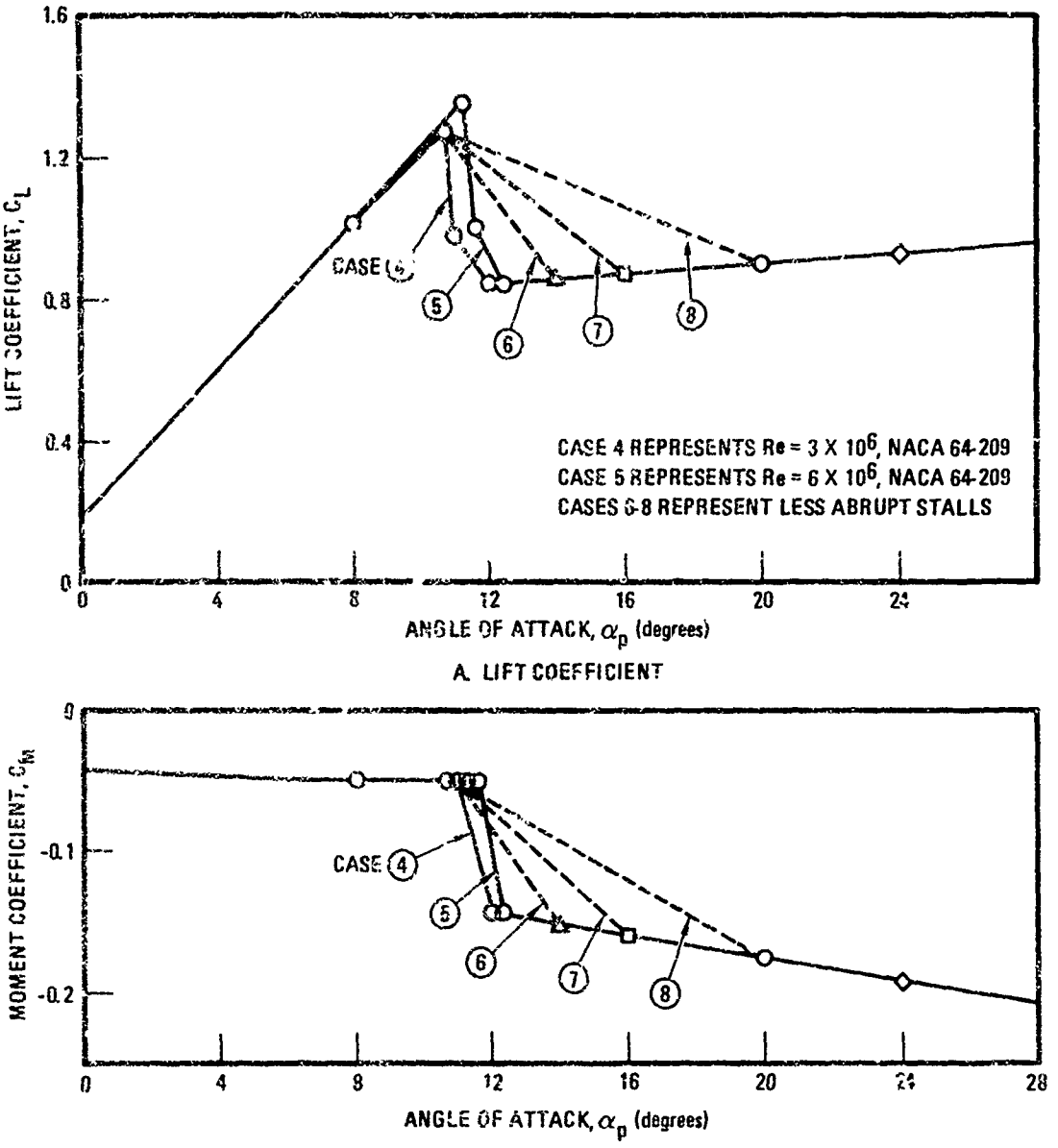

Figure 18. Nonlinear Airfoil Section Characteristics Used for Parametric Calculations

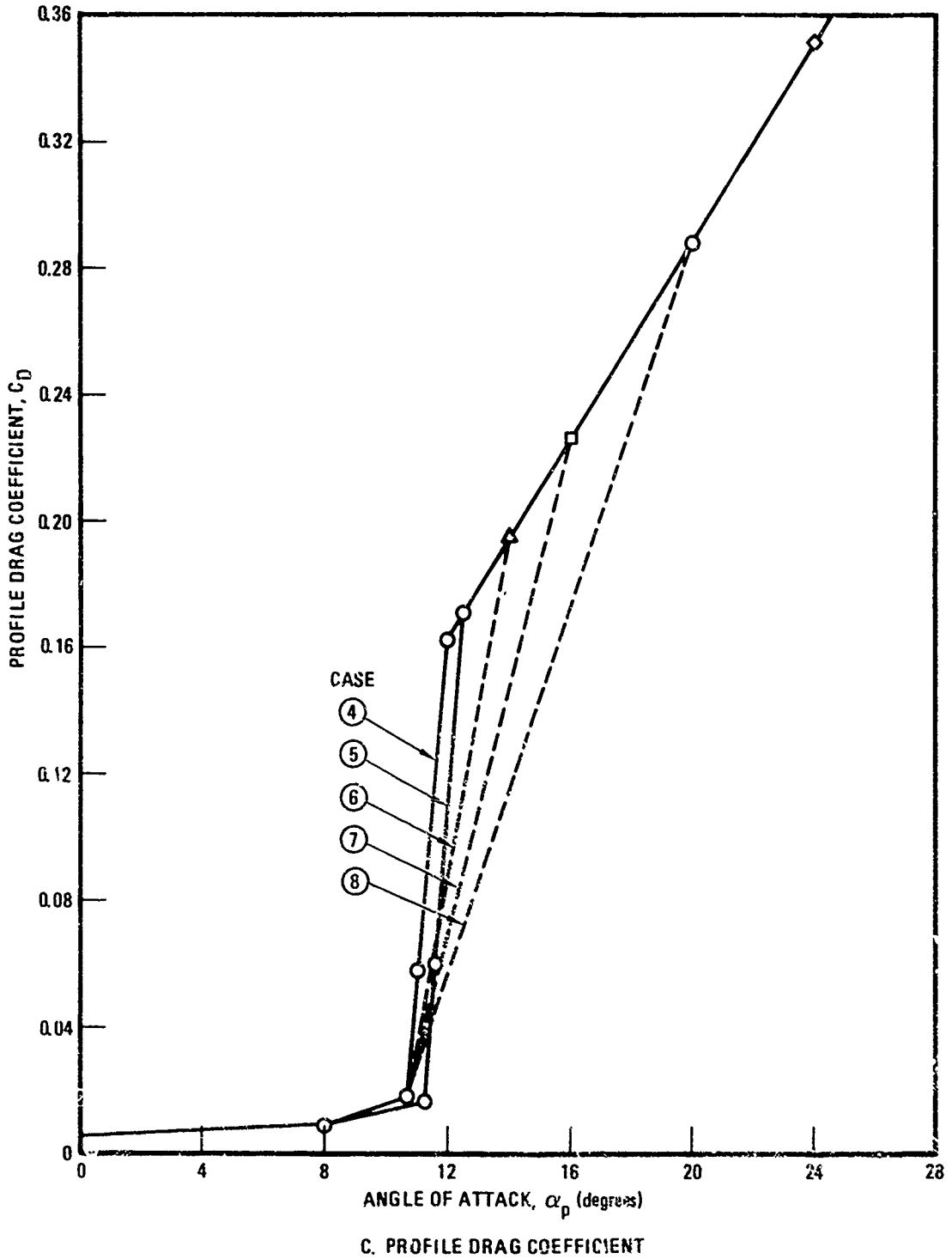

Figure 18. Nonlinear Airfoil Section Characteristics Used for Parametric Calculations (Concluded)

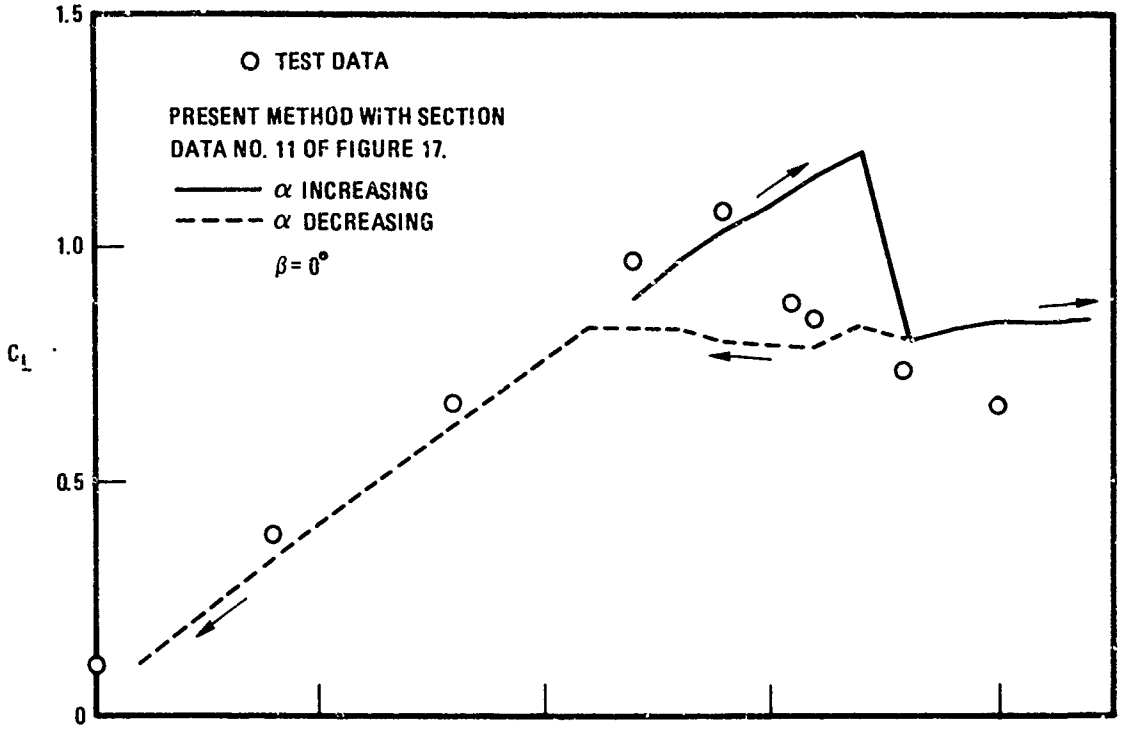

A. ZERO YAW ANGLE

T-2C DATA FROM REF. 23.
M_∞ = 0.20, Re_c = 4 X 10^6
GRIT OFF

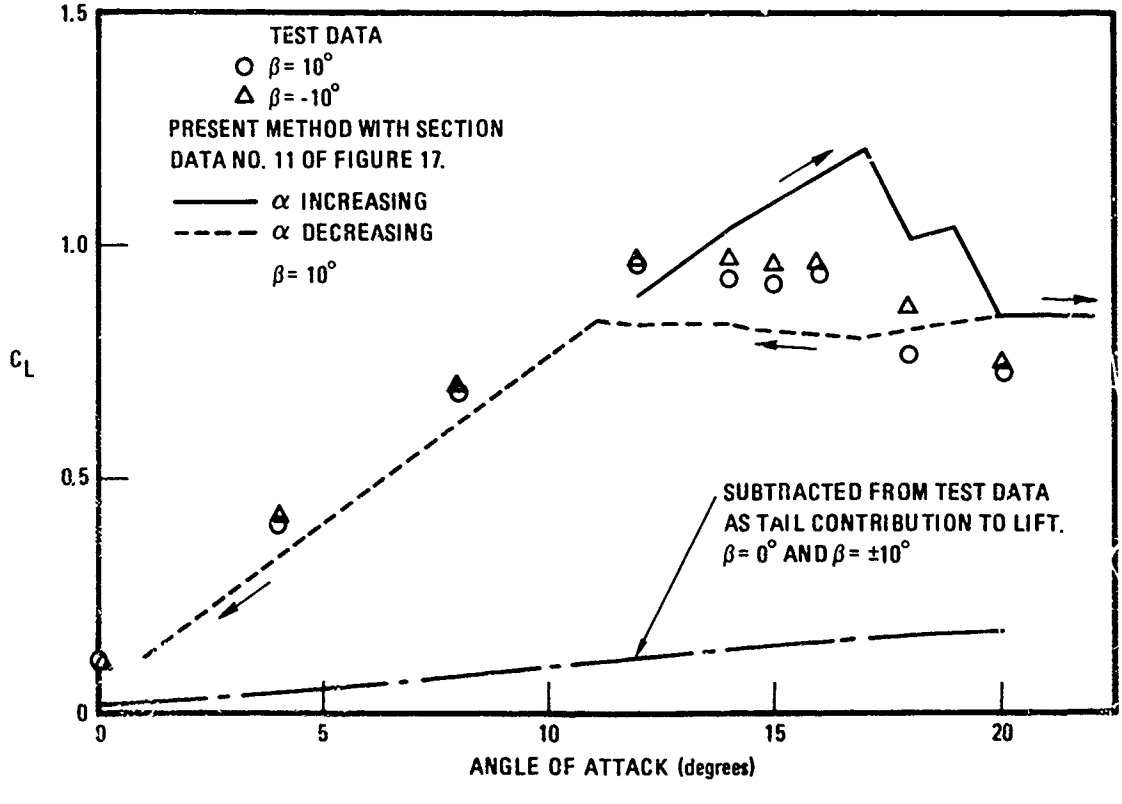

B. ±10° YAW ANGLE

Figure 19. Comparison of Present Method with T-2C Wind Tunnel Data for Lift

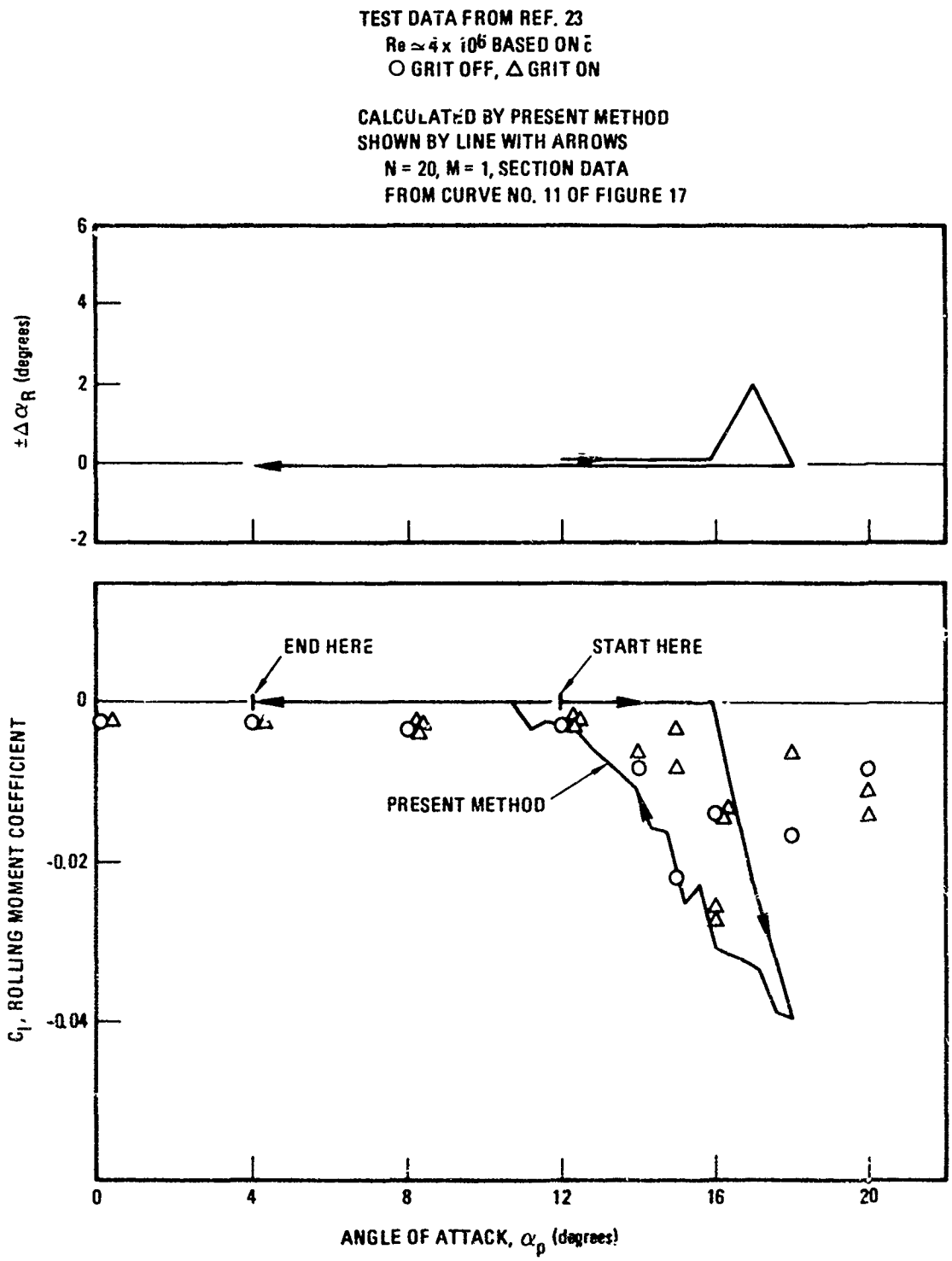

Figure 20. Comparison of Present Method with T-2C Wind Tunnel Data for Rolling Moment at Zero Yaw Angle

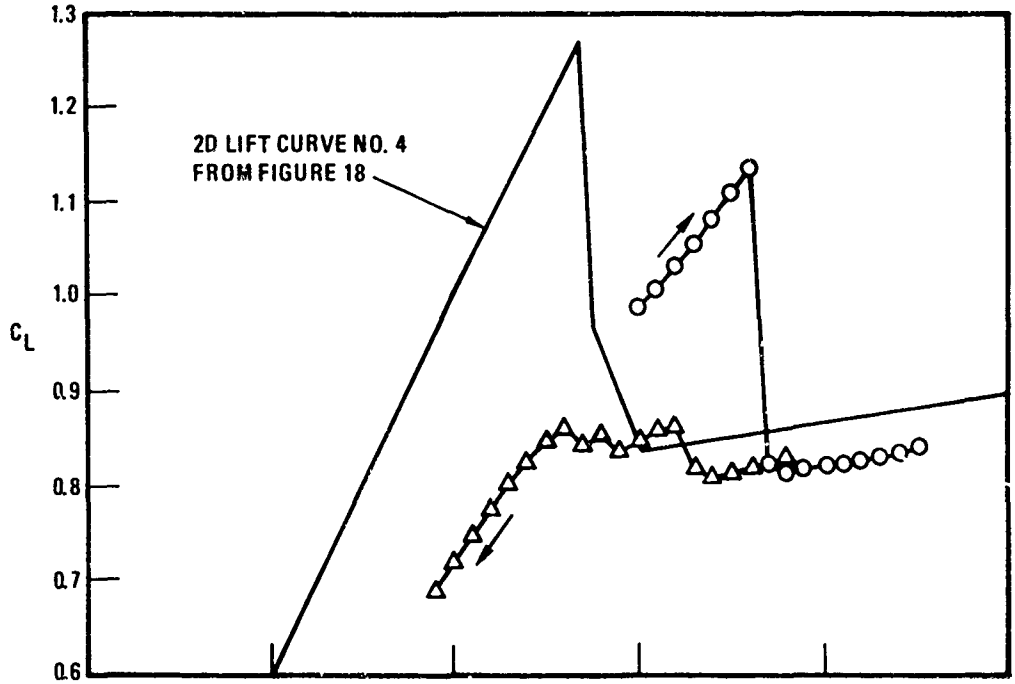

A. NEGATIVE LIFT CURVE SLOPE = 0.97 PER DEGREE

AR = 5.07, τ = 0.495, Λ = 2.27°
i_w = 0°, α_T = 0°, γ = 0°, R_B = 0.119 b/2
PITCH RATE = 8 DEG/SEC
SIDESLIP = 0, $\Delta\alpha_R$ = 0
N = 14, M = 4

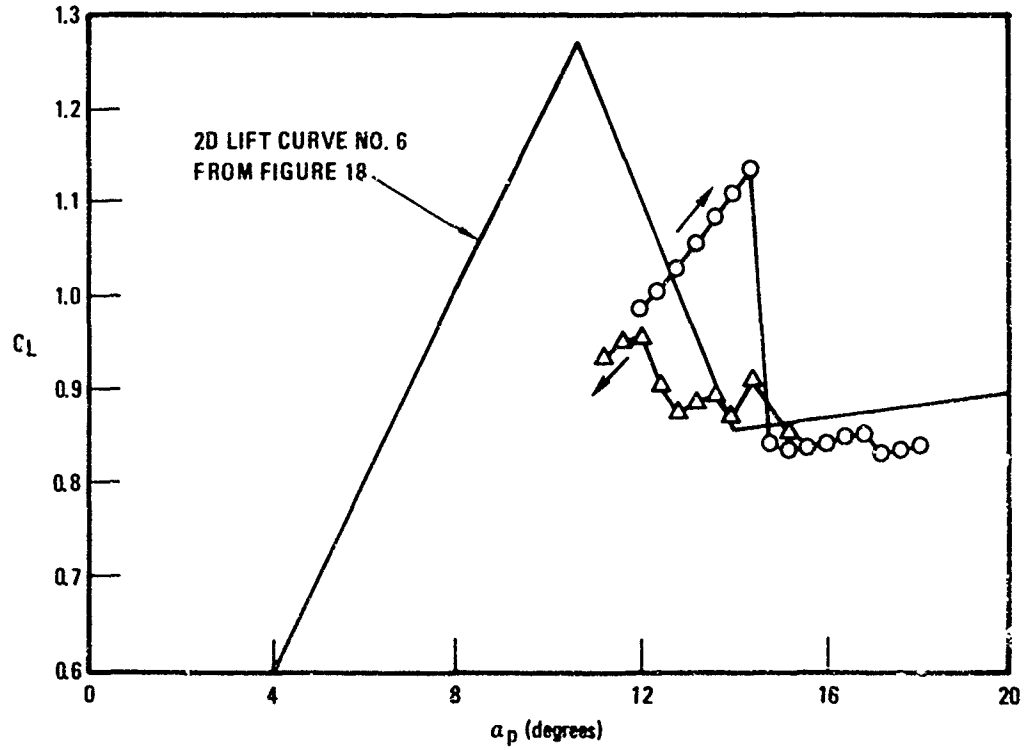

B. NEGATIVE LIFT CURVE SLOPE = 0.125 PER DEGREE

Figure 21. Effect of Negative Lift Curve Slope on Lift Hysteresis, Aspect Ratio 5.07

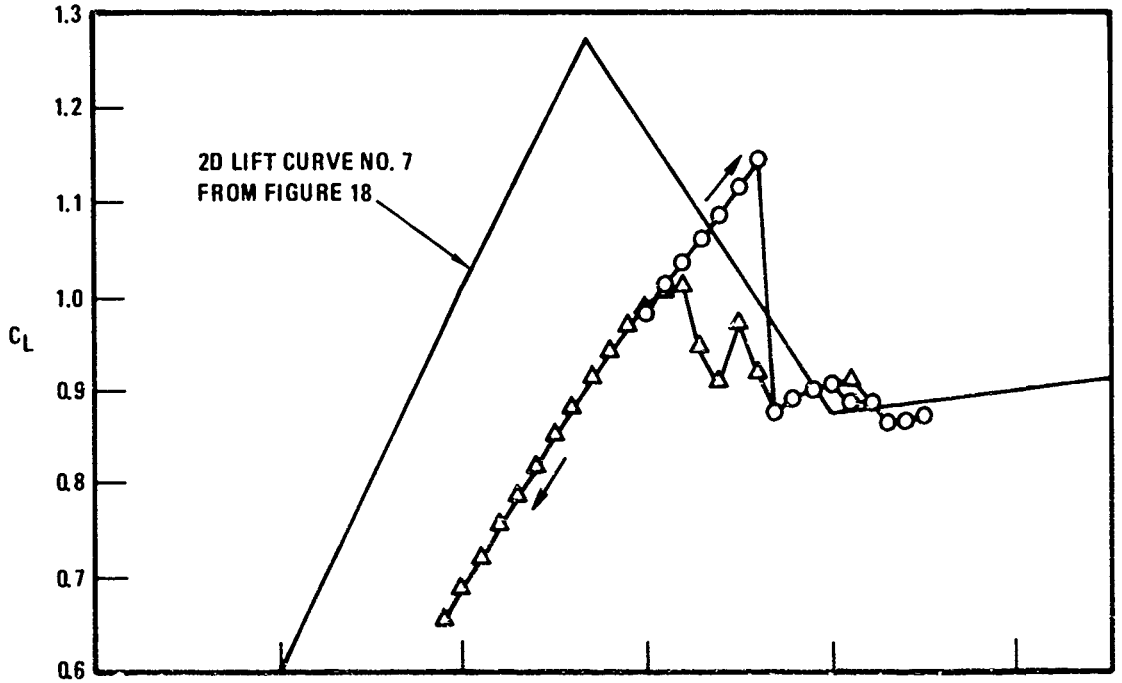

C. NEGATIVE LIFT CURVE SLOPE = 0.075 PER DEGREE

NOTATIONS ON FIGURES A & B

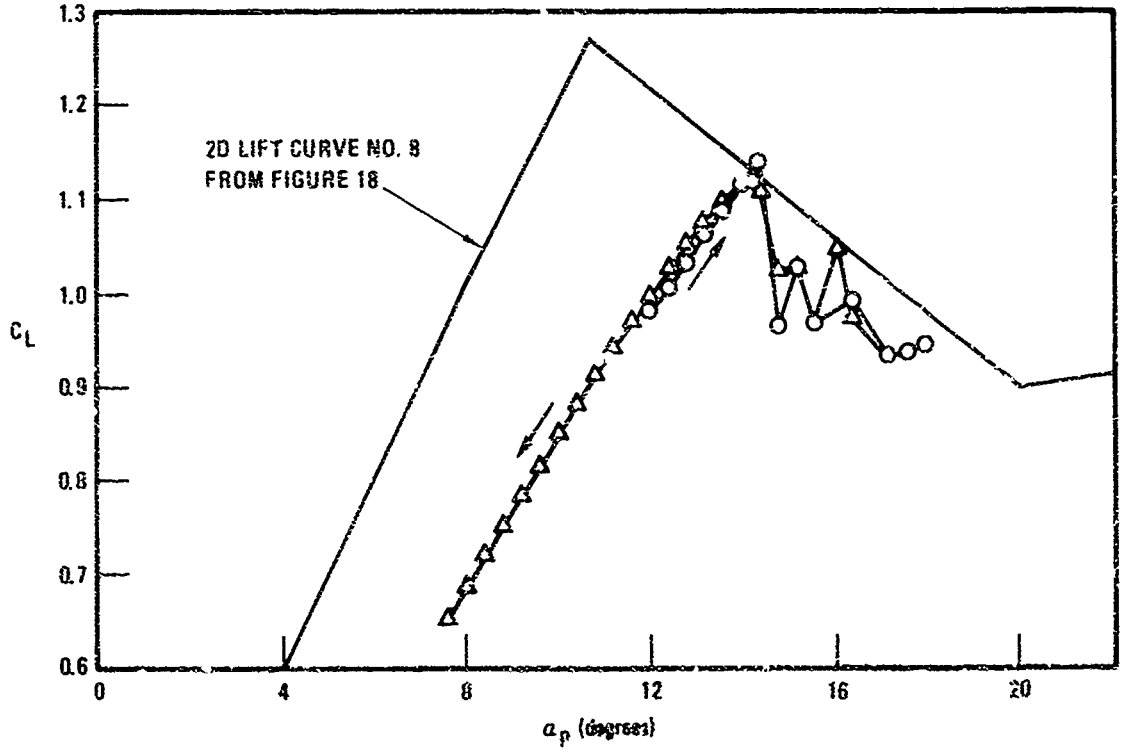

D. NEGATIVE LIFT CURVE SLOPE = 0.040 PER DEGREE

Figure 21. Effect of Negative Lift Curve Slope on Lift Hysteresis, Aspect Ratio 5.07 (Concluded)

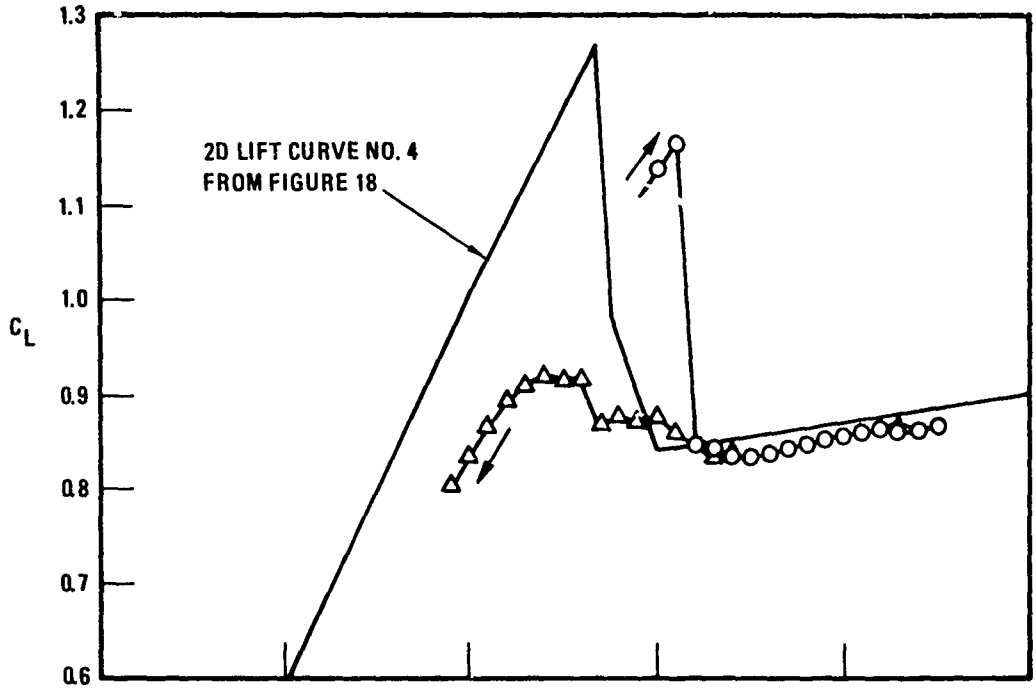

A. NEGATIVE LIFT CURVE SLOPE = 0.97 PER DEGREE

AR = 8.0, τ = 0.495, Λ = 2.27°
i_w = 0°, α_T = 0°, γ = 0°, R_B = 0.119 b/2
PITCH RATE 8 DEG/SEC
SIDESLIP = 0, $\Delta\alpha_R$ = 0
N = 14, M = 4

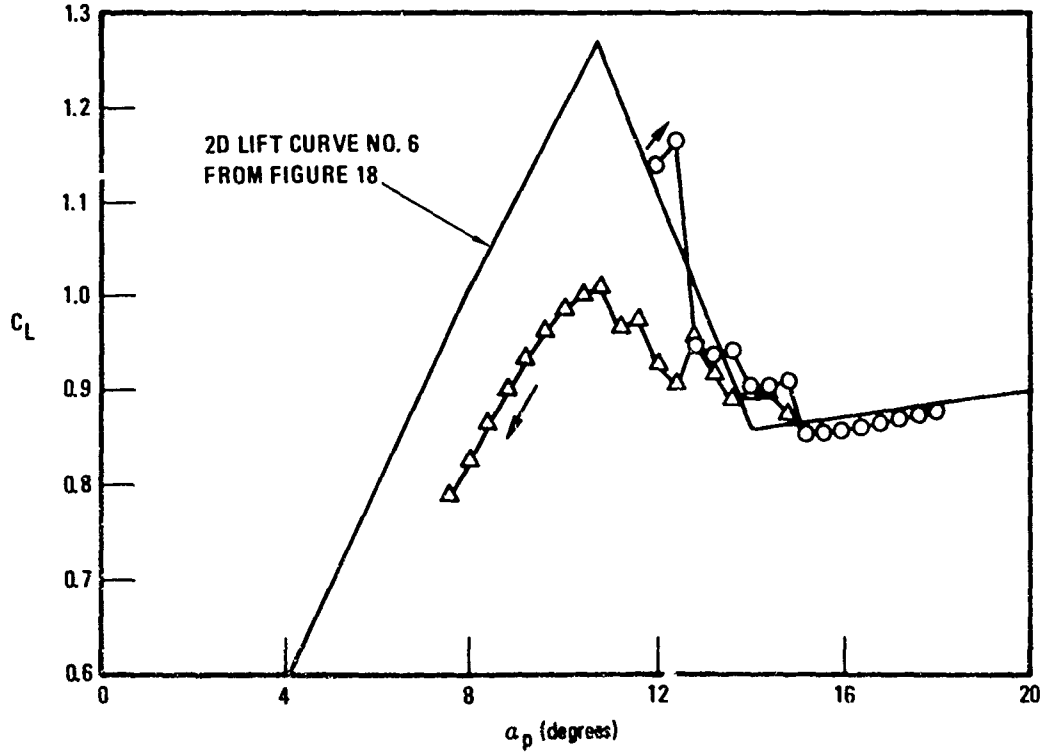

B. NEGATIVE LIFT CURVE SLOPE = 0.125 PER DEGREE

Figure 22. Effect of Negative Lift Curve Slope on Lift Hysteresis, Aspect Ratio 8.0

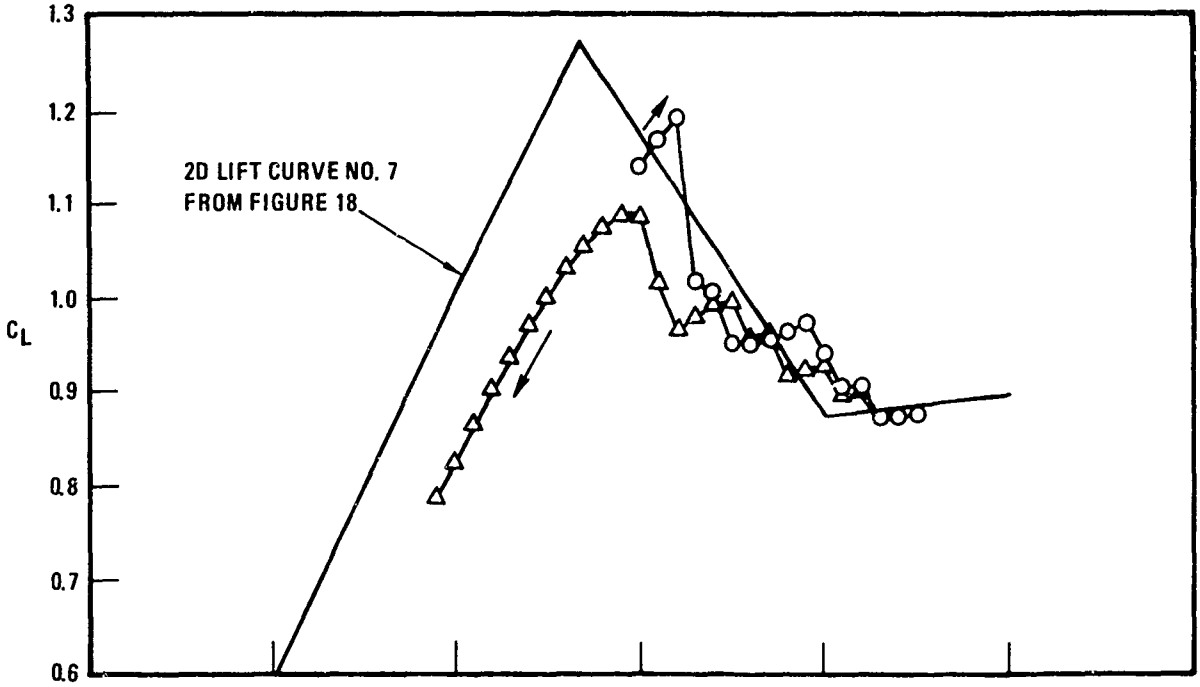

C. NEGATIVE LIFT CURVE SLOPE = 0.075 PER DEGREE

NOTATIONS ON FIGURES A & B

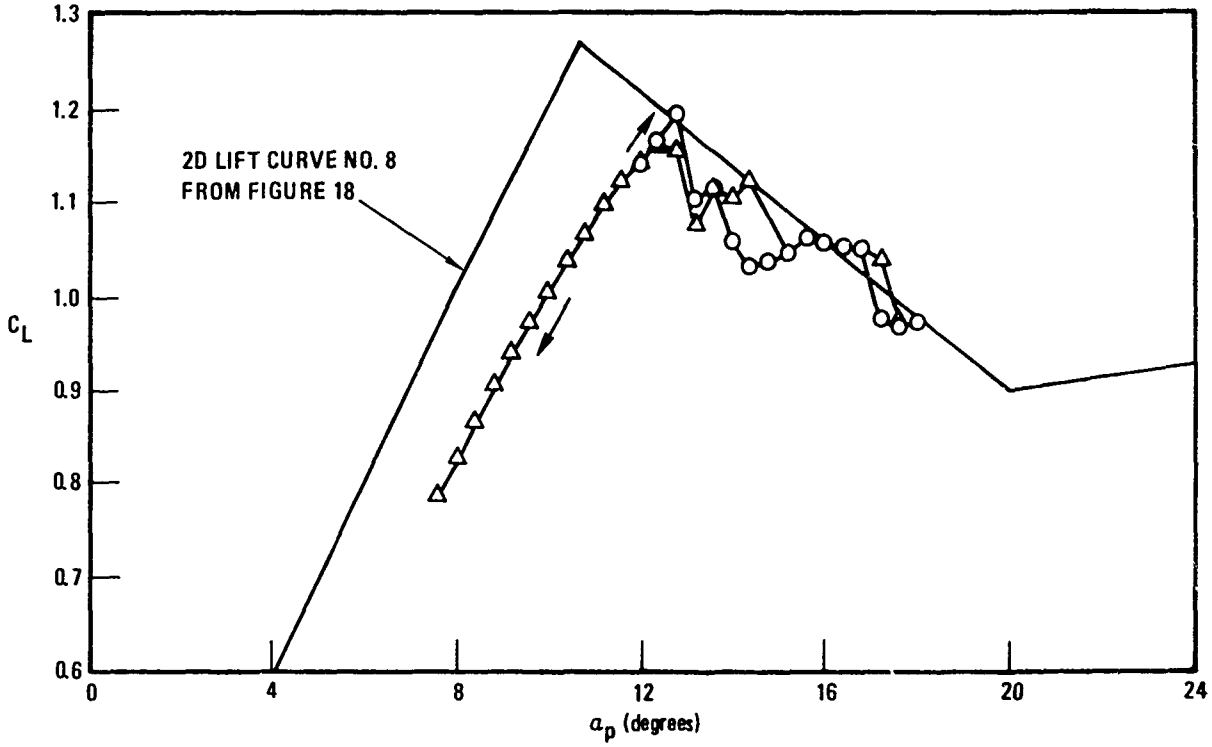

D. NEGATIVE LIFT CURVE SLOPE = 0.040 PER DEGREE

Figure 22. Effect of Negative Lift Curve Slope on Lift Hysteresis, Aspect Ratio 8.0 (Concluded)

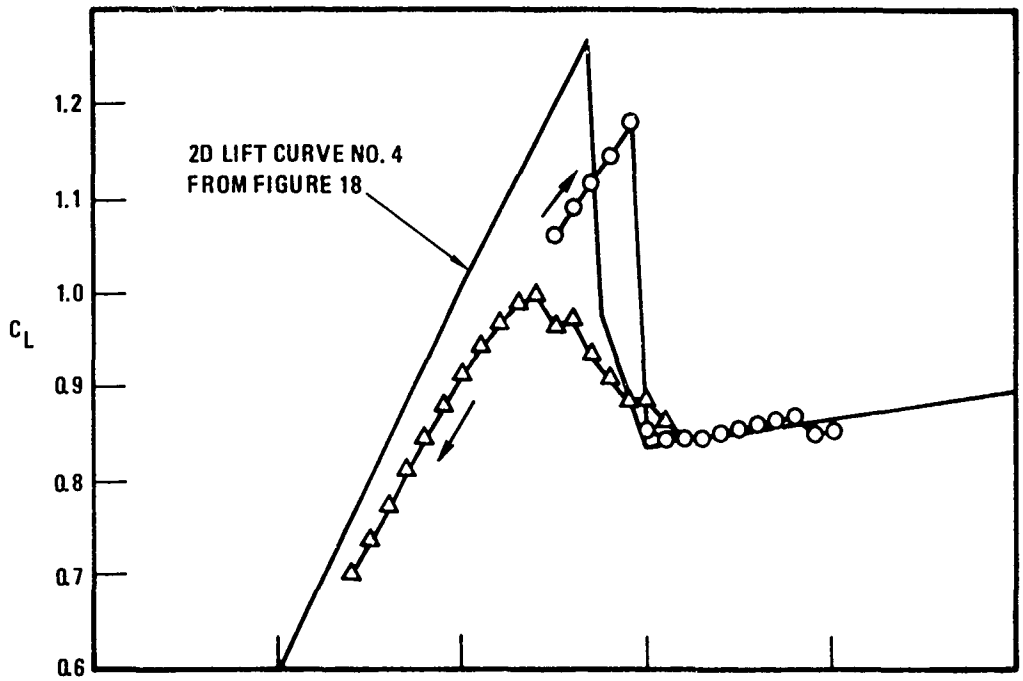

A. NEGATIVE LIFT CURVE SLOPE = 0.97 PER DEGREE

AR = 12.0, τ = 0.495, Λ = 2.27°
i_w = 0°, α_T = 0°, γ = 0°, R_B = 0.119 b/2
PITCH RATE 8 DEG/SEC
SIDESLIP = 0, $\Delta\alpha_R$ = 0°
N = 14, M = 4

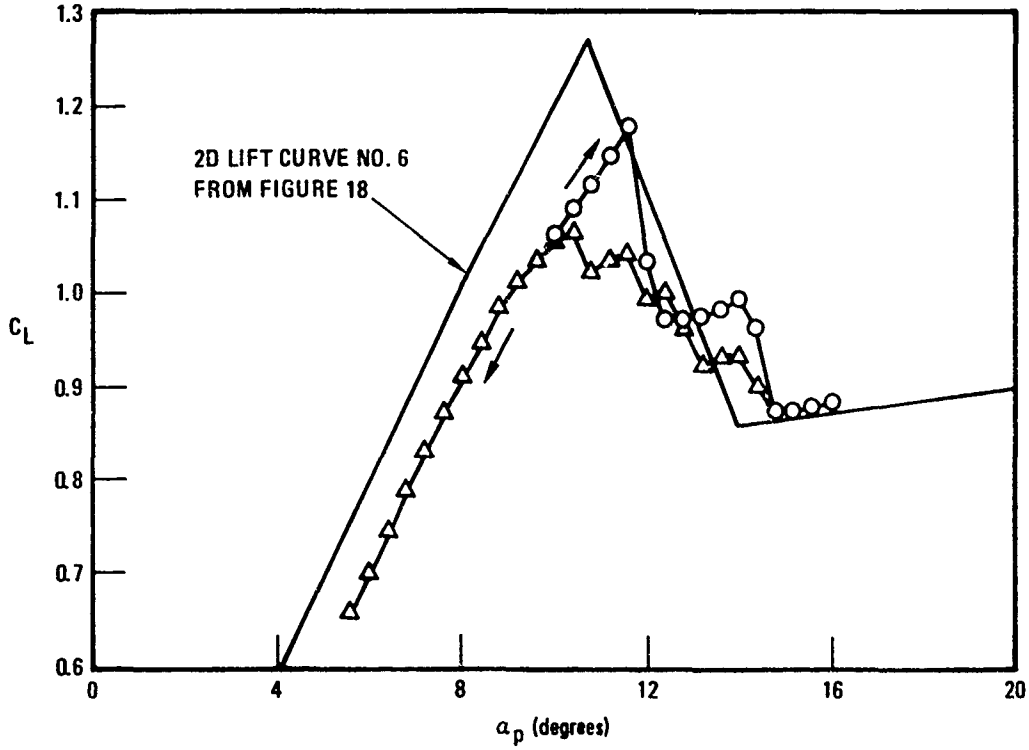

B. NEGATIVE LIFT CURVE SLOPE = 0.125 PER DEGREE

Figure 23. Effect of Negative Lift Curve Slope on Lift Hysteresis, Aspect Ratio 12.0

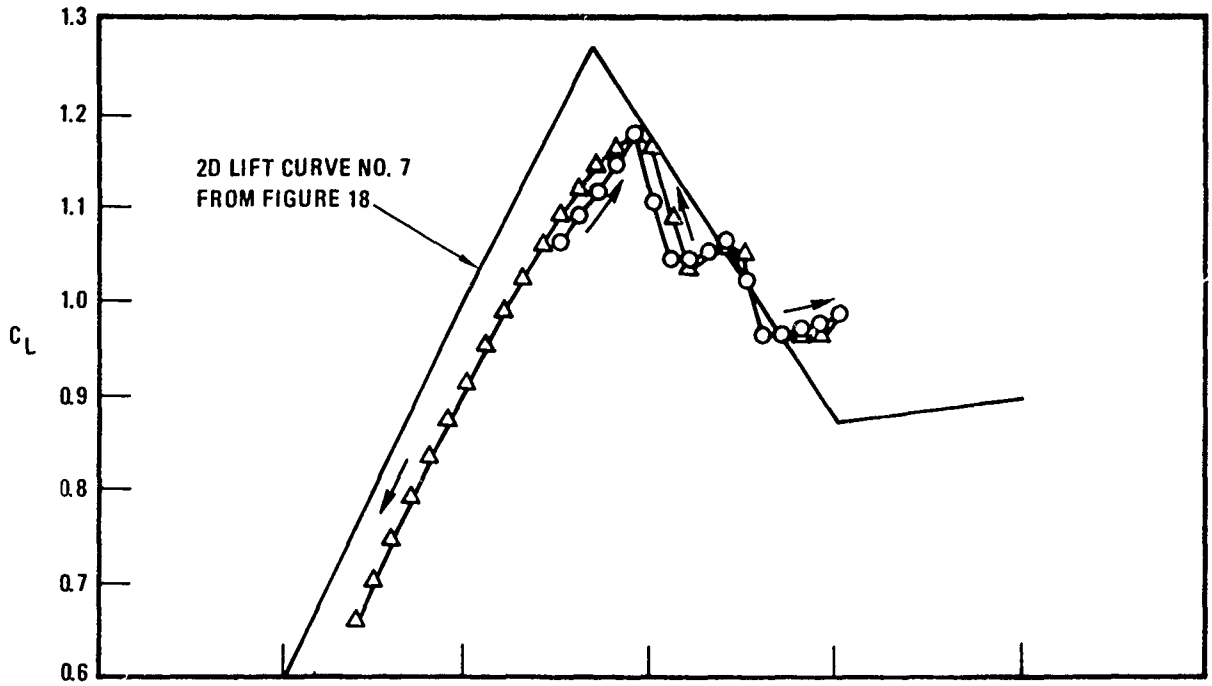

C. NEGATIVE LIFT CURVE SLOPE = 0.075

NOTATIONS ON FIGURES A & B

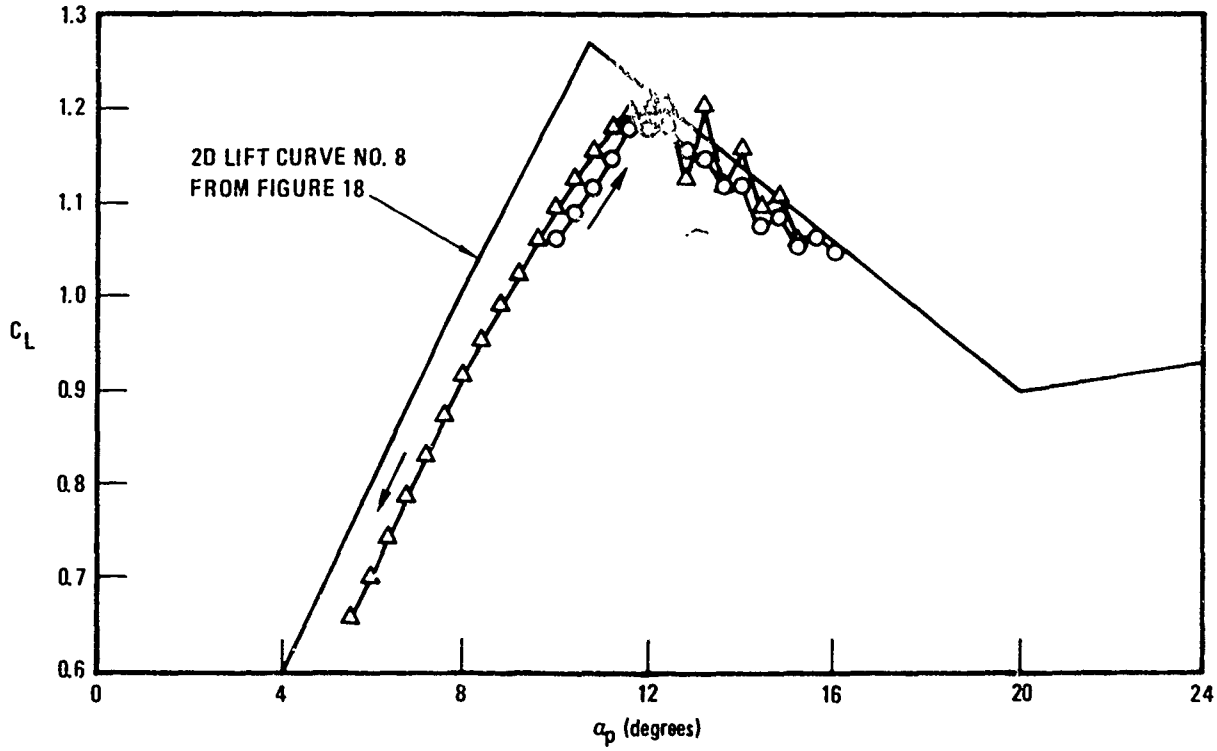

D. NEGATIVE LIFT CURVE SLOPE = 0.040

Figure 23. Effect of Negative Lift Curve Slope on Lift Hysteresis, Aspect Ratio 12.0 (Concluded)

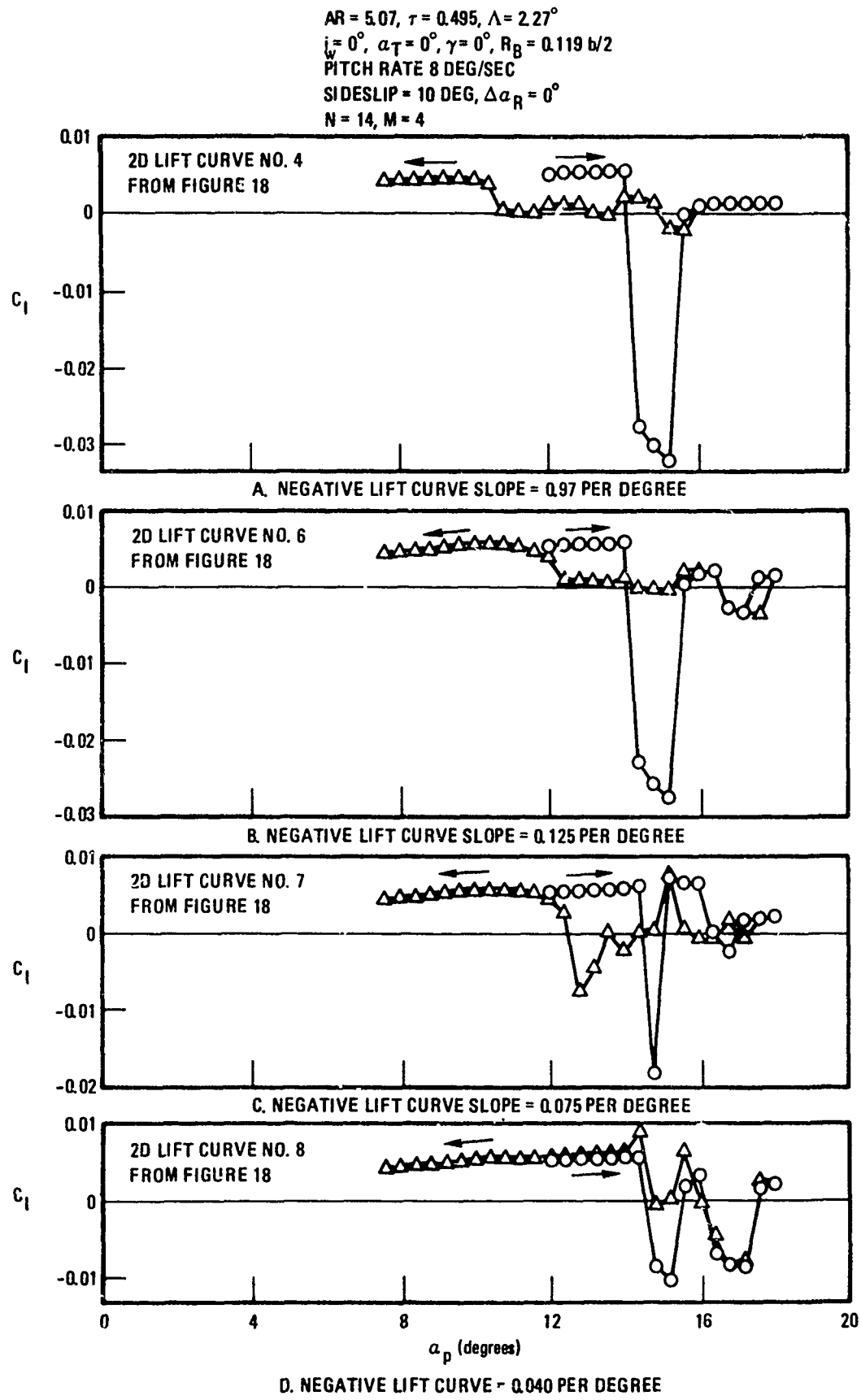

Figure 24. Effect of Negative Lift Curve Slope on Rolling Moment Hysteresis at 10° Sideslip Angle, Aspect Ratio 5.07

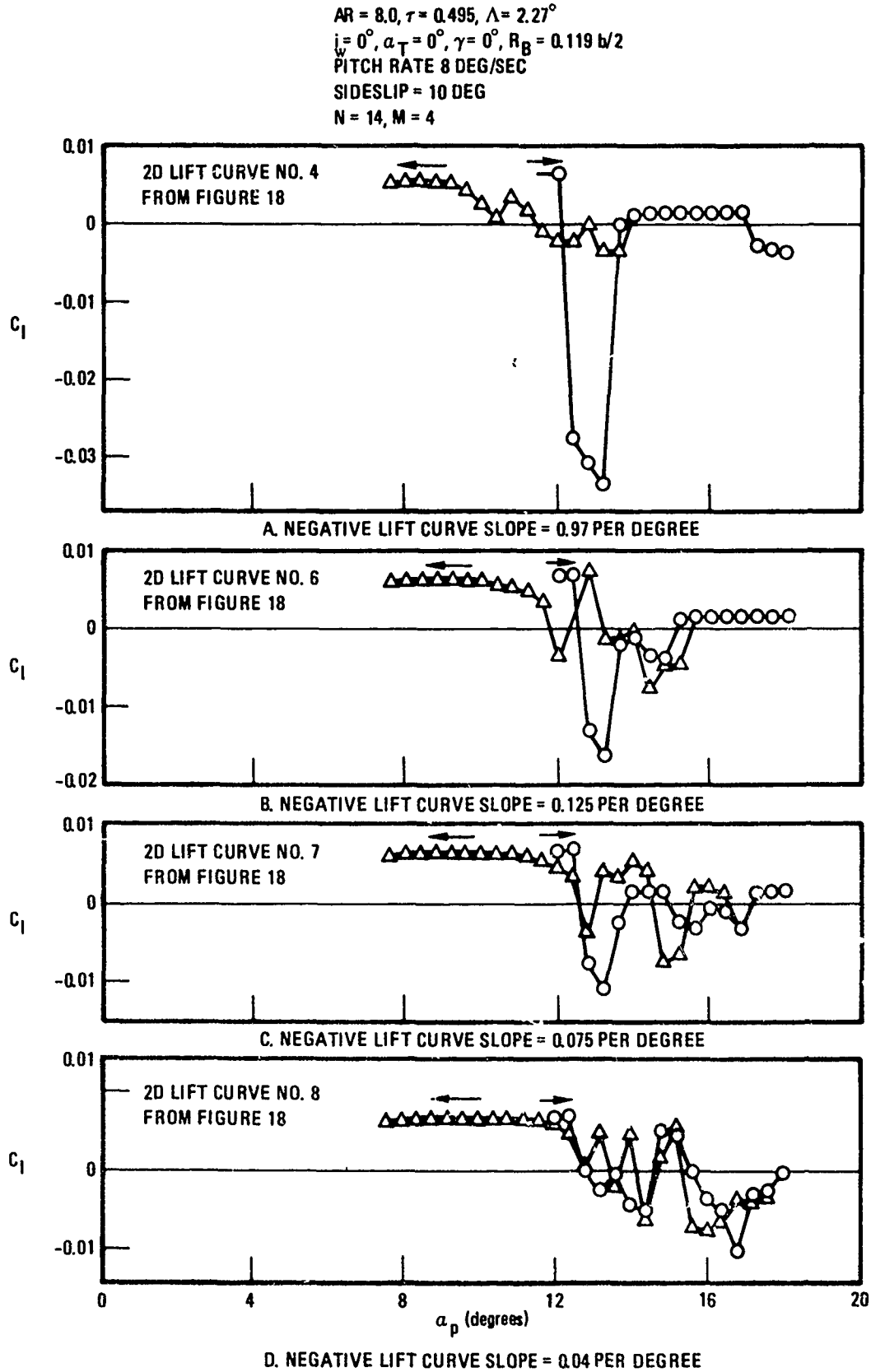

Figure 25. Effect of Negative Lift Curve Slope on Rolling Moment Hysteresis at 10° Sideslip Angle, Aspect Ratio 8.0

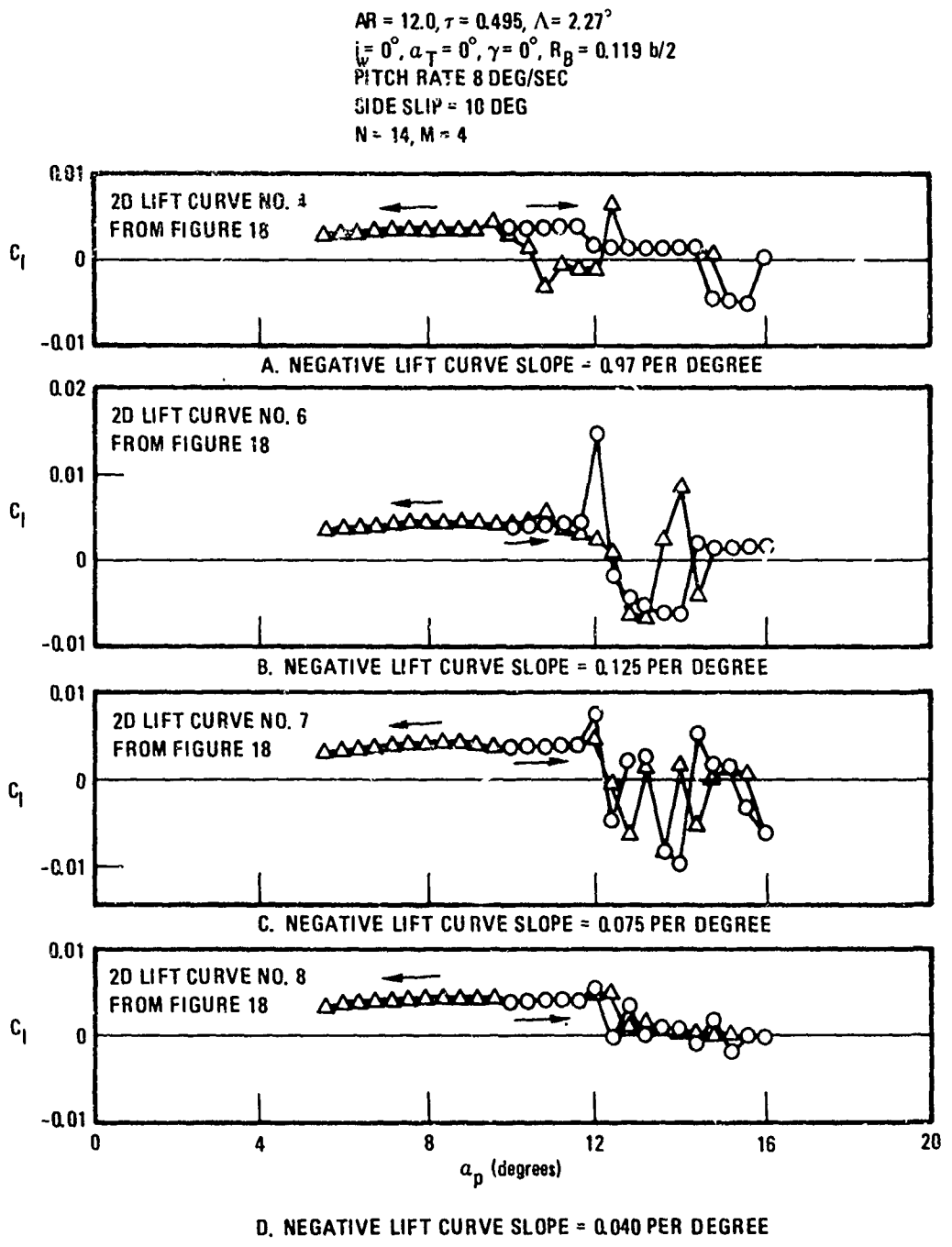

Figure 26. Effect of Negative Lift Curve Slope on Rolling Moment Hysteresis at 10° Sideslip Angle, Aspect Ratio 12.0

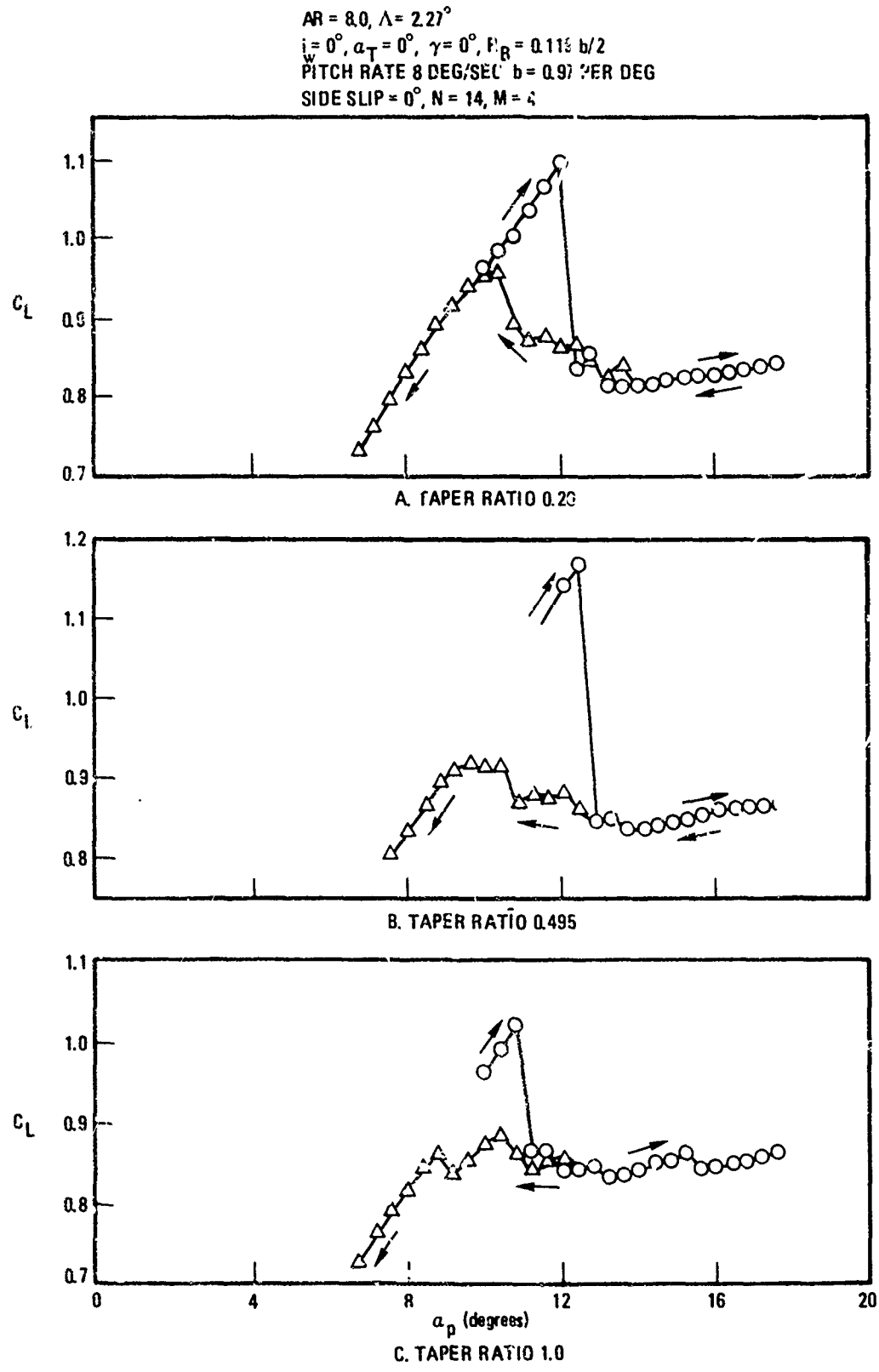

Figure 27. Effect of Taper Ratio on Lift Hysteresis, Aspect Ratio 8.0, Lift Curve #4 from Figure 18

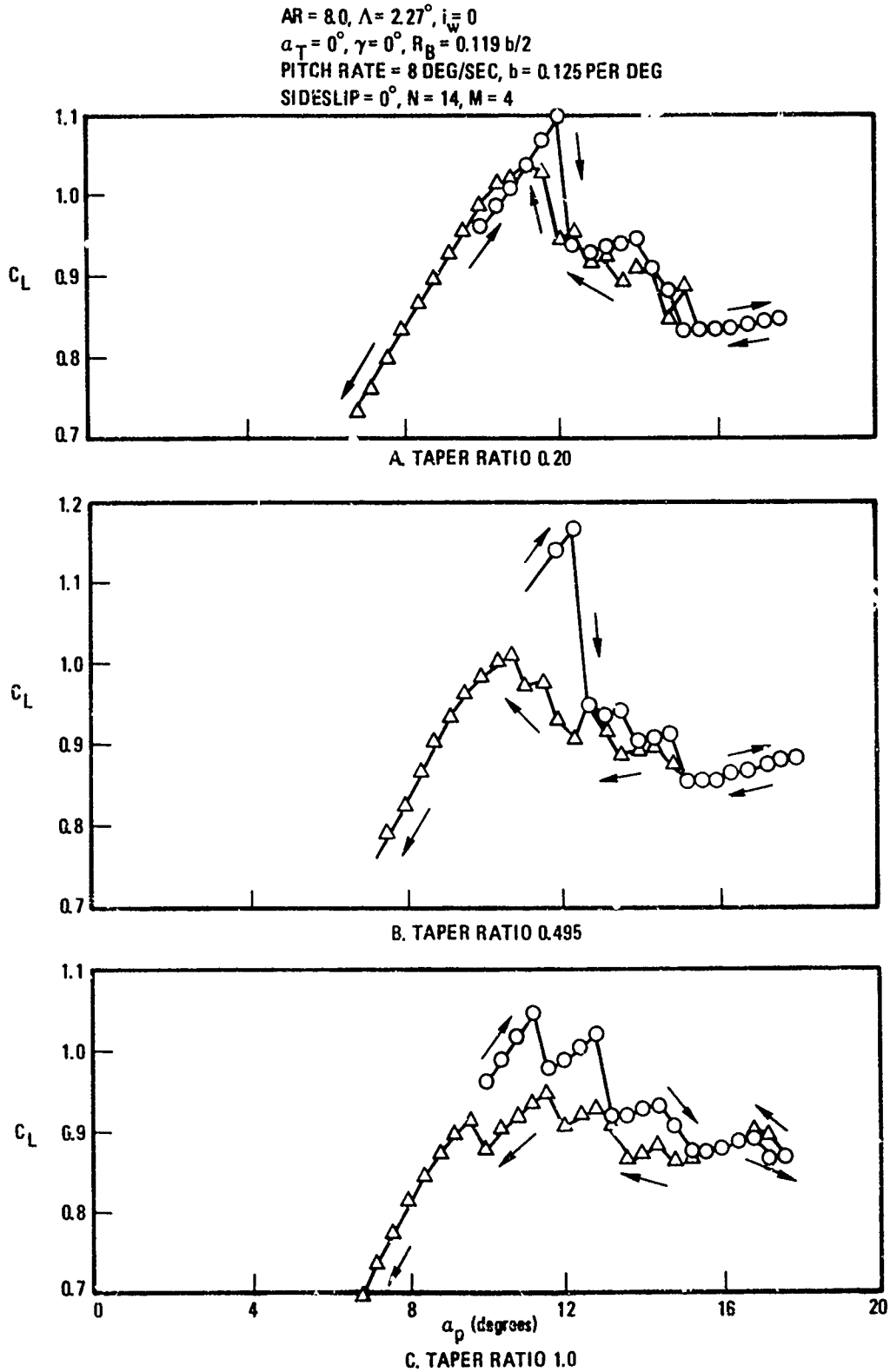

Figure 28. Effect of Taper Ratio on Lift Hysteresis, Aspect Ratio 8.0, Lift Curve #6 from Figure 18

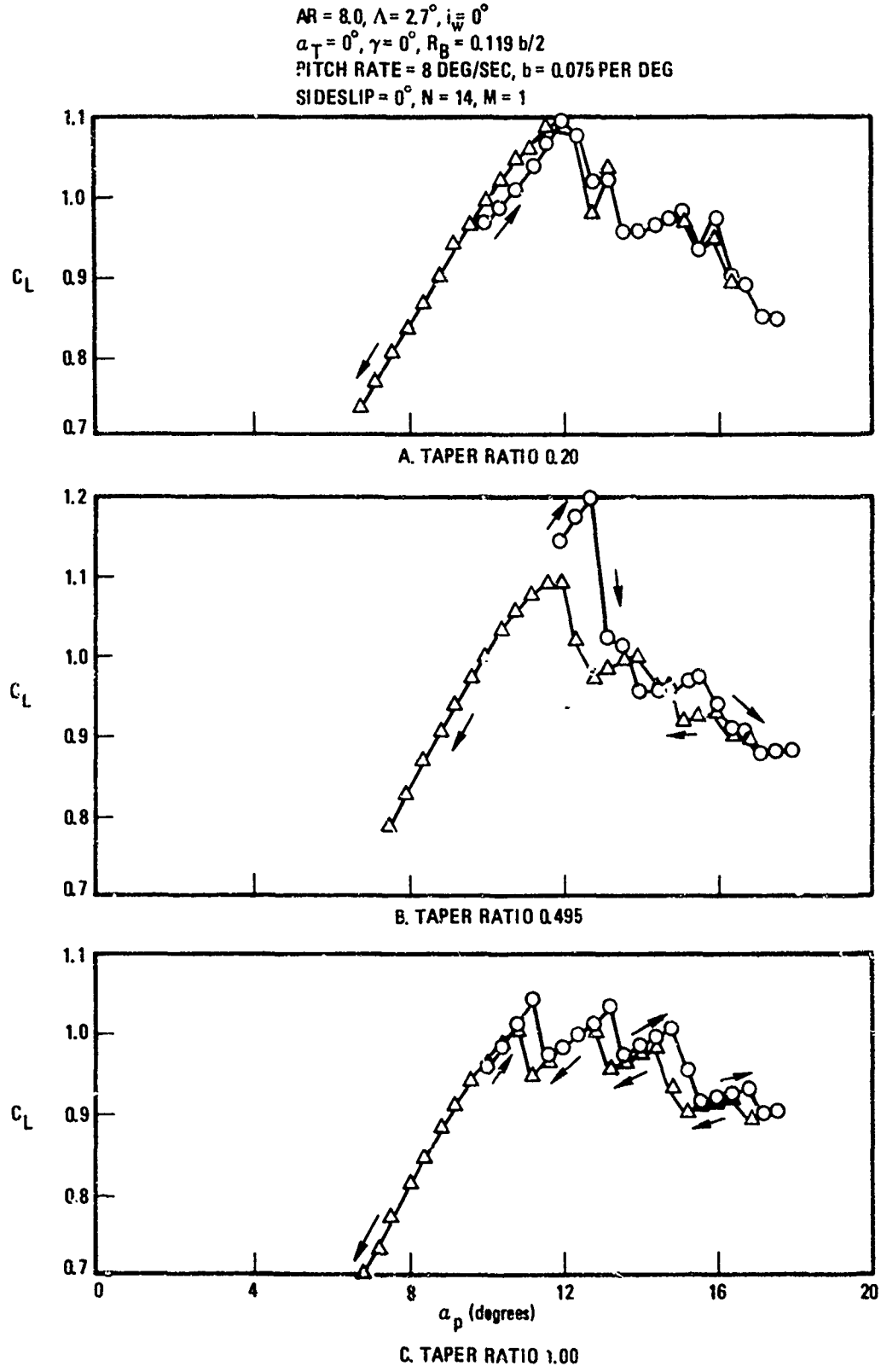

Figure 29. Effect of Taper Ratio on Lift Hysteresis, Aspect Ratio 8.0, Lift Curve #7 from Figure 18

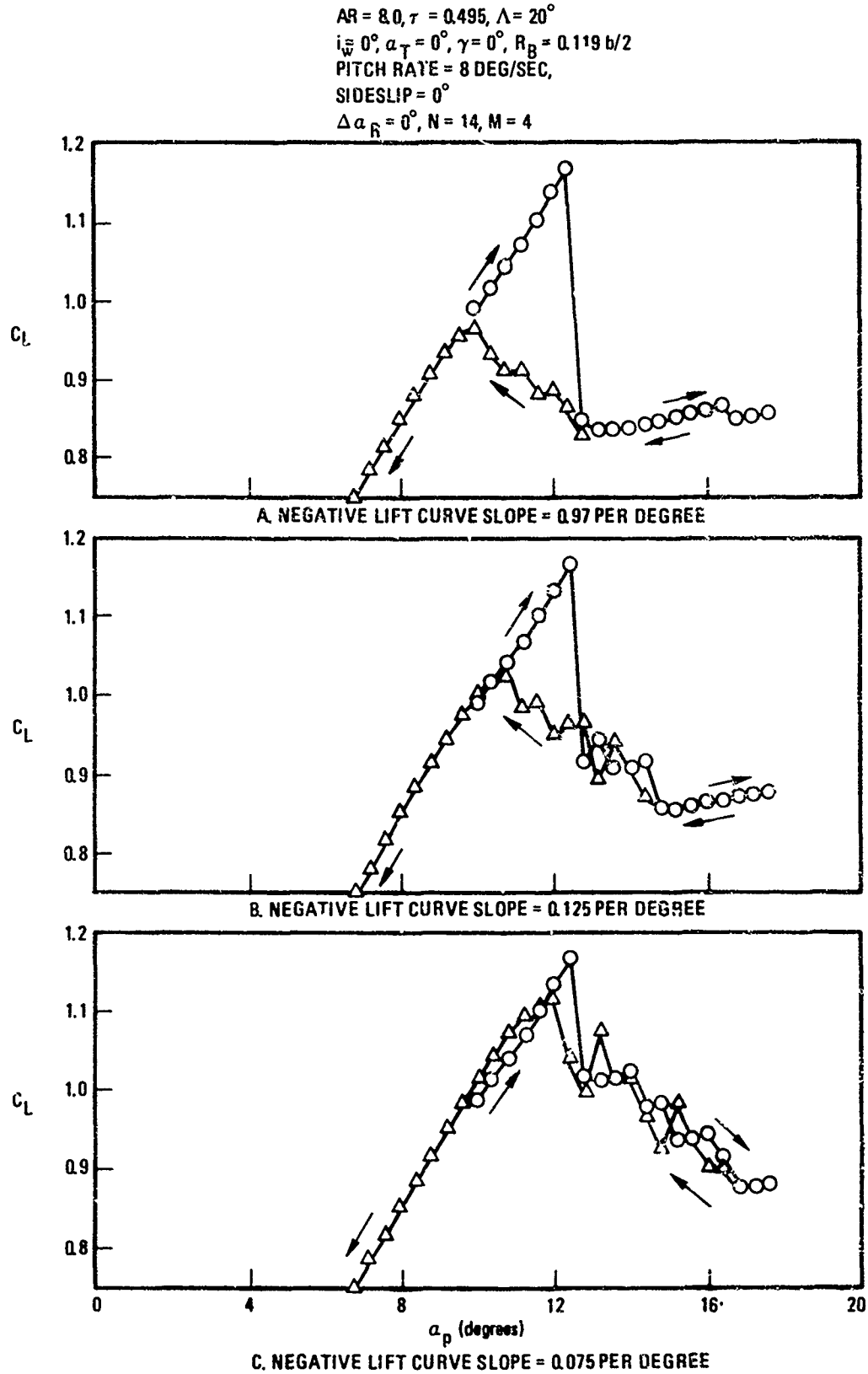

Figure 30. Effect of Negative Lift Curve Slope on Lift Hysteresis, Aspect Ratio 8.0, Sweepback Angle 20°.

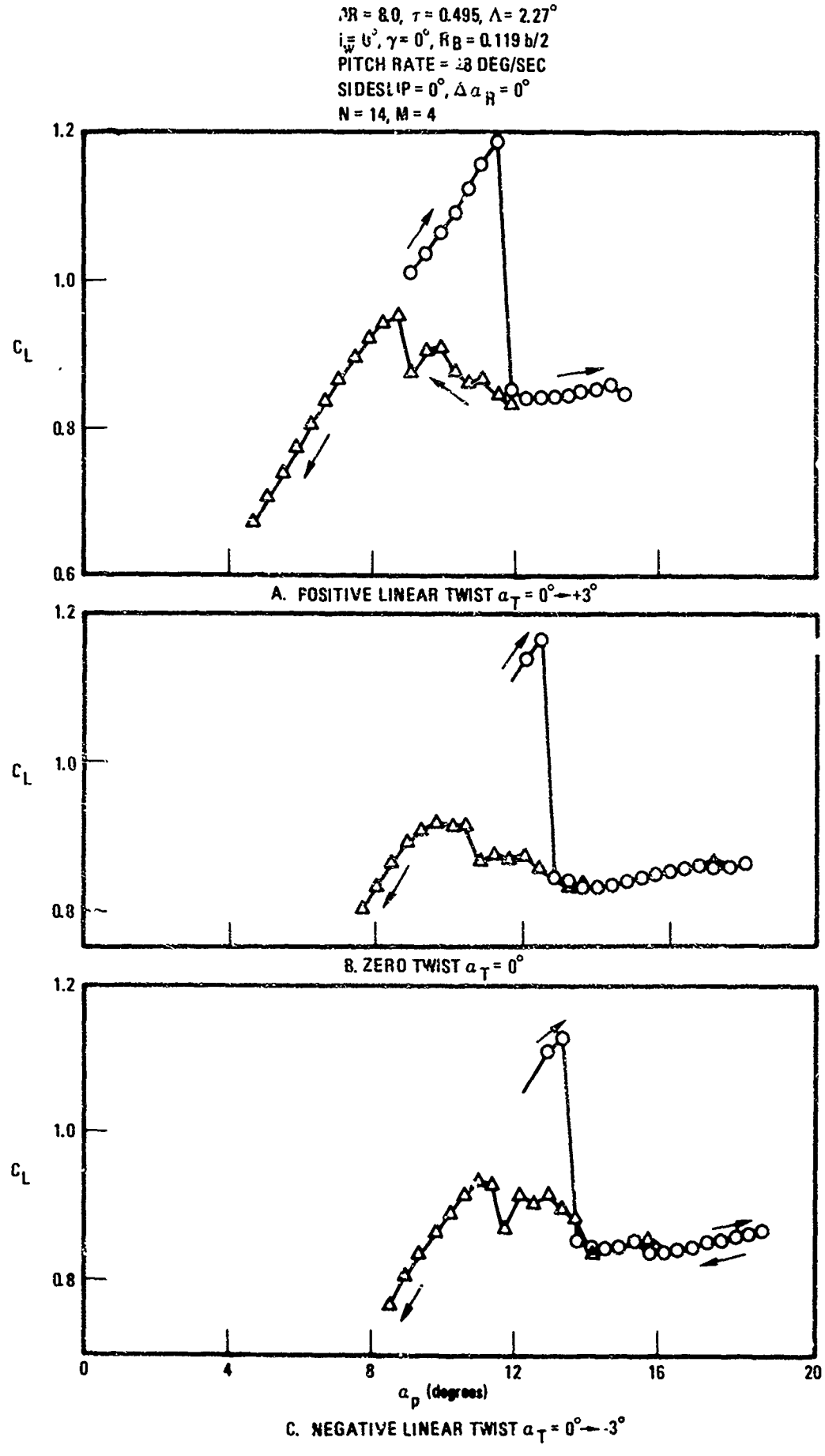

Figure 31. Effect of Twist on Lift Hysteresis, Aspect Ratio 8.0, 2D Lift Curve #4 from Figure 18

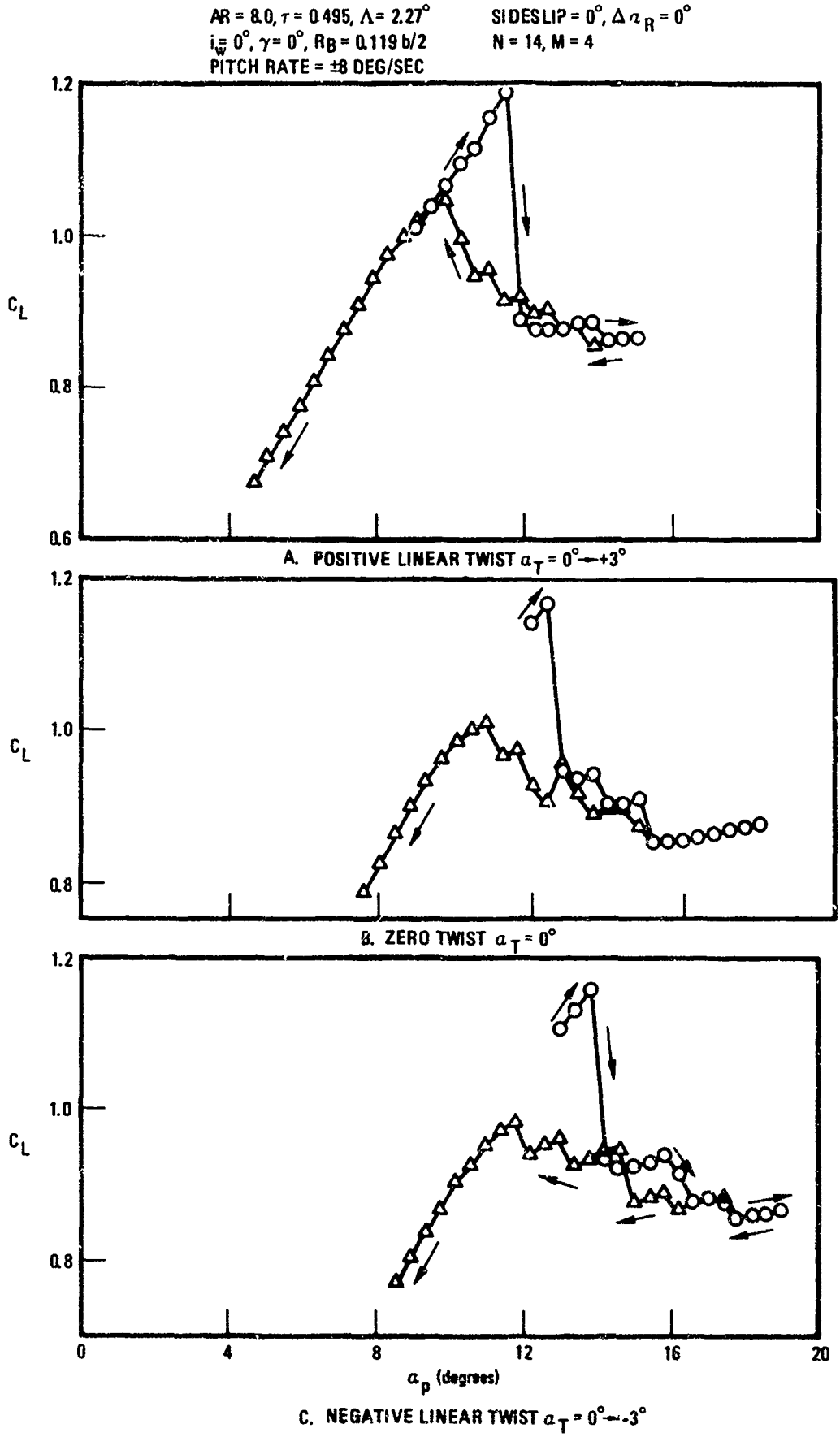

Figure 32. Effect of Twist on Lift Hysteresis, Aspect Ratio 8.0, 2D Lift Curve #6 from Figure 18

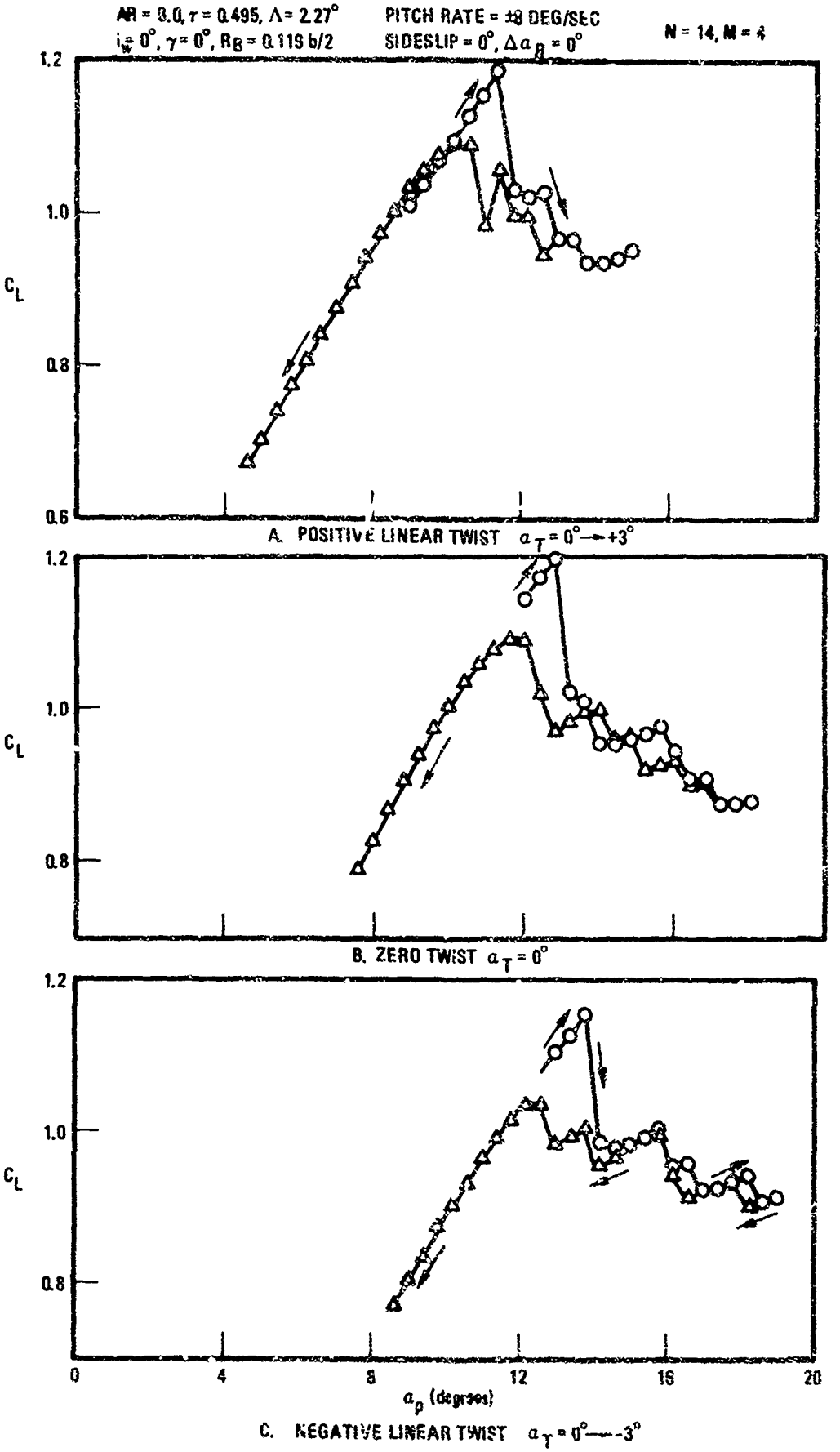

Figure 33. Effect of Twist on Lift Hysteresis, Aspect Ratio 8.0, 2D Lift Curve #7 From Figure 18

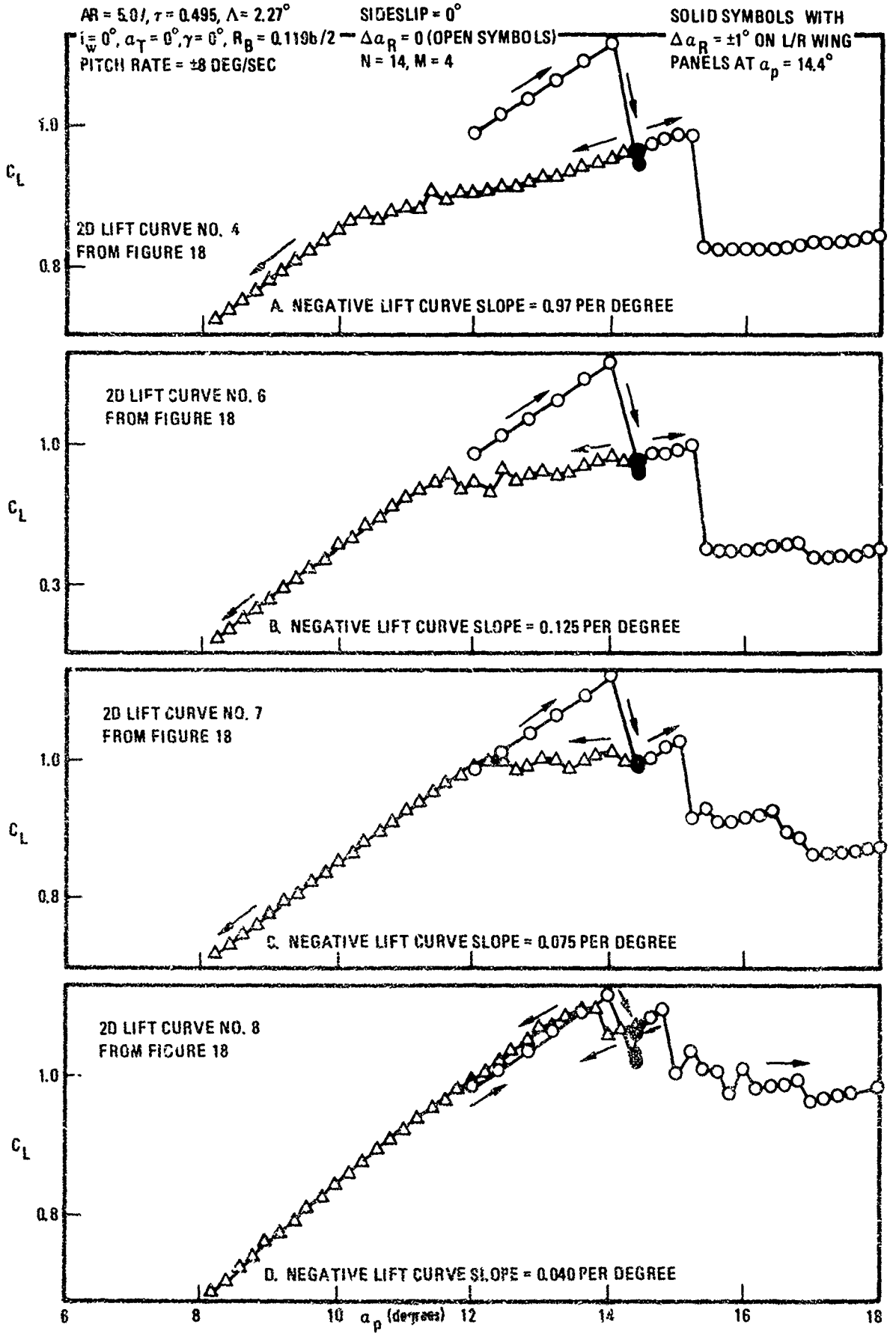

Figure 34. Effect of Roll Perturbation at α_p = 14.4 Degrees on Lift Hysteresis, Aspect Ratio 5.07

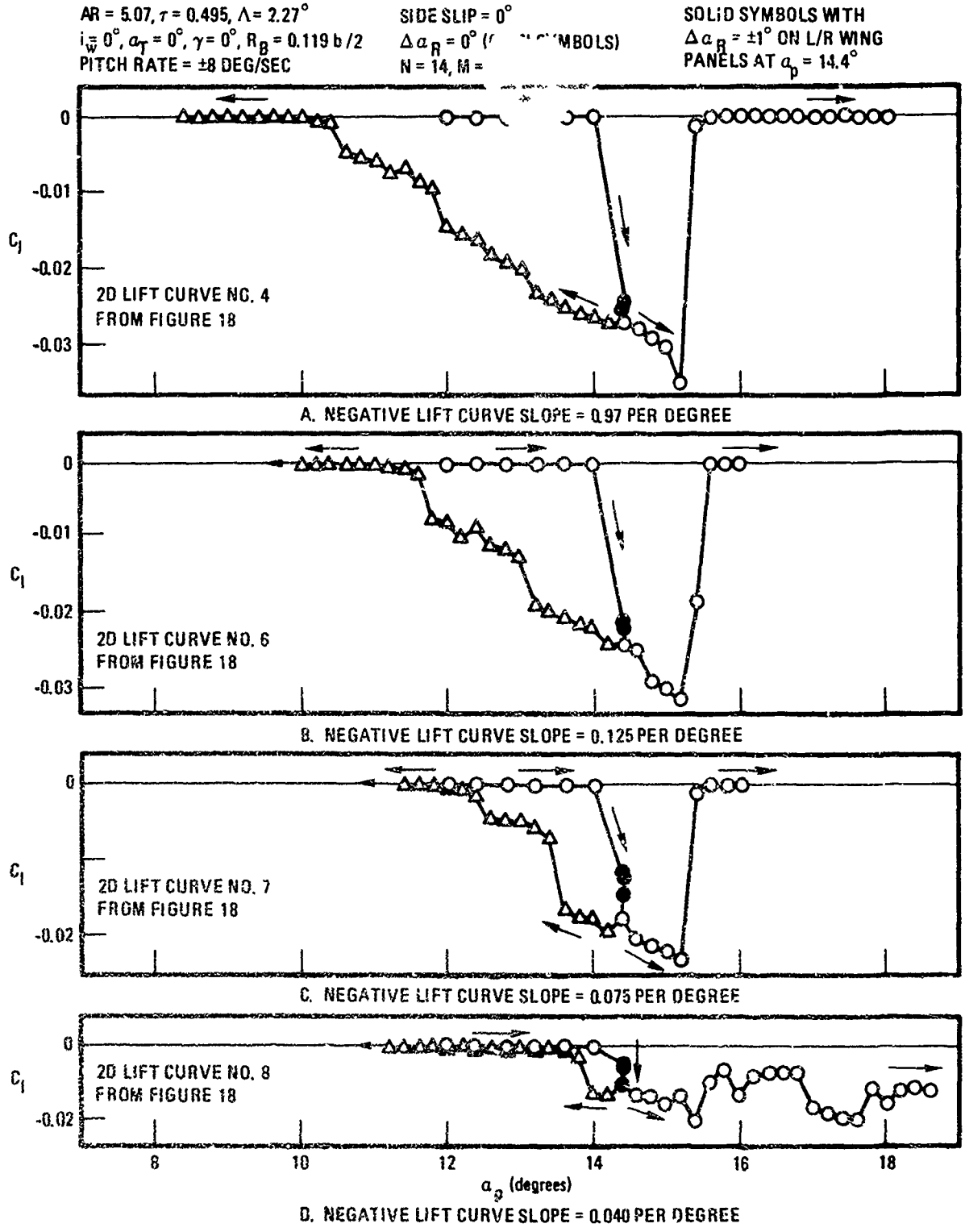

Figure 35. Effect of Roll Perturbation at α_p 14.4 Degrees on Zero Beta Rolling Moment, Aspect Ratio 5.07

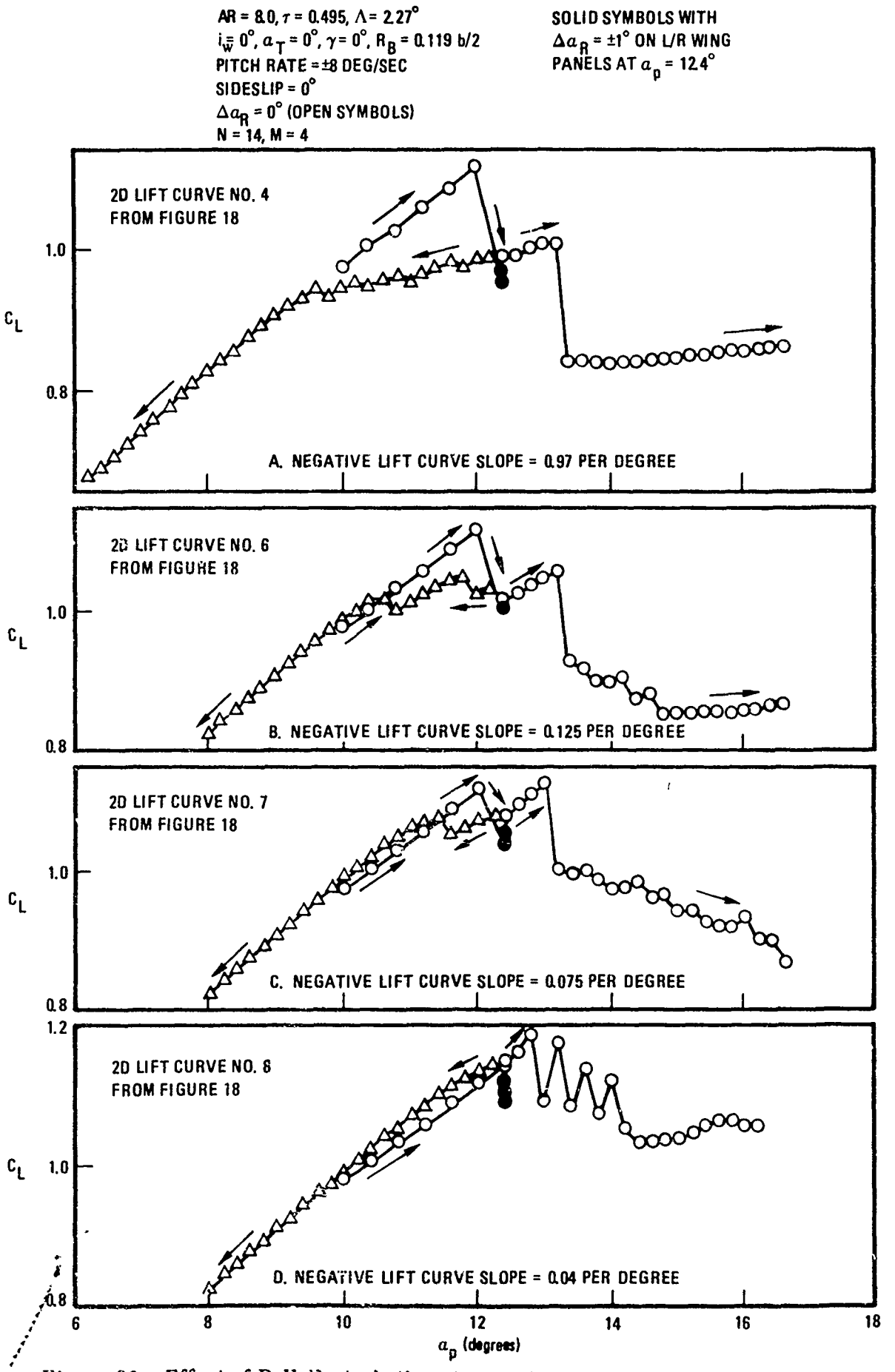

Figure 36. Effect of Roll Perturbation at α_p = 12.4 Degrees on Lift Hysteresis Aspect Ratio 8.0

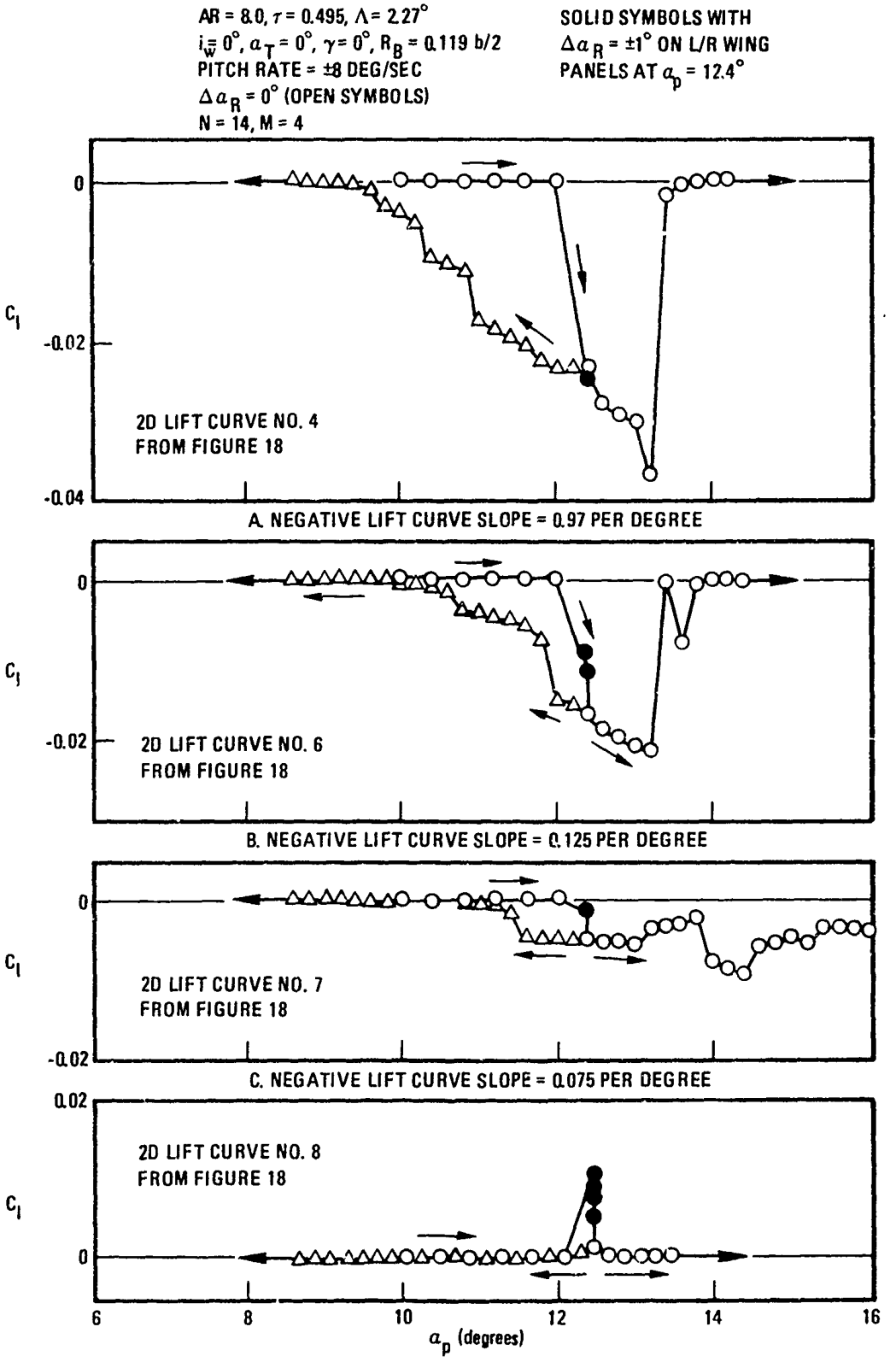

Figure 37. Effect of Roll Perturbation at α_p = 12.4 Degrees on Zero Beta Rolling Moment, Aspect Ratio 8.0

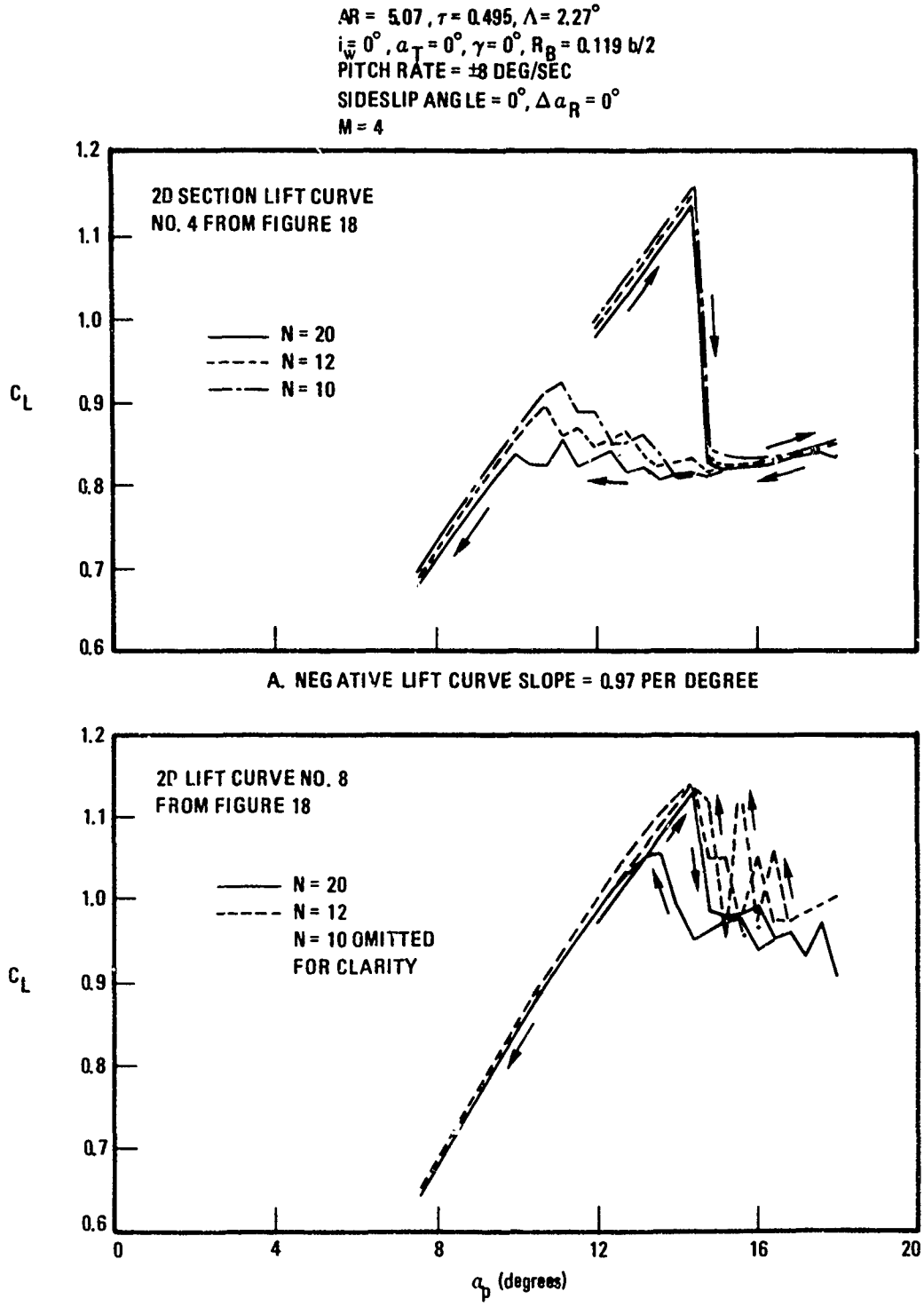

Figure 38. Effect on Number of Spanwise Vortex Elements N on Lift Hysteresis, Aspect Ratio 5.7

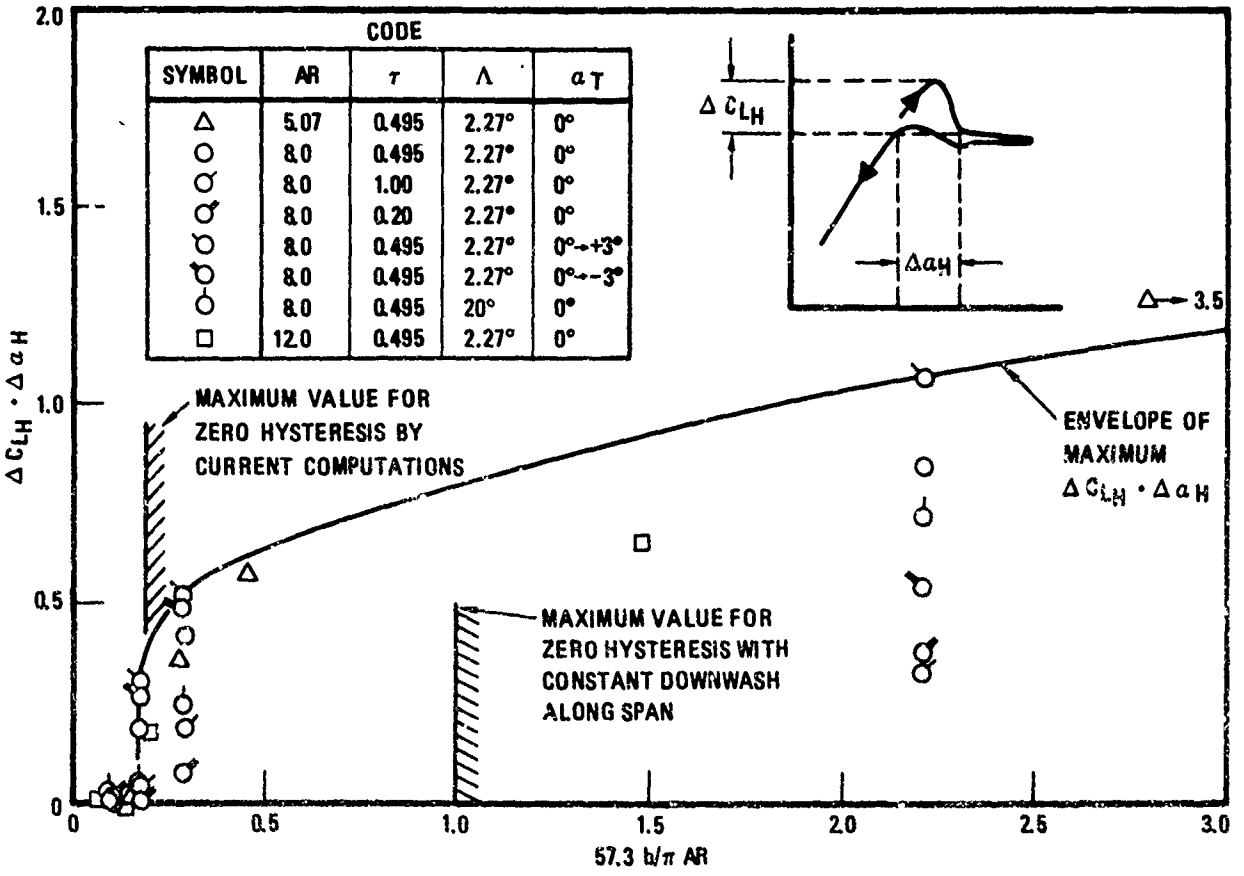

Figure 39. Lift Hysteresis Correlation